Aus dem Biomedizinischen Centrum
Lehrstuhl Physiologische Chemie
Institut der Ludwig-Maximilians-Universität München
Vorstand: Prof. Andreas Ladurner

Dissecting the role of ISW1a in preventing cryptic transcription

Dissertation
zum Erwerb des Doktorgrades der Naturwissenschaften
an der Medizinischen Fakultät der
Ludwig-Maximilians-Universität München

vorgelegt von
Andreia Almeida

aus
Lisboa

2025

Mit Genehmigung der Medizinischen Fakultät
der Ludwig-Maximilians-Universität München

Betreuer:	Prof. Dr. Andreas Ladurner
Zweitgutachter:	Prof. Dr. Philipp Korber
Dekan:	Prof. Dr. med. Thomas Gudermann
Tag der mündlichen Prüfung:	03. Februar 2026

Affidavit

Rafael de Almeida, Andreia Sofia

Surname, first name

I hereby declare, that the submitted thesis entitled:

Dissecting the role of ISW1a in preventing cryptic transcription

is my own work. I have only used the sources indicated and have not made unauthorized use of services of a third party. Where the work of others has been quoted or reproduced, the source is always given.
I further declare that the submitted thesis or parts thereof have not been presented as part of an examination degree to any other university.

Karlsruhe, 15.February.2026

Place, date

Andreia Almeida

Signature doctoral candidate

Confirmation of congruency

Rafael de Almeida, Andreia Sofia

Surname, first name

I hereby declare that the electronic version of the submitted thesis, entitled:

Dissecting the role of ISW1a in preventing cryptic transcription

is congruent with the printed version both in content and format.

Karlsruhe, 15.February.2026

Place, date

Andreia Almeida

Signature doctoral candidate

Acknowledgements

I would like to express my gratitude to those who, in various ways, contributed to my doctorate experience over the course of nearly five years.

Michaela Smolle, for adding me to her research group and giving me the opportunity to expand my scientific expertise while working on this and other projects. Her support outside the lab during a very vulnerable time is something that I am deeply grateful for and will not forget.

My lab colleagues, Ameirika, Lena Bergmann, and Lingling Yang, for sharing this journey with me. I am also grateful to Julia Schluckebier for her assistance in the lab.

Andreas Ladurner, for integrating me into his group during the last year of my doctorate. I had a lovely experience being part of Ladurner's lab meetings. I am thankful for his lab members, for being so nice and welcoming. I would like to give a special thanks not just to Andreas and Carla for their valuable input and ideas, but also to Magdalena.

My TAC members, Peter Becker and Sigurd Braun, for their valuable feedback and guidance. A special thanks to Peter Becker for being so helpful.

Tobias Straub and Tamas Schauer, for their support during my learning curve with bioinformatics at the computer biology core facility, and every time after that when I would get "stuck" with data analysis.

Marianne and Zdenka for helping keeping the department running and for being so nice. On top of that, I am going to miss Zdenka's baking skills.

Christine and Anton for their administrative, technical, and at times emotional support. I always felt like I could count on them for anything. Anton, for being always funny and chatty, and for bringing his sweet dog to work.

Elizabeth Schroeder-Reiter, for her role in coordinating the IRTG program, including the trip to Venice, and for being one who cares and is always ready to help PhD students such as myself.

My roommates, Janina and Brunella. I could always count on them to let go of stress and just have fun.

Garyfallia, for being my first weird roommate and now my dearest and best friend. For all the late nights watching Rupaul or Harry Potter. For all the brunches, dinners, dances, and for showing me Greece.

The MAPS group, Rita, Abu and Marcel, thank you so much for the fun moments, trips, and emotional support.

Last but not least, my family. My mother, for the support and care during both surgery recoveries. Her readiness to drop everything to be by my side during my most vulnerable moments meant the world to me. And my father, for being so strong and positive - for not letting go of his essence. He was fearful that his battle against cancer would make me spiral during my PhD, so he made sure to show me his strength and optimism every single day, even during his worst moments. I love you so much.

Preface

The research presented herein builds upon earlier work initiated by my former principal investigator, Michaela Smolle. Given the collaborative nature of this project, it is important to distinguish my ownership over this work, and the contribution, support and guidance from others.

For this research project, I have made significant contributions through various molecular biology methods and bioinformatics analyses. I was responsible for the total RNA extraction, the preparation of strand-specific RNA-seq libraries, and the 5′cap-seq library preparation. Additionally, I played a vital role in the experimental procedure and analysis of strand-specific multiplexed RT-qPCR, with the support of our former lab technician, Julia Schluckebier, on the experimental procedure. My bioinformatics responsibilities included the processing and downstream analysis of RNA-seq, 5′cap-seq, and CUT&RUN data, as well as the annotation and validation of Isw1 and Chd1-repressed antisense transcripts. Importantly, I generated all the figures presented in this thesis, with the exception of figures 1.6.3 A, 1.6.3 C, and 1.6.4, which are derived from preliminary data collected in our lab. Furthermore, I was also responsible for comparing my data with the GEO data sets referred herein.

I collaborated closely with Lingling Yang, a fellow member of our lab group, who carried out the ChIP-seq experiments and processed the respective sequencing data. I used the normalized ChIP-seq data generated by Lingling to compare with my RNA-seq and 5′cap-seq data and generate the figures 3.7.1, 3.7.2 and 3.7.3. Additionally, I deeply appreciate Julia Schluckebier's effort in trying to establish the CUT&RUN approach in our lab. While I was establishing the pipeline for the 5′cap-seq data analysis, Julia generated the CUT&RUN libraries referred in this study. I would also like to point out that not only me, but also other lab members (André Marschall, Lingling Yang, Lisa Schuster), former lab technician (Ina Koeva),

as well as our former principal investigator (Michaela Smolle), contributed to making the strains used in this study.

Tamas Schauer, a former member of the Bioinformatics Core Facility, shared examples of R functions for plotting metagene profiles and heatmaps, which I then optimized and incorporated into my R scripts. I would also like to extend my heartfelt thanks to Tobias Straub, head of the Bioinformatics Core Facility, for giving me the opportunity to spend a few weeks in his department, where I received guidance and training while conducting my first bioinformatic analysis. I am also deeply grateful for his problem-solving insights, which helped me navigate challenges during my transcriptomics analyses.

In conclusion, this thesis predominantly derives from my contributions, with a portion deriving from a close collaboration with Lingling Yang. I am grateful for the support from my fellow lab members and technicians, as well as the valuable help from other departments.

Table of Contents

Affidavit i

Confirmation of congruency ii

Acknowledgements iii

Preface v

Table of Contents vii

List of Abbreviations xi

List of Figures xviii

List of Tables xxii

Summary xxiii

Zusammenfassung xxv

1 Introduction 1

1.1 The basics of chromatin 1

1.2 Nucleosome arrangement within genes 2

1.3 Chromatin remodelers 3

1.4 The coordinated action of chromatin factors regulates transcriptional chromatin dynamics 6

1.5 Cryptic transcription 9

1.5.1 Cryptic transcripts in wild-type yeast 10

1.5.2 Maintenance of chromatin structure prevents cryptic events 11

1.6 Isw1 remodeling complexes in yeast 12

1.6.1 Isw1 ATPase and its complexes 12

1.6.2 Importance of Isw1 complexes in chromatin remodeling 14

1.6.3 The role of Isw1 remodelers in transcription regulation....16
1.6.4 Structure and mechanism of the ISW1a complex....17
1.6.5 Regulation of ISW1a complex....19
1.6.6 Genetic interactions involving ISW1a....20
1.6.7 Recruitment of ISW1a....21
1.6.8 Role of ISW1a Complex in Transcriptional Fidelity....22
1.7 Aims of this thesis....24
2 Methods....26
2.1 Molecular biology methods....26
2.1.1 Yeast strains....26
2.1.2 Total RNA extraction....29
2.1.3 Strand-specific RNA-seq libraries....30
2.1.4 5′cap-seq library preparation....31
2.1.5 Multiplexed strand-specific RT-qPCR....34
2.1.6 CUT&RUN and library preparation....36
2.1.7 Chromatin immunoprecipitation followed by quantitative PCR (ChIP-qPCR) 37
2.1.8 Western blotting....40
2.1.9 ChIP-seq library preparation....41
2.2 Bioinformatics methods....42
2.2.1 RNA-seq data processing....42
2.2.2 5′cap-seq data processing....43
2.2.3 Annotation and Validation of Isw1 and Chd1-Repressed Antisense Transcripts (ICRATs)....47
2.2.4 CUT&RUN data processing....50

2.2.5 ChIP-seq data processing 51
3 Results....52
3.1 Isw1 and Chd1 prevent cryptic initiation at thousands of genes....52
3.2 Characterization of Isw1 and Chd1-repressed antisense transcripts....57
3.3 Individual contributions of Isw1 and Chd1 chromatin remodelers to suppressing cryptic transcription 65
3.4 The role of chromatin remodelers Chd1 and ISW1a in preventing the exposure of cryptic promoters....72
3.5 Rrp6 masks the cryptic phenotype in cells lacking ISW1a 77
3.6 ISW1a and Chd1 remodelers repress cryptic transcription in sporulation and transmembrane transport-related genes 81
3.7 ISW1a prevents incorporation of H2A.Z at intragenic promoters....85
3.8 H2A.Z facilitates cryptic transcription in *ioc3Δ* and *isw1Δ* cells 89
3.9 H2A.Z promotes ISW1a recruitment *in vivo* 94
3.10 Supplementary figures 99
4 Discussion 105
4.1 High-resolution characterization of the cryptic transcriptional phenotype in *isw1Δ chd1Δ* cells 105
4.2 Distinct and overlapping contributions of ISW1a and CHD1 remodelers to cryptic transcription 108
4.3 Why do cryptic intragenic RNAs accumulate in chromatin remodeler-deficient cells? 112
4.4 H2A.Z is important for the cryptic phenotype in cells lacking Isw1 chromatin remodelers 113
4.5 ISW1a recruitment may be facilitated by H2A.Z 115

4.6 Proposed model for Isw1 remodeling complexes in suppressing cryptic transcription in wild-type yeast 116
4.7 Outlook 120
4.7.1 Link between intragenic DNA exposure and cryptic transcription 120
4.7.2 Role of ISW1a in suppressing cryptic transcription initiation at intergenic regions 121
4.7.3 Stability and fate of remodeler-repressed cryptic transcripts 122
4.7.4 Relationship between Isw1, Chd1, and the FACT complex 122
4.7.5 The importance of Swr1 and H2A.Z in enabling cryptic transcription in *ioc3Δ* cells 123
4.7.6 Recruitment of ISW1a 123
4.7.7 Concluding remarks 124
References 125

List of Abbreviations

5′cap-seq	5′cap sequencing
Abf1	Autonomously replicating sequence (ARS) binding factor 1
ACT1	Actin
ADA	Ada2-Gcn5-Ada3
ADH1	Alcohol dehydrogenase 1
AIM23	Altered inheritance rate of mitochondria protein 23
asDEGs	antisense differentially expressed genes
asRNA	antisense RNA
ATP	Adenosine triphosphate
ATPase	Adenosine triphosphatase
bps	base pairs
Bre1	Brefeldin A-sensitivity protein 1
BROMO	Bromodomain
CAG	Cytosine-adenosine-guanine
cDNA	Complementary DNA
CHD	Chromodomain-Helicase-DNA binding
Chd1	Chromodomain-helicase-DNA binding protein 1
ChIP	Chromatin immunoprecipitation
ChIP-seq	ChIP sequencing
CHRV	Chromosome V
CIP	Calf intestinal alkaline phosphatase
CLB	Coil-Linker-DNA-Binding
CPM	Counts per million
Ct	Cycle threshold
CTD	C-terminal domain

CUTs	Cryptic unstable transcripts
DAVID	Database for Annotation, Visualization and Integrated Discovery
DCV1	Demands Cdc28 kinase activity for viability 1
DMSO	Dimethyl sulfoxide
DNA	Deoxyribonucleic acid
DNase	Deoxyribonuclease
dNTPs	Deoxynucleotide triphosphates
EDTA	Ethylenediaminetetraacetic acid
EGTA	Ethyleneglycol-bis (beta-aminoethylether)- N,N'-tetraacetic acid
EMSA	Electrophoretic mobility shift assay
FAA2	Fatty acid activation 2
FACT	Facilitates chromatin transcription
FDR	False discovery rate
FLO10	Flocculation 10
FUN26	Function unknown now 26
GAL10-7	Galactose metabolism protein 10 - Galactose metabolism protein 7
GCN5	General control nonderepressible 5
GEO	Gene expression omnibus
GO	Gene ontology
h	hour
HEPES	N-2-hydroxyethylpiperazine-N'-2-ethane sulfonic acid
HFM1	Helicase family member 1
Hho1	Histone H one
HLB	Helical-Linker-DNA-Binding
Hmo1	High mobility group family member 1
HOP1	Homologous pairing 1

HSA	helicase–SANT-associated
HSS	HAND SANT and SLIDE
HSSB	HSS-Binding
HTA2	Histone h two A
HTB2	Histone h two B
Htz1	Histone Two A Z
HXT10	Hexose transporter 10
ICRATs	Isw1 and Chd1-repressed antisense transcripts
IgG	Immunoglobulin G
IGV	Integrative genomics viewer
IME1	Inducer of meiosis 1
IME4	Inducer of meiosis 4
INO80	Inositol requiring 80
Ioc	ISWI one complex
Ioc2	ISWI one complex protein 2
Ioc3	ISWI one complex protein 3
Ioc4	ISWI one complex protein 4
IP	Immunoprecipitated
IRC18	Increased recombination centers 18
ISW1	Imitation switch 1
ISW1a	Imitation switch 1 complex a
ISW1b	Imitation switch 1 complex b
ISW2	Imitation switch 2
ISWI	Imitation switch
kB	kilobase
Log_2FC	Logarithm base 2 fold-change
M	Molar
MATa	Mating-type a

MATα	Mating-type alpha
MCD4	Morphogenesis checkpoint dependent 4
MEC1	Mitosis entry checkpoint 1
min	minute
ml	milliliter
mm	millimeter
MNase	Micrococcal nuclease
MNase-seq	MNase sequencing
mRNA	messenger RNA
MUT	Mutant
n	number in a group
ncRNA	non-coding RNA
NDR	Nucleosome-depleted region
NET-seq	Native elongating transcript sequencing
nM	nanomolar
NMD	nonsense-mediated decay
NP-40	Nonoxynol-40
Npl3	Nuclear protein localization 3
NuA4	Nucleosome acetyltransferase of histone H4
OD_{600}	Optical density at 600 nm
ORF	Open reading frame
Paf1	Polymerase-associated factor 1
pAG-MNase	Protein A and protein G IgG binding domains fused to micrococcal nuclease
PCA	Principal component analysis
PCA1	P-type cation-transporting ATPase
PCR	Polymerase chain reaction
PDC1	Pyruvate decarboxylase 1
PEG	Polyethylene glycol

Pgk1	Phosphoglycerate kinase 1
PIC	Pre-initiation complex
PIPES	[1,4-piperazinebis(ethane sulfonic acid)]
PMA1	Plasma membrane ATPase 1
POG1	Promoter of growth 1
poly(A)	Polyadenylate
qPCR	quantitative PCR
RAD30	Radiation sensitive 30
Rad6	Radiation sensitive protein 6
Rap1	Repressor/activator protein 1
Reb1	RNA polymerase I Enhancer Binding protein
RecA	Recombinase A
RNA	Ribonucleic acid
RNA-seq	RNA sequencing
RNAPII	RNA polymerase II
RNase	Ribonuclease
Rpd3S	Reduced potassium dependency-3 small complex
rpm	revolutions per minute
rRNA	Ribosomal RNA
Rrp6	Ribosomal RNA-processing protein 6
RRT	Resize-reduce-trim
RSC	Remodels the Structure of Chromatin
RT	Reverse transcription
RT-qPCR	Reverse transcription-quantitative PCR
Rtt109	Regulator of Ty1 transposition 109
S. cerevisiae	*Saccharomyces cerevisiae*
S2P	Phosphorylated serine 2
S5P	Phosphorylated serine 5

SAGA	Spt-Ada-Gcn5-Acetyltransferase
sDEGs	sense differentially expressed genes
SDS	Sodium dodecyl sulfate
SEM	Standard error of the mean
Set1	SET (Su(var)3-9, enhancer-of-zeste and trithorax) domain-containing 1
Set2	SET domain-containing 2
Set3C	Set3 complex
Siz1	SAP and miz-finger domain 1
Siz2	SAP and miz-finger domain 2
SMARCA1	SWI/SNF related, matrix associated, actin dependent regulator of chromatin, subfamily a, member 1
SMARCA5	SWI/SNF related, matrix associated, actin dependent regulator of chromatin, subfamily a, member 5
Snf2	Sucrose nonfermenting 2
snoRNA	Small nucleolar RNA
snRNA	Small nuclear RNA
SPO22	Sporulation-specific gene 22
SPR28	Sporulation regulated 28
Spt10	Suppressor of Ty protein 10
Spt21	Suppressor of Ty protein 21
Spt6	Suppressor of Ty 6
SRATs	Set2-repressed antisense transcripts
STE3	Sterile 3
SUMO	Small ubiquitin-like modifier
SUTs	Stable unannotated transcripts
SWI/SNF	Switch/sucrose non-fermentable
SWR1	SWI2/SNF2-related 1
SWR1C	SWR1 complex

TBP	TATA-box-binding protein
TC	TSS cluster
TES	Transcription end site
TF	Transcription factor
TNRs	Trinucleotide repeats
tRNA	Transfer RNA
TSS	Transcription start site
TSS-seq	TSS sequencing
UDG	Uracil-DNA glycosylase
Ume6	Unscheduled meiotic gene expression 6
UMI	Unique molecular identifier
WCE	Whole cell extract
Yaf9	Yeast homolog of the human leukemogenic protein AF9
YPD	Yeast extract peptone dextrose
ZIP2	Zipping up meiotic chromosomes 2
µg	microgram
µl	microliter
µM	Micromolar

List of Figures

Figure 1.3.1 Overview of chromatin remodeling families, their ATPase domains, as well as the existing ATPases and the complexes these belong in *Saccharomyces cerevisiae.* 4

Figure 1.4.1 Simplified overview of the chromatin dynamics taking place over genic regions during transcription....8

Figure 1.6.1 Subunit composition of the two most studied Isw1 remodeling complexes in *S. cerevisiae*: ISW1a and ISW1b. 13

Figure 1.6.2 Schematic representation of domain organization for ISW1a components....18

Figure 1.6.3 *IOC3* interacts genetically with histone variant *HTZ1* and *SET3* histone acetyltransferase. 21

Figure 1.6.4 Loss of *IOC3* derepresses cryptic transcription and histone turnover. 24

Figure 2.1.1 RNA integrity (25S and 18S rRNA) prior to library preparation. 30

Figure 2.1.2 Ioc3-Flag occupancy expressed in percentage of input. 40

Figure 2.2.1 PCA plot of sense and antisense transcript profiles. 43

Figure 2.2.2 Sample distances from the first (A) and second (B) 5′cap-seq experiments. 46

Figure 2.2.3 The Resize-Reduce-Trim method successfully improved the annotation of potential ICRATs. 49

Figure 3.1.1 Deleting Isw1 and Chd1 leads to transcription derepression at thousands of genes. 53

Figure 3.1.2 Loss of both ISW1 and CHD1 leads to exposure of thousands of intragenic promoters. 55

Figure 3.1.3 Representative gene *PCA1* shows increased sense and antisense TSS and RNA expression in *isw1Δ chd1Δ* compared to wild-type....56

Figure 3.1.4 Distribution of intragenic TSS clusters across gene regions in wild-type and *isw1Δ chd1Δ* yeast. 57

Figure 3.2.1 Annotated Isw1 and Chd1-repressed antisense transcripts (ICRATs). 59

Figure 3.2.2 Capped ICRATs and promoter motif analysis. 61

Figure 3.2.3 SRATs are the most derepressed group of annotated ncRNAs in yeast, yet they show poor overlap with ICRATs. 62

Figure 3.2.4 The FACT complex, among other factors involved in chromatin structure, may also regulate ICRAT expression. 64

Figure 3.3.1 *IOC3* deletion does not influence the overall levels of Ioc4 protein in cells, and vice-versa. 65

Figure 3.3.2 Relationships between *isw1Δ chd1Δ* and/or single remodeler mutants compared to wild-type yeast. 67

Figure 3.3.3 Chd1 is a major suppressor of cryptic transcription, and cooperates with ISW1a remodeler at hundreds of genes. 68

Figure 3.3.4 Increased antisense transcription in the remodeler mutants generally does not result in down-regulation of gene expression *in cis*. 69

Figure 3.3.5 Derepressed asDEGs containing ICRATs, as determined by differential expression analysis on *ioc3Δ*, *isw1Δ*, *chd1Δ* and *ioc3Δ chd1Δ* mutants versus wild-type. 70

Figure 3.3.6 Isw1 and Chd1 suppress distinct antisense transcripts. 71

Figure 3.3.7 Isw1 and Chd1 remodelers prevent antisense transcription accumulation at opposite ends of genes. 72

Figure 3.4.1 Deletion of *IOC3* and *CHD1* exposes new promoters. 73

Figure 3.4.2 Density and expression changes of sense intragenic TSS clusters in *ioc3Δ* and *chd1Δ* cells. 73

Figure 3.4.3 Genome-wide mapping of TSSs reveals that ISW1a and Chd1 remodelers impact sense transcription in different ways. 74

Figure 3.4.4 ISW1a and Chd1 prevent exposure of antisense promoters predominantly at different regions of genes. 76

Figure 3.4.5 Chd1 prevents exposure of cryptic promoters at intergenic regions. 77

Figure 3.5.1 ISW1a represses intergenic promoters and divergent transcription initiated at gene promoters. 79

Figure 3.5.2 *IOC3* deletion has heightened cryptic effects on the antisense transcriptome in *rrp6Δ* background compared to wild-type cells. 80

Figure 3.6.1 Gene ontology analysis revealed sporulation and transmembrane transport enrichment in genes with derepressed sense and antisense transcription, respectively. 82

Figure 3.6.2 ISW1a regulates non-coding transcription in sporulation-related genes. 83

Figure 3.6.3 TATA box and transcription rate analysis of differentially expressed genes in various remodeler mutants and whole *S.cerevisiae* genome. 84

Figure 3.7.1 H2A.Z marks the TSSs of intragenic transcripts in *ioc3Δ* and *isw1Δ* cells. 86

Figure 3.7.2 Representative genes showing increased H2A.Z and H3K4me3 levels near the start of asRNAs. 88

Figure 3.7.3 H2A.Z and H3K4me3 accumulate in the gene bodies of derepressed genes in *isw1Δ* and *ioc3Δ* cells. 89

Figure 3.8.1 Multiplexed strand-specific RT-qPCR strategy. 90

Figure 3.8.2 *HTZ1* deletion suppresses the cryptic phenotype in *isw1Δ* and *ioc3Δ* cells. 91

Figure 3.8.3 *SWR1* deletion suppresses the cryptic phenotype in *isw1Δ* cells. 92

Figure 3.8.4 Impact of *RAD6* and *SET1* deletions on the cryptic transcription phenotype in Isw1 remodeler mutants. 93

Figure 3.9.1 Ioc3 accumulates at nucleosome-depleted regions in wild-type yeast. 95

Figure 3.9.2 Ioc3 seems to be enriched at Reb1 and Rap1 binding sites in wild-type yeast. 96

Figure 3.9.3 Potential reduction in Ioc3 recruitment to the start of genes upon loss of H2A.Z. ChIP-qPCR analysis of Ioc3-Flag in wild-type and *htz1Δ*, *gcn5Δ*, and *htz1Δ gcn5Δ* cells. 98

Figure 3.10.1 RNA-seq and 5′cap-seq coverage tracks of three biological replicates from wild-type and *isw1Δ chd1Δ* strains over representative genes *PCA1* (A) and *FLO10* (B). 99

Figure 3.10.2 Results of de-novo motif search performed by HOMER on TSS clusters from capped ICRATs. 100

Figure 3.10.3 Individual replicate data from metagene analysis of antisense expression levels across genes longer than 2 kb (n = 1148).....101

Figure 3.10.4 Results of sense differential expression analysis performed on each remodeler mutant versus wild-type yeast. 101

Figure 3.10.5 Results of antisense differential expression analysis performed on each remodeler mutant versus wild-type yeast. 102

Figure 3.10.6 Individual replicate data for transcriptional changes in meiotic genes caused by deletion of *IOC3*, *ISW1*, and *CHD1*. 103

Figure 3.10.7 Individual replicate data for H2A.Z and H3K4me3 levels data over derepressed genes. 104

Figure 4.6.1 Proposed model for the role of Isw1 and Chd1 remodelers in the suppression of cryptic transcription. 119

List of Tables

Table 1.3.1 Chromatin remodelers in *S. cerevisiae*: genomic localization, recruitment factors, and functional outcomes. 5

Table 2.1.1 All strains used in this study. 27

Table 2.1.2 Oligos used for genomic deletions. 29

Table 2.1.3 Oligos used for 5′cap-seq. 33

Table 2.1.4 Oligos used for multiplexed strand-specific RT-qPCR. 35

Table 2.1.5 Oligos used for ChIP-qPCR. 39

Table 2.2.1 Final library sizes for the first 5′cap-seq experiment. 45

Table 2.2.2 Final library sizes for the second 5′cap-seq experiment. 45

Summary

Eukaryotic genomes are organized into chromatin, comprising nucleosomes that wrap DNA around an octamer of canonical histones (H2A, H2B, H3, and H4). The SWR1 complex (SWR1C) is responsible for H2A/H2A.Z exchange at the +1 nucleosome in yeast. H2A.Z-containing nucleosomes are less stable, facilitating disassembly and therefore RNA polymerase II (RNAPII) access during transcription initiation. In *Saccharomyces cerevisiae*, Isw1 and Chd1 chromatin remodelers space nucleosomes into organized arrays. Isw1 acts as the ATPase subunit of Isw1a (Isw1/Ioc3) and Isw1b (Isw1/Ioc2/Ioc4) complexes, which differ in their subunit composition. Loss of Isw1, combined with *CHD1* deletion, enhances cryptic intragenic transcription. However, the specific roles of Isw1, Chd1, and ISW1a in controlling cryptic transcription remain unexplored.

Herein, I used RNA-seq and 5′cap-seq to dissect the extent of the cryptic phenotype in the *isw1Δ chd1Δ* double mutant and to determine the individual contributions of CHD1 and ISW1a to cryptic transcription. Then I integrated ChIP-seq data with my transcriptomic data, and used multiplexed RT-qPCR, CUT&RUN, and ChIP-qPCR experiments to elucidate the mechanism through which ISW1a prevents cryptic transcription in yeast.

Deleting both Isw1 and Chd1 resulted in a significant increase in cryptic transcription, with 35% of yeast genes exhibiting elevated antisense RNA (asRNA) expression and 698 genes showing increased sense transcription. I identified 1918 antisense RNAs in the *isw1Δ chd1Δ* double mutant, most of which were capped and polyadenylated. Longer genes were particularly susceptible to harboring these cryptic transcripts. ISW1a and CHD1 exhibited distinct and complementary roles in suppressing antisense transcription. I uncovered that CHD1 primarily represses antisense transcription at 3′ ends of genes, which initiate near gene transcription end sites, while ISW1a suppresses antisense transcription initiation at 5′ ends of genes. Additionally, I uncovered a potential role for ISW1a in preventing divergent

transcription from intergenic regions, including the production of the nuclear exosome-degraded cryptic unstable transcripts. Furthermore, I found that the ISW1a and CHD1 impact sense transcription differently. ISW1a suppresses sense transcription initiation at intragenic regions, preventing accumulation of cryptic transcripts in the mid-to-end regions of genes. CHD1 represses both intragenic and gene promoters, thus affecting cryptic and mRNA transcription. In all remodeler mutants, derepressed antisense transcription was enriched in genes related to transmembrane transport, while derepressed sense transcription was associated with genes involved in sporulation, highlighting the critical dependence of these genes on chromatin structure for transcription fidelity.

The work I present here shows an association between changes in chromatin composition and cryptic transcription in *isw1Δ* and *ioc3Δ* cells, as increased levels of H2A.Z overlapped with the start of cryptic transcripts. Additional deletion of *HTZ1* (yeast H2A.Z) suppressed antisense transcription in these mutants, highlighting the importance of H2A.Z in cryptic transcription initiation. A similar suppression of antisense transcription was observed in a *swr1Δ* background, particularly in *isw1Δ* cells, suggesting that SWR1C may be needed for H2A.Z incorporation at the start of antisense transcripts. CUT&RUN experiments targeting Flag-tagged Ioc3 confirmed previous findings, demonstrating Ioc3 recruitment to gene boundaries in wild-type yeast. Earlier *in vitro* findings from our lab found that ISW1a preferentially binds to H2A.Z-containing nucleosomes and slides them faster than H2A-containing nucleosomes. My follow-up ChIP-qPCR experiments support this observation, as they showed diminished Ioc3 occupancy at the start of genes upon *HTZ1* deletion, indicating that H2A.Z may partially contribute to ISW1a recruitment to these regions *in vivo*.

I propose a mechanism where loss of ISW1a destabilizes chromatin particularly at the 5′ end of genes, exposing DNA stretches that may attract SWR1C, leading to intragenic H2A.Z incorporation in these regions. This weakens histone-DNA contacts, facilitating RNAPII-mediated cryptic transcription. Together, my findings provide novel insights into the distinct yet cooperative roles of ISW1a and CHD1 in preserving transcription fidelity.

Zusammenfassung

Eukaryotische Genome sind in Chromatin organisiert, das aus Nukleosomen besteht, die DNA um ein Oktamer aus kanonischen Histonen (H2A, H2B, H3 und H4) wickeln. Der SWR1-Komplex (SWR1C) ist für den Austausch von H2A gegen H2A.Z im +1-Nukleosom in Hefe verantwortlich. H2A.Z-haltige Nukleosomen sind weniger stabil, was die Disassemblierung erleichtert und somit der RNA-Polymerase II (RNAPII) während der Transkriptionsinitiation Zugang verschafft. In Saccharomyces cerevisiae positionieren die Chromatin-Remodeler Isw1 und Chd1 die Nukleosomen in geordneten Arrays. Isw1 fungiert als ATPase-Untereinheit der Isw1a (Isw1/Ioc3) und Isw1b (Isw1/Ioc2/Ioc4) Komplexe, die sich in ihrer Untereinheitenzusammensetzung unterscheiden. Der Verlust von Isw1, kombiniert mit der Deletion von CHD1, verstärkt die kryptische, intragene Transkription. Die spezifischen Rollen von Isw1, Chd1 und ISW1a bei der Kontrolle kryptischer Transkription sind jedoch noch unerforscht.

In dieser Arbeit habe ich RNA-seq und 5′cap-seq eingesetzt, um das Ausmaß des kryptischen Phänotyps in *isw1Δ chd1Δ* Doppelmutanten zu untersuchen und die individuellen Beiträge von CHD1 und ISW1a zur kryptischen Transkription zu bestimmen. Anschließend habe ich ChIP-seq-Daten mit meinen Transkriptomdaten integriert und Multiplex RT-qPCR, CUT&RUN sowie ChIP-qPCR Experimente durchgeführt, um den Mechanismus zu klären, durch den ISW1a die kryptische Transkription in Hefe verhindert.

Die Deletion von Isw1 und Chd1 führte zu einem signifikanten Anstieg kryptischer Transkription, wobei 35 % der Hefegene eine erhöhte Expression von antisense RNAs (asRNA) und 698 Gene eine erhöhte sense-Transkription zeigten. Ich identifizierte 1918 antisense-RNAs in der *isw1Δ chd1Δ* Doppelmutante, die überwiegend gekappt und poly-adenyliert waren. Längere Gene waren besonders anfällig für das Auftreten dieser kryptischen Transkripte. ISW1a und CHD1 zeigten unterschiedliche, sich jedoch ergänzende Rollen bei der Unterdrückung der

antisense Transkription. Ich konnte zeigen, dass CHD1 antisense-Transkription hauptsächlich an den 3′-Enden von Genen unterdrückt, die in der Nähe der Transkriptions-Endstellen initiieren, während ISW1a die Initiation der antisense-Transkription an den 5′-Enden der Gene verhindert. Darüber hinaus entdeckte ich eine potenzielle Rolle von ISW1a bei der Verhinderung divergenter Transkription in intergenen Regionen, einschließlich der Produktion nuklearer Exosom-abgebauter kryptisch instabiler Transkripte.

Zusätzlich fand ich heraus, dass ISW1a und CHD1 die sense-Transkription unterschiedlich beeinflussen. ISW1a unterdrückt die Initiation von sense-Transkription in intragenen Regionen und verhindert so die Ansammlung kryptischer Transkripte in den mittleren bis endständigen Regionen von Genen. CHD1 unterdrückt sowohl intragene als auch Genpromotoren, was sich auf kryptische und mRNA-Transkription auswirkt. In allen Remodeler-Mutanten war deregulierte antisense Transkription in Genen angereichert, die mit dem transmembranen Transport assoziiert sind, während deregulierte sense-Transkription mit Genen der Sporulation verbunden war, was die entscheidende Abhängigkeit dieser Gene von der Chromatinstruktur für eine korrekte Transkriptionsregulation unterstreicht.

Die hier vorgestellten Arbeiten zeigen einen Zusammenhang zwischen Änderungen in der Chromatin-Zusammensetzung und kryptischer Transkription in *isw1Δ* und *ioc3Δ* Zellen, da erhöhte H2A.Z-Werte mit dem Beginn kryptischer Transkripte überlappten. Die zusätzliche Deletion von *HTZ1* (Hefe-H2A.Z) unterdrückte die antisense-Transkription in diesen Mutanten und hob die Bedeutung von H2A.Z bei der Initiation kryptischer Transkription hervor. Eine ähnliche Unterdrückung der antisense-Transkription wurde in einem *swr1Δ* Hintergrund beobachtet, insbesondere in *isw1Δ*-Zellen, was darauf hindeutet, dass SWR1C für die H2A.Z-Inkorporation am Beginn kryptischer Transkripte erforderlich sein könnte. CUT&RUN-Experimente mit Flag-markiertem Ioc3 bestätigten frühere Ergebnisse und zeigten die Rekrutierung von Ioc3 an Gen-Grenzen in Wildtyp-Hefe. Frühere *in vitro* Ergebnisse aus unserem Labor zeigten, dass ISW1a bevorzugt an

H2A.Z-haltige Nukleosomen bindet und diese schneller verschiebt als H2A-haltige Nukleosomen. Meine anschließenden ChIP-qPCR Experimente stützen diese Beobachtung, da sie eine verringerte Ioc3 Besetzung am Beginn von Genen nach der Deletion von *HTZ1* zeigten, was darauf hindeutet, dass H2A.Z teilweise zur Rekrutierung von ISW1a an diese Regionen *in vivo* beiträgt.

Ich schlage einen Mechanismus vor, bei dem der Verlust von ISW1a das Chromatin insbesondere am 5′-Ende von Genen destabilisiert und DNA-Bereiche freilegt, die SWR1C anziehen könnten, was zu einer intragenen H2A.Z-Inkorporation in diesen Regionen führt. Dies schwächt die Histon-DNA-Kontakte und erleichtert die kryptische Transkription durch RNAPII. Insgesamt liefern meine Ergebnisse neue Einblicke in die unterschiedlichen, aber kooperativen Rollen von ISW1a und CHD1 bei der Erhaltung der Transkriptionsgenauigkeit.

1 Introduction

1.1 The basics of chromatin

Genetic information is stored within DNA, which can stretch up to approximately two meters in humans (Piovesan, Pelleri et al. 2019). To overcome the large genome-to-nucleus size ratio, eukaryotes have the ability to fit large DNA molecules into the nuclei of microscopic cells by compacting the DNA into higher-order chromatin structures, such as chromosomes (Thelen, Defourny et al. 2021).

The nucleosome is the basic unit of chromatin, consisting of approximately 147 bps of DNA wrapped around a histone octamer (two histone H2A-H2B dimers and one core histone H3-H4 tetramer) (Jiang and Pugh 2009). The wrapping of DNA around the histone octamer occurs through electrostatic interactions and hydrogen bonds formed between histones and the phosphate oxygen of the DNA (White, Suto et al. 2001). The primary chromatin structure, also known as beads-on-a-string, consists of an array of spaced nucleosomes (Jiang and Pugh 2009). The linker DNA between the nucleosome cores is associated with the linker histone H1. Although histone H1 is not a component of the histone octamer, it facilitates nucleosome stability by binding to DNA at the entry and exit sites of the nucleosome, and it is associated with higher nucleosome compaction structures (Kalashnikova, Rogge et al. 2016) (Ricci, Manzo et al. 2015).

In higher eukaryotes, chromatin morphologies are typically classified into two states: euchromatin and heterochromatin, wherein the former is less compacted and generally more transcriptionally active, and the latter is more compacted and often transcriptionally inactive (Bassett, Cooper et al. 2009). The beads-on-a-string structure is an example of euchromatin, while higher-order structures form heterochromatin. A hierarchical chromatin organization model points to the presence of ordered higher-order structures, including secondary structures, formed by interactions between nucleosomes (i.e. 30 nm chromatin fiber), which in

turn can interact with themselves leading to tertiary structures (Woodcock and Dimitrov 2001). However, a number of *in vivo* imaging studies have questioned this traditional model of hierarchical chromatin organization, particularly the existence of a 30-nm fiber (Ricci, Manzo et al. 2015). A more flexible model for chromatin fibre organization *in vivo* has been proposed, wherein nucleosomes form "clutches" of different sizes and densities which are spaced by longer linker DNA (Ricci, Manzo et al. 2015).

Importantly, chromatin structure can be affected by DNA properties and by a series of factors that delineate DNA accessibility during vital biological processes that take place in the nucleus, such as gene expression. The next subchapter delves deeper into how nucleosomes are arranged within genes.

1.2 Nucleosome arrangement within genes

In the promoter region of genes lies a particularly longer stretch of linker DNA, known as the nucleosome depleted region (NDR). In budding yeast, NDRs are enriched in homopolymeric stretches of deoxyadenosine nucleotides known as poly(dA:dT) sequences, which inherently disfavor nucleosome formation (Baldi, Korber et al. 2020).

Flanking the NDR are two nucleosomes: the + 1 nucleosome is downstream the NDR and covers the transcription start site (TSS) while the -1 nucleosome is situated upstream of the NDR. Rather than the canonical histone H2A, the +1 nucleosome contains the histone variant H2A.Z, as well as other histone tail modifications that contribute to the disruption of the octamer (Topal, Vasseur et al. 2019, Li, Wei et al. 2023). Previous research has suggested that the -1 nucleosome is actually a +1 nucleosome of a divergent gene or upstream non-coding RNA due to the bidirectional nature of promoters (Bagchi, Battenhouse et al. 2020).

The 5′ end of genes is characterized by well-positioned and regularly spaced nucleosomes. This chromatin structure has been re-established *in vitro* by adding important chromatin factors, in the absence of transcription (Krietenstein, Wal et al. 2016). The 3′ of genes, however, displays a fuzzy nucleosome distribution. The

fuzziness observed could be attributed to the less conserved arrangement of nucleosomes within these regions, which may suggest that the start of genes relies on more functional pressures on chromatin organization (Jiang and Pugh 2009). Following the terminal nucleosome at the 3′ end, there is a 3′ NDR where transcription termination takes place (Jiang and Pugh 2009).

Nucleosomes can hide DNA regulatory elements crucial for the recruitment of transcription machinery components. On the other hand, chromatin structure needs to be rapidly re-established to ensure transcription fidelity. Therefore, chromatin structure undergoes continuous modulation through mechanisms such as nucleosome sliding, nucleosome assembly/disassembly, histone replacement, and histone tail modifications. Chromatin remodelers are some of the key players involved in chromatin organization along genes, together with histone chaperones and other histone modifying enzymes.

1.3 Chromatin remodelers

Chromatin remodelers consist of a catalytic subunit that may interact with additional subunits to form complexes, or act as a monomer (Eustermann, Patel et al. 2023). Additional subunits typically target the complexes to specific genomic regions by recognizing particular features of DNA sequences or nucleosomes.

In eukaryotes, chromatin remodelers are classified into four distinct families: SWI/SNF, INO80, ISWI, and CHD (Eustermann, Patel et al. 2023). Regardless of the family, the catalytic subunits contain a similar Snf2-type ATPase domain consisting of two RecA domains, RecA1 and RecA2, resulting in a two-lobed structure (Eustermann, Patel et al. 2023). Different ATPases are distinguished by their amino-terminal or carboxyl-terminal regions, which can bear unique domains that are often responsible for interacting with nucleosomes and additional subunits (Figure 1.3.1) (Eustermann, Patel et al. 2023).

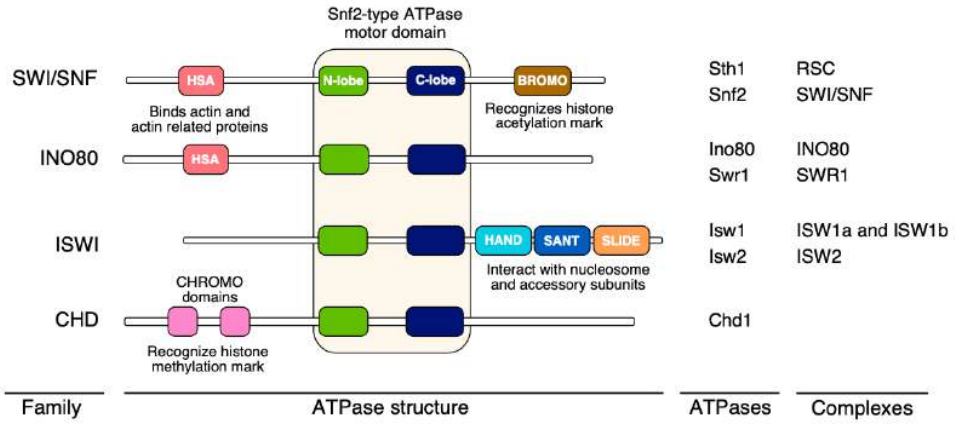

Figure 1.3.1 Overview of chromatin remodeling families, their ATPase domains, as well as the existing ATPases and the complexes these belong in *Saccharomyces cerevisiae.* The ATPase motor domain forms a two lobed structure (N-lobe, C-lobe). Family specific domains include helicase–SANT-associated (HSA) domain, bromodomain (BROMO), tandem chromodomains, and HSS domain (HAND, SANT, and SLIDE).

Chromatin remodelers use the energy of ATP hydrolysis to translocate DNA, which can lead to various outcomes (Table 1.3.1). Successive transitions between chromatin-bound and chromatin-free states of the ATPase disrupt histone-DNA contacts and induce DNA translocation by creating a 1 bp bulge (Reyes, Marcum et al. 2021). Remodelers exhibit notably short chromatin-bound times, typically ranging from 4 to 7 seconds (Kim, Visanpattanasin et al. 2021). Transient interactions with chromatin are a common feature of remodeling complexes which may challenge the study of their recruitment *in vivo* (Kim, Visanpattanasin et al. 2021).

Table 1.3.1 Chromatin remodelers in *S. cerevisiae*: genomic localization, recruitment factors, and functional outcomes.

Family	Complexes	Localization	Recruitment	Outcome	Ref.
SWI/SNF (switch/sucrose non-fermentable)	RSC	NDRs; 5′ end and -1 nucleosomes	Poly(dA:dT) sequences; histone acetylation	Nucleosome eviction or sliding away from NDR	(Yen, Vinayachandran et al. 2012, Singh and Mueller-Planitz 2021, Eustermann, Patel et al. 2023)
	SWI/SNF	NDRs; 5′ end and -2 nucleosomes	Histone acetylation	Nucleosome eviction or sliding away from NDR	(Yen, Vinayachandran et al. 2012, Singh and Mueller-Planitz 2021, Eustermann, Patel et al. 2023)
INO80 (Inositol requiring 80)	INO80	NDRs; -1 nucleosome	Longer DNA stretches	+1 nucleosome positioning; nucleosome spacing; H2A.Z/H2A exchange; nucleosome eviction	(Yen, Vinayachandran et al. 2012, Yen, Vinayachandran et al. 2013, Singh and Mueller-Planitz 2021, Eustermann, Patel et al. 2023)
	SWR1	NDRs; +1 nucleosome	Longer DNA stretches; histone acetylation	H2A/H2A.Z exchange	(Clapier, Iwasa et al. 2017, Singh and Mueller-Planitz 2021, Eustermann, Patel et al. 2023)
ISWI (Imitation switch)	ISW2	NDRs, centromeres, +1 nucleosome	Poly(dA:dT) sequences; transcription factor Ume6	+1 nucleosome positioning	(Goldmark, Fazzio et al. 2000, Yen, Vinayachandran et al. 2012, Zentner, Tsukiyama et al. 2013, Eustermann, Patel et al. 2023)
	ISW1a	NDRs; Ends of genes; +1 and terminal nucleosomes	Unknown	+1 nucleosome positioning; nucleosome spacing	(Smolle, Venkatesh et al. 2012, Yen, Vinayachandran et al. 2012, Zentner, Tsukiyama et al. 2013, Singh and Mueller-

					Planitz 2021, Eustermann, Patel et al. 2023)
	ISW1b	Mid-3′ end of genes; 5′ end and -1 nucleosomes	H3K36me3	Regularly spaced nucleosome arrays	(Smolle, Venkatesh et al. 2012, Yen, Vinayachandran et al. 2012, Li, Bergmann et al. 2022)
CHD (Chromodomain-Helicase-DNA binding)	CHD1	NDRs; gene bodies	Paf1 complex; poly(dA:dT) sequences	Regularly spaced nucleosome arrays	(Zentner, Tsukiyama et al. 2013, Park, Shivram et al. 2014, Lee, Park et al. 2017, Eustermann, Patel et al. 2023)

1.4 The coordinated action of chromatin factors regulates transcriptional chromatin dynamics

The coordinated action between chromatin remodelers and other factors modulates chromatin changes during gene expression, inevitably contributing to transcription fidelity. Chromatin remodelers RSC and SWI/SNF are involved in NDR formation through the disassembly of nucleosomes from the promoter region, as well as by pushing the +1 and -1 nucleosomes away from each other (Kubik, Bruzzone et al. 2019, Eustermann, Patel et al. 2023). This facilitates the binding of essential TATA-box-binding protein (TBP), transcription factors and RNAPII, allowing for the assembly of the pre-initiation complex (PIC) (Kubik, O'Duibhir et al. 2018). While RSC and SWI/SNF push the +1 nucleosome away from the NDR, INO80, ISW2, and ISW1a chromatin remodelers shift it towards the NDR, resulting in a tight regulation of the +1 nucleosome positioning (Eustermann, Patel et al. 2023).

General regulatory factors such as Reb1, Abf1, and Rap1 have also been implicated in NDR formation. Reb1 and Abf1 act as barriers to nucleosome mobility, preventing the repositioning of nucleosomes and maintaining the promoter region free for recruitment of subsequent transcriptional machinery (Oberbeckmann, Niebauer et al. 2021, Chen, Kharerin et al. 2022). Rap1 not only disrupts local

higher-order chromatin structure but also guides nucleosome rearrangements with a defined directionality, thereby regulating gene expression and repression of divergent transcription (Kubik, O'Duibhir et al. 2018, Wu, Patel et al. 2018, Mivelaz, Cao et al. 2020).

Another promoter-prevalent chromatin feature is histone turnover, meaning the replacement of "old" histones by soluble histones. Histone turnover is particularly high at active promoters and repressed within the gene body (Ferrari and Strubin 2015). Histone chaperones participate in the process of histone turnover by facilitating either the assembly or disassembly of nucleosomes (Ferrari and Strubin 2015). For example, the histone chaperone complex FACT (Facilitates Chromatin Transcription) destabilizes nucleosomes at promoter regions, facilitating the passage of RNAPII through chromatin (Gurova, Chang et al. 2018). With the help of the chromatin remodeler Chd1, FACT extends its influence to downstream nucleosomes where it facilitates nucleosome assembly after RNAPII passage, maintaining chromatin integrity throughout the elongation process (Gurova, Chang et al. 2018, Jeronimo, Angel et al. 2021). Other histone chaperones cooperate with histone acetyltransferase Rtt109 to incorporate “new” acetylated histones, contributing to higher histone turnover and acetylation, weakening DNA-histone contacts (Tsubota, Berndsen et al. 2007, Topal, Vasseur et al. 2019).

As before-mentioned, actively transcribed genes are further characterized by a H2A.Z-containing nucleosome marking the TSS. So far, SWR1 remodeling complex seems to be the sole responsible for the incorporation of the histone variant H2A.Z at the +1 nucleosome (Eustermann, Patel et al. 2023). H2A.Z-containing nucleosomes are generally more unstable than canonical H2A-containing nucleosomes. This increased instability facilitates the disassembly of the nucleosome during transcription initiation (Li, Wei et al. 2023).

The ISW1 and CHD1 chromatin remodelers maintain regularly spaced nucleosomes and prevent histone turnover within the gene body (Smolle, Venkatesh et al. 2012, Kubik, Bruzzone et al. 2019, Eustermann, Patel et al. 2023). Research suggests CHD1 governs shorter spacing while ISW1 activity results in longer spacing (Ocampo, Chereji et al. 2016). Additionally, ISW1 and CHD1 remodelers

have been implicated in dinucleosome resolution, a process that likely occurs due to nucleosome collisions post-RNAPII passage (Eustermann, Patel et al. 2023).

During transcription elongation, critical pathways involving histone modifying enzymes contribute to the maintenance of chromatin structure. Phosphorylated serine 5 (S5P) of the C-terminal domain (CTD) of RNAPII recruits the Set1 methyltransferase, which methylates histone H3 at lysine 4 over the 5′ transcribed regions (Kim and Buratowski 2009). Subsequently, the histone deacetylase Set3 recognizes the H3K4me2 mark, deposited by Set1, and initiates the removal of acetylation marks. This process allows for the rapid regeneration of chromatin over the 5′ regions of genes following RNAPII passage. A similar pathway operates at the 3′ end of genes, where phosphorylated serine 2 (S2P) of RNAPII CTD recruits the methyltransferase Set2, whose H3K36me2 marks recruit the Rpd3S histone deacetylase complex (Figure 1.4.1) (Woo, Dam Ha et al. 2017). In the absence of some of these factors, chromatin fails to re-establish its structure after RNAPII passage. This failure can result in the exposure of intragenic promoters that can lead to the accumulation of cryptic transcripts (Venkatesh, Li et al. 2016).

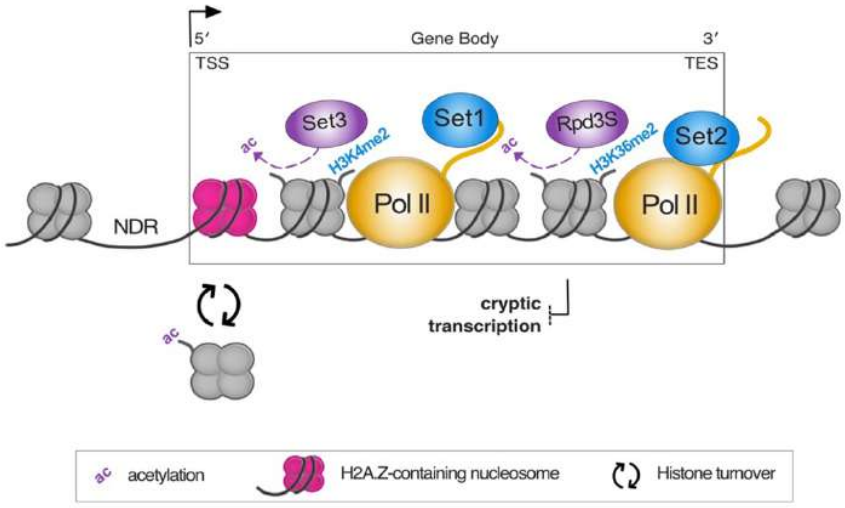

Figure 1.4.1 Simplified overview of the chromatin dynamics taking place over genic regions during transcription. The 5′ and 3′ NDRs are indicated. Surrounding active promoter regions, there is higher histone turnover and incorporation of acetylated histones. The first nucleosome of the gene body usually contains histone variant H2A.Z instead of H2A. The Set1/Set3 pathway maintains chromatin structure at the 5′ ends of genes while the Set2/Rpd3S pathway acts similarly at the 3′ end.

1.5 Cryptic transcription

Genomes from yeast to humans express a multitude of non-coding RNAs (ncRNAs) (Mattick, Amaral et al. 2023). Non-coding RNAs can come in different sizes, structures, and a large part of ncRNAs are highly regulatory and crucial for vital biological processes. Among these, are the infrastructure ncRNAs such as transfer RNAs (tRNAs), ribosomal RNAs (rRNAs), small nuclear RNAs (snRNAs), and small nucleolar RNAs (snoRNAs). Small interfering RNAs (siRNAs), microRNAs (miRNAs) and small PIWI-interacting RNAs (piRNAs) are also highly functional in eukaryotes, as these have been reported to negatively affect gene expression (Mattick, Amaral et al. 2023).

Numerous long non-coding RNAs (lncRNAs), whose sequences are less evolutionarily conserved and longer than 200 nucleotides, have been shown to be involved in a multitude of processes (Mattick, Amaral et al. 2023). These lowly transcribed ncRNAs have been associated to cell differentiation and development, cell cycle, cellular adhesion, DNA damage, glucose metabolism, cellular signal transduction, transport pathways, stress response, DNA methylation, phase-separated condensates, and cell membranes (Mattick, Amaral et al. 2023).

Another subset of ncRNAs includes the so-called cryptic transcripts. Cryptic transcripts emerge from DNA sequences that are not canonical promoters. These DNA sequences may become exposed under certain conditions such as chromatin structure changes (Venkatesh, Workman et al. 2013). Like many regulatory lncRNAs, cryptic transcripts are usually also less expressed when compared to mRNA expression levels (Venkatesh, Workman et al. 2013, Mattick, Amaral et al. 2023). While intragenic transcripts overlap with genes either in the same direction (sense) or in the opposite direction (antisense), intergenic transcripts are those that do not overlap with genes. Cryptic transcription often originates from NDRs, but it may also originate from intragenic regions (Venkatesh, Workman et al. 2013). While there are ncRNAs that can be transcribed by RNA polymerase I, II, and III, cryptic transcripts are usually products of RNAPII transcription (Venkatesh, Workman et al. 2013, Mattick, Amaral et al. 2023). Primarily, cryptic RNAs are considered as by-

products of “unintended” transcription, and may be rapidly degraded to prevent interference with cellular processes (Venkatesh, Workman et al. 2013, Li, Liu et al. 2021).

1.5.1 Cryptic transcripts in wild-type yeast

Although wild-type yeast cells produce many capped and polyadenylated cryptic transcripts, these are usually rapidly degraded. Deleting decapping enzymes, nuclear, cytoplasmic 5′ end exonucleases, and other RNA-binding factors that are critical for RNA surveillance pathways enabled researchers to identify and annotate cryptic transcripts (Li, Liu et al. 2021). In particular, disruption of the nuclear exosome by depleting its catalytic component, Rrp6, leads to the production of a group of RNA species called Cryptic Unstable Transcripts (CUTs) (Xu, Wei et al. 2009). Xu et al. have identified 925 CUTs where the vast majority initiates from 5′ and 3′ NDRs that are shared with promoters of protein-coding genes (Xu, Wei et al. 2009). The expression of divergent CUTs has been suggested to promote DNA exposure due to the high correlation between increased gene expression (Vera and Dowell 2016). On the other hand, these transcripts have also been shown to cause transcriptional interference (Vera and Dowell 2016). Deletion of Rrp6 is vastly used in combination with other deletions when studying the role of other factors in the regulation of cryptic transcription.

Despite most cryptic RNAs being unstable and rapidly targeted by termination and nuclear RNA degradation systems, some transcripts are stable in wild-type yeast and some may even exhibit regulatory functions. Stable Unannotated Transcripts (SUTs) represent a subset of RNA species that are only partially susceptible to degradation by the nuclear exosome; instead, SUTs are primarily targeted by cytoplasmic decay pathways (Xu, Wei et al. 2009). Consequently, these transcripts persist for a longer period of time, allowing their detection in wild-type yeast. Interestingly, SUTs have been proposed to act *in trans* for the regulation of target genes. Deletion of certain SUTs results in alterations in gene expression and causes fitness defects (Balarezo-Cisneros, Parker et al. 2021).

In mitotically growing yeast, meiotic gene expression is repressed by non-coding RNAs (Pondugala and Mishra 2022). In haploid cells, the expression of *IME1*, the master regulator of meiosis, is suppressed by the transcription of a ncRNA at the promoter region (Pondugala and Mishra 2022). Another meiotic gene, *IME4*, typically expressed in MATa/MATα heterozygous diploids, is repressed in haploid cells by an overlapping non-coding transcript from the antisense strand (Pondugala and Mishra 2022).

Certain cellular stimuli such as heat can trigger the accumulation of intragenic transcripts (Kim, Liu et al. 2010). Stress-responsive genes have been associated with higher sense and antisense cryptic transcription (Kim, Liu et al. 2010, Garcia-Martinez, Ayala et al. 2012). Upon stress, RNAPII accumulation at the 3′ end of genes increases significantly, as does the initiation mark H3K4me3, and overlapping non-coding transcripts like CUTs and SUTs (Kim, Liu et al. 2010). It is possible that the accumulation of cryptic RNAs in cells under stress comes from changes in the response of factors of RNA degradation pathways. Importantly, as newer methodologies are employed to study previously identified cryptic transcripts, their potential regulatory role and fate are being gradually unveiled.

1.5.2 Maintenance of chromatin structure prevents cryptic events

Chromatin regulators can be recruited onto genes during transcription elongation, either by RNAPII or other mechanisms. Impairing chromatin regulators such as histone chaperones, methyltransferases, and chromatin remodelers can lead to defects in chromatin, resulting in the exposure of intragenic cryptic promoters (Smolle, Venkatesh et al. 2012, Venkatesh, Li et al. 2016, Viktorovskaya, Chuang et al. 2021, Jeronimo and Robert 2022).

The cryptic transcriptional phenotype associated with cells disrupted for FACT histone chaperone has been demonstrated from yeast to mammals (Jeronimo and Robert 2022). Moreover, FACT impairment also triggers the incorporation of H2A.Z at intragenic regions, potentially facilitating the initiation of cryptic transcripts (Jeronimo, Watanabe et al. 2015). Mutations compromising the full functionality of

the Spt6, another histone chaperone, result in numerous intragenic TSSs appearing on both sense and antisense strands of genes, with a preference for the 5′ ends of genes in the induced antisense TSSs (Viktorovskaya, Chuang et al. 2021). Furthermore, the antisense TSS-seq signal in Spt6-deficient cells exhibited a strong correlation with the wild-type positions of the +1, +2, and +3, indicating a potential link between these nucleosomes and antisense transcription (Viktorovskaya, Chuang et al. 2021).

The Set2/Rpd3S pathway has been shown to suppress cryptic transcription (Venkatesh, Li et al. 2016). Antisense transcripts annotated in yeast lacking the Set2 histone methyltransferase are referred to as SRATs (Set2-repressed antisense transcripts) and were found to cover 11% of the yeast genome without causing transcriptional interference (Venkatesh, Li et al. 2016). Set2-mediated H3K36me3 is crucial for concealing cryptic promoters, as these transcripts originate from the intragenic regions where H3K36me3 is deposited during mRNA transcription (Venkatesh, Li et al. 2016).

Interestingly, research suggests that Isw1 and Chd1 suppress cryptic transcription in cooperation with Set2 by preventing histone turnover at mid-3′ end of genes (Smolle, Venkatesh et al. 2012). However, the extent of individual contributions from Isw1 complexes and Chd1 remain to be elucidated. While RNA surveillance factors control the accumulation levels of cryptic transcripts, it appears that chromatin regulators primarily act to prevent their initiation.

1.6 Isw1 remodeling complexes in yeast

1.6.1 Isw1 ATPase and its complexes

In yeast, there are two ISWI proteins: Isw1 and Isw2 (Tsukiyama, Palmer et al. 1999). Likewise, mammals also have two ISWI proteins: SNF2L and SNF2H, encoded by the *SMARCA1* and *SMARCA5* genes, respectively, which show approximately 65% similarity to their counterparts in yeast (Lazzaro and Picketts 2001). These ATPases interact with distinct additional subunits to form complexes that are recruited to different genomic regions. The yeast ISWI ATPases contain two regulatory domains

flanking its motor domain: AutoN and NegC. The N-terminal autoinhibitory region, AutoN, negatively regulates ATP hydrolysis and can be relieved by interactions with the basic patch of the histone H4 tail. The NegC domain inhibits the coupling of ATP hydrolysis to DNA translocation and can be relieved by the HSS domain binding to extranucleosomal DNA (Clapier and Cairns 2012, Eustermann, Patel et al. 2023). Together, these domains control the catalytic activity of ISWI proteins.

In this study, the emphasis is on Isw1 remodelers. Isw1 can interact with Ioc3 to form the ISW1a complex (Figure 1.6.1) (Vary, Gangaraju et al. 2003). Alternatively, it can interact with both Ioc4 and Ioc2, leading to the formation of the ISW1b complex (Figure 1.6.1) (Vary, Gangaraju et al. 2003). Loss of any Ioc subunit prevents complex formation (Vary, Gangaraju et al. 2003). Additionally, Isw1 has been previously co-purified with Esc8, suggesting the existence of a third Isw1 complex in yeast (Cuperus and Shore 2002). Unpublished Isw1-TAP purification and mass spectrometry data from our lab further supports the existence of an Isw1/Esc8 complex, which we designate as Isw1c. *In vitro* studies from our lab have started, to our knowledge, the characterization of the remodeling functions of Isw1c complex, showing that it can hydrolyze ATP to slide nucleosomes, preferably those containing acetylated histone H4 at lysine residues K5,8, and 12.

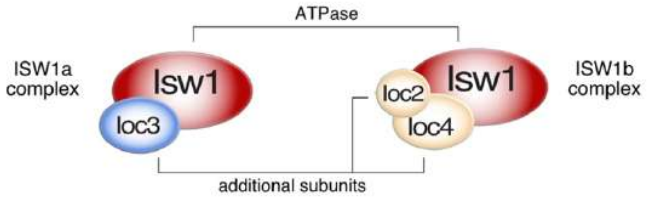

Figure 1.6.1 Subunit composition of the two most studied Isw1 remodeling complexes in *S. cerevisiae*: ISW1a and ISW1b. Ioc3 interacts with Isw1 to form ISW1a while both Ioc2 and Ioc4 subunits interact with Isw1 to form ISW1b complex.

The HAND-SANT-SLIDE (HSS) domain, located in the C-terminal end of Isw1 (Figure 1.3.1), has been reported to interact with the Ioc subunits of Isw1 complexes, ISW1a and ISW1b, and to facilitate interaction with DNA and nucleosomes (Pinskaya, Nair et al. 2009, Shen, Beyrouthy et al. 2017). The SANT

and SLIDE domains not only allow optimal Isw1-chromatin interaction, but are also responsible for Isw1 interactions with both Ioc2 and Ioc4 (Pinskaya, Nair et al. 2009). Ioc3 interacts with the SLIDE domain of Isw1 and multiple SUMOylation residues caused by the Siz1/Siz2 SUMO E3 ligases over the HSS domain stabilize the Isw1a complex *in vivo* (Pinskaya, Nair et al. 2009, Yamada, Frouws et al. 2011, Shen, Beyrouthy et al. 2017). Additionally, the HSS domain promotes ISW1a ability to bind to DNA and nucleosomes (Reyes, Marcum et al. 2021).

Isw1 remodeling activities have been implicated in essential biological processes such as DNA replication, DNA repair, transcription, and mRNA maturation (Smolle, Venkatesh et al. 2012, Aydin, Vermeulen et al. 2014, Babour, Shen et al. 2016, Bellush and Whitehouse 2017). Like other chromatin remodelers, Isw1 remodelers have also been associated with neurodegenerative diseases as well as cancer (Goodwin and Picketts 2018, Li, Gong et al. 2021). In particular, *SMARCA1* gene has been associated to schizophrenia spectrum disorders (Goodwin and Picketts 2018). In yeast, Isw1 has been reported to be involved in preserving genomic stability. Changes in the length of trinucleotide repeats (TNRs) have been linked to various heritable neurodegenerative diseases, such as Huntington's disease and ataxia (Koch, House et al. 2018). ISWI remodelers may play a role in preventing the expansions of TNRs since yeast Isw1 ATPase was observed to prevent CAG repeat expansions during transcription elongation (Koch, House et al. 2018). While Isw1 remodelers participate in numerous biological processes, the central focus of this study revolves around their involvement in transcription regulation.

1.6.2 Importance of Isw1 complexes in chromatin remodeling

Both ISW1a and ISW1b are considered spacers, as these remodelers can determine the distance between intragenic nucleosomes (Kubik, Bruzzone et al. 2019). The contributions of Isw1 remodelers in modulating chromatin structure have been investigated both *in vitro* and *in vivo*. *In vitro* studies show that ISW1a contributes to the positioning of the +1 nucleosome and the establishment of NDRs

and regular nucleosome arrays (Krietenstein, Wal et al. 2016). Both ISW1a and ISW1b regulate nucleosome positioning downstream of the TSS (Yen, Vinayachandran et al. 2012, Bhardwaj, Hailu et al. 2020). While ISW1a complex promotes nucleosome shifting in the 5′ direction, ISW1b shifts nucleosomes in the 3′ direction (Yen, Vinayachandran et al. 2012, Bhardwaj, Hailu et al. 2020).

ISW1b has been proposed to be the major contributor for nucleosome spacing and dinucleosome resolving *in vivo* downstream of 5′ NDRs, compared to ISW1a (Eriksson and Clark 2021). However, a more recent study revealed that in the absence of ISW1a, nucleosome positioning downstream of the TSS was significantly altered over thousands of genes, particularly at the +2 and +3 nucleosome positions (Bhardwaj, Hailu et al. 2020). Previously, a tendency for tightly packed nucleosomes at 5′ends of genes was observed in the *isw1Δ chd1Δ* double mutant, highlighting a role in dinucleosome resolution (Ocampo, Chereji et al. 2019). When delving into the individual contributions of the remodelers regarding dinucleosome resolution, researchers have identified ISW1b and Chd1 as the main contributors for dinucleosome resolution (Eriksson and Clark 2021).

Loss of Isw1 results in transcription-associated chromatin changes within gene bodies. Specifically, an increase in histone turnover over mid-3′ end regions of longer and infrequently transcribed genes (Smolle, Venkatesh et al. 2012). This effect is primarily ascribed to the absence of the ISW1b complex (Smolle, Venkatesh et al. 2012). Deleting *ISW1* further results in higher levels of transcription-coupled H4 acetylation over the coding regions, weakening histone-DNA contacts (Smolle, Venkatesh et al. 2012).

The occupancy profiles of Isw1 and Chd1 ATPases reveal their presence over the extended linker DNA of NDRs (Zentner, Tsukiyama et al. 2013). Authors linked this binding preference to the role of these remodelers in transcription-coupled nucleosome turnover, given their predominant activity within gene bodies (Zentner, Tsukiyama et al. 2013). On the other hand, a more recent study revealed the lack of Isw1 binding at promoters and a higher signal within the coding regions when compared to other yeast chromatin remodelers (Kubik, Bruzzone et al. 2019).

Moreover, the authors showed a significant correlation between Isw1 and Chd1 occupancies (Kubik, Bruzzone et al. 2019).

Overall, it appears Isw1 remodelers play a crucial role in maintaining a repressive chromatin state during transcription, with their actions exerting diverse effects on nucleosome positioning, spacing, and dictating levels of histone turnover, and acetylation.

1.6.3 The role of Isw1 remodelers in transcription regulation

Morillon et al. observed increased density of engaged RNAPII in Isw1 catalytic mutant beyond the poly(A) site of *GAL10-7* when compared to wild-type yeast (Morillon, Karabetsou et al. 2003). The authors suggested a potential role in transcription termination for Isw1; however, alternative explanations such as antisense transcription were not addressed. Nonetheless, the differences in nascent RNAPII density align with a more recent study where native elongating transcript sequencing (NET-seq) was used to assess the role of multiple chromatin factors in regulating RNAPII levels during transcription (Couvillion, Harlen et al. 2022). The levels of pausing RNAPII were shown to be reduced at the TSSs and increased at poly(A) sites in *isw1Δ* compared to wild-type yeast (Couvillion, Harlen et al. 2022). Although NET-seq is not the most direct method to measure transcriptional differences, differential expression analysis revealed a tendency towards gene derepression in the absence of Isw1 ATPase, with fewer than 100 protein-coding genes differentially expressed (Couvillion, Harlen et al. 2022).

Similarly, microarray expression profiling conducted by Vary *et al.* revealed a modest impact on transcription in *isw1Δ* cells, with 175 genes showing derepression (Vary, Gangaraju et al. 2003). As expected, loss of Ioc3 or Ioc2, subunits of ISW1a and ISW1b respectively, revealed a subtle impact relative to loss of Isw1 ATPase. Vary and colleagues observed a 1.5-fold-change up-regulation of 27 and 23 genes in *ioc3Δ* and *ioc2Δ* mutants, respectively, with only few down-regulated genes (Vary, Gangaraju et al. 2003). In striking contrast, RNA-seq data identified 766 genes differentially expressed in *ioc3Δ* (Bhardwaj, Hailu et al. 2020).

RNA-seq is a more direct strategy to measure transcriptional phenotypes. However, the study contained analytical and experimental limitations including a false discovery rate (FDR) greater than 5%.

The involvement of Isw1 in suppressing cryptic transcription was initially supported by northern blot analysis targeting the 3′ end of a limited number of genes, revealing an accumulation of multiple cryptic transcripts in *isw1Δ* cells and, to a lesser extent, in *ioc4Δ* cells compared to wild-type (Smolle, Venkatesh et al. 2012). It was proposed that ISW1b, recruited to mid-3′ end of genes via H3K36me3, prevents histone turnover during transcription alongside Chd1, thereby preventing the exposure of intragenic cryptic promoters in those regions (Smolle, Venkatesh et al. 2012). However, investigations regarding the involvement of ISW1a in cryptic transcription have not yet been published.

1.6.4 Structure and mechanism of the ISW1a complex

Cryo-EM studies have characterized ISW1a structure and mechanism within a dinucleosome model, suggesting that ISW1a operates by simultaneously interacting with two neighbouring nucleosomes to regulate the length of linker DNA between them (Yamada, Frouws et al. 2011, Li, Chen et al. 2024).

The Ioc3 subunit of ISW1a contains distinct domains which are crucial for its spacing function and for interactions with Isw1 ATPase as well as chromatin (Figure 1.6.2). The Helical-Linker-DNA-Binding (HLB) domain, characterized by alpha-helices, plays a pivotal role in DNA interaction (Yamada, Frouws et al. 2011). Unlike ISW1b, ISW1a exhibits a distinctive preference for binding dinucleosomes over mononucleosomes *in vitro* (Bhardwaj, Hailu et al. 2020). This preference is particularly attributed to the HLB domain of Ioc3 and requires HLB interaction with extranucleosomal DNA (Bhardwaj, Hailu et al. 2020). The HSS-Binding (HSSB) domain, which forms a loop structure, interacts with the corresponding HSS region on the Isw1 ATPase (Yamada, Frouws et al. 2011). This interaction is rigid, contributing to the stability of the complex (Yamada, Frouws et al. 2011). Additionally, the proposed function of the HSS-Ioc3 module is to act as a protein

ruler, binding two DNA segments to establish the spacing between nucleosomes (Yamada, Frouws et al. 2011, Li, Chen et al. 2024). Ioc3 also contains two Coil-Linker-DNA-Binding (CLB) motifs, N-coil and C-coil, which primarily engage with DNA phosphate groups (Yamada, Frouws et al. 2011).

In the dinucleosome model, sensing of a neighboring nucleosome by Ioc3 subunit is likely facilitated by the histone H4 tail, the nucleosome acidic patch and the nucleosomal DNA (Li, Chen et al. 2024). The SANT and SLIDE domains of Isw1 distinctly bind to the DNA minor groove of the internal-linker DNA while the HLB domain of Ioc3 binds to the major groove of the entry DNA (~30 bps) (Yamada, Frouws et al. 2011, Li, Chen et al. 2024). The CLB motifs in Ioc3 have been shown to recognize external-linker DNA, which might contribute to the stability of Ioc3-DNA complex (Yamada, Frouws et al. 2011). The Isw1 ATPase translocates the linker DNA into the nucleosome until the linker DNA is too short to support a stable HSS-Ioc3 binding (Li, Chen et al. 2024).

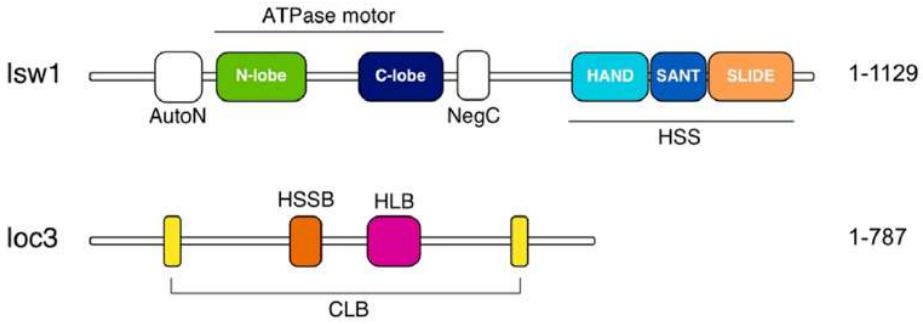

Figure 1.6.2 Schematic representation of domain organization for ISW1a components. The Isw1 catalytic subunit has a total of 1129 amino acids while Ioc3 has 787 amino acids. Isw1 ATPase contains two regulatory domains flanking its motor domain: AutoN and NegC. The C-terminal end of Isw1 harbors the HAND-SANT-SLIDE (HSS) domain, which is crucial for interaction with the Ioc subunits of ISW1a and ISW1b complexes. The Ioc3 subunit features a Helical-Linker-DNA-Binding (HLB) domain and Coil-Linker-DNA-Binding (CLB) motifs for DNA interaction, and an HSS-Binding (HSSB) domain for interaction with the Isw1 catalytic subunit. Further details on the respective domains can be consulted in the main text.

1.6.5 Regulation of ISW1a complex

Previous research has contributed to elucidate the factors that may influence the function of the ISW1a remodeling complex. Studies have revealed contrasting effects between the RSC and ISW1a complexes, particularly at promoter regions (Parnell, Schlichter et al. 2015). While RSC functions to widen the NDR, ISW1a acts in opposition, causing its shrinkage. Poly(dA:dT) tracts are particularly enriched at linker DNA of NDRs and have been reported to stimulate RSC "pusher" activity (Amigo, Raiqueo et al. 2023). However, poly(dA:dT) tracts seem to have the opposite effect for ISW1a complex as these hinder its sliding activity (Amigo, Raiqueo et al. 2023). In agreement, genes exhibiting ISW1a-mediated nucleosome shifts towards the NDR displayed reduced frequencies of poly(dA:dT) tracts within the promoter region (Amigo, Raiqueo et al. 2023). On the other hand, linker histone H1, Hho1, has been shown to impede RSC nucleosome remodeling while stimulating ISW1a sliding activity (Amigo, Farkas et al. 2022). The high mobility group box protein Hmo1, functionally similar to a linker histone H1, also enhances ISW1a activity, further implicating the involvement of linker histones in ISW1a function (Hepp, Alarcon et al. 2014).

Moreover, transcription factors (TFs) have been postulated to potentially modulating ISW1a remodeling activities (Li, Hada et al. 2015). In particular, *in vitro* studies have shown that during ISW1a-mediated remodeling, nucleosomes are positioned relative to promoter-bound TF, Gal4, suggesting the role of TFs as reference points for ISW1a activity (Li, Hada et al. 2015).

As before-mentioned, ISW1a demonstrates a preference for nucleosomes with approximately 30 base pairs of extranucleosomal DNA, further influencing its targeting and activity (Gangaraju and Bartholomew 2007). This binding preference is attributed to the ISW1a accessory subunit Ioc3, as it is the main part of the complex that associates with extranucleosomal DNA. This suggests Ioc3 plays a pivotal role in guiding the complex to specific chromatin regions (Gangaraju and Bartholomew 2007).

1.6.6 Genetic interactions involving ISW1a

Investigating genetic interactions involving ISW1a can provide intriguing insights into its involvement in molecular pathways. A notable observation, as reported by Linstrom et al., is the robust stress dependent synthetic phenotype manifested between Isw1 and the constituent of both the NuA4 histone H4 acetyltransferase and SWR1 complexes, Yaf9 (Lindstrom, Vary et al. 2006). This genetic interaction is attributed to Yaf9 function in the NuA4 complex as well as in the Swr1 complex (Lindstrom, Vary et al. 2006). *In vivo*, NuA4 and SWR1 cooperate to open chromatin at promoters, reflecting a positive role in transcription (Auger, Galarneau et al. 2008). Acetylation by NuA4 is essential for preparing the promoter for chromatin remodeling and transcription activation (Auger, Galarneau et al. 2008). A synthetic phenotype between Ioc3 and Yaf9 under stress conditions suggests that ISW1a may function in parallel with these complexes (Bhardwaj, Hailu et al. 2020). However, because ISW1a is responsible has a repressive effect on chromatin structure at the promoter regions, it is likely that it antagonizes NuA4 and Swr1 actions. Additionally, growth defects in YPD medium and 10 mM caffeine have been observed in preliminary investigations of genetic interactions between components of Isw1 remodeler complexes and Htz1 (Figure 1.6.3 A).

Preliminary data from our lab also showed a synthetic effect between Ioc3 and histone acetyltransferase Set3 under normal conditions, as demonstrated through growth assays and Northern blotting techniques (Figure 1.6.3 B and C). The accumulation of cryptic transcripts detected by northern blot is markedly pronounced in the double mutant *ioc3Δ set3Δ*, raising the question whether ISW1a cooperates with the Set1/Set3 pathway to maintain chromatin structure at the start of genes.

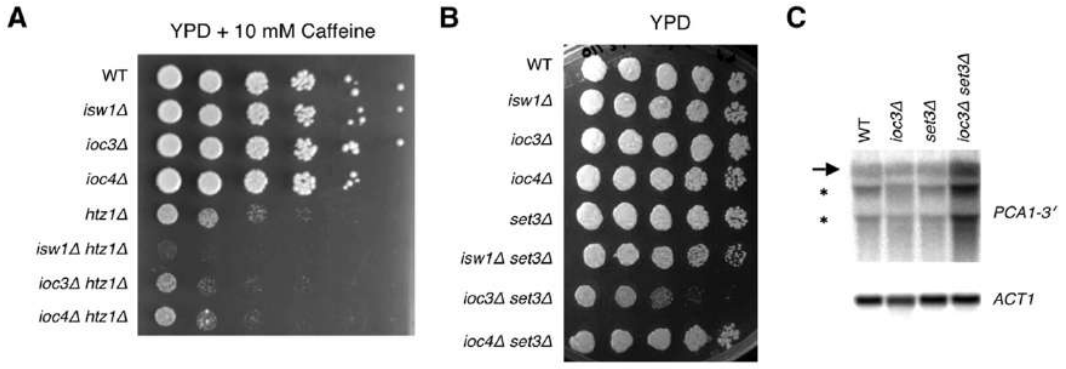

Figure 1.6.3 *IOC3* interacts genetically with histone variant *HTZ1* and *SET3* histone acetyltransferase. (A, B) Spotting assays for Isw1 remodeler mutants with and without *htz1Δ* or *set3Δ* background. Cells were grown until reaching two divisions. Cultures with an initial optical density (OD600) of 0.5 were subjected to 5-fold serial dilutions. Subsequently, these dilutions were spotted onto YPD medium with 10 mM Caffeine (A) or without (B) and incubated at 30°C for a duration of 4 (A) or 2 days (B). (C) Northern blot analysis of *PCA1* transcripts. Northern blot analysis was conducted using RNA isolated from each strain. To target *PCA1* transcripts, probes were directed against the 3′ end. *ACT1* served as a measure of loading control. The full-length (→) and cryptic transcripts (*) are indicated.

1.6.7 Recruitment of ISW1a

Recent work demonstrated that ISW1a localizes to centromeres, hinting at a broader role for ISWI remodelers beyond transcriptional regulation (Litwin, Nowicka et al. 2023). However, the majority of published research highlights ISW1a's occupancy at the ends of genes.

Interactions between Isw1 remodelers and nucleosomes were elucidated through MNase-ChIP-seq, with Ioc3 and Ioc4, revealing specific binding patterns (Yen, Vinayachandran et al. 2012). Notably, Ioc3 exhibited strong binding to +1 and -1 nucleosomes, while Ioc4 displayed an affinity for intragenic nucleosomes (Yen, Vinayachandran et al. 2012). Consequently, Isw1 ATPase-nucleosome interactions were observed throughout gene bodies (Yen, Vinayachandran et al. 2012). ChIP-chip experiments using yeast genomic tiling arrays provided further insights into the genomic occupancy of Ioc3 and Ioc4. Smolle et al. demonstrated that Ioc3 is recruited to regions surrounding the start and end of genes, contrasting with Ioc4's predominant localization within mid-3′ coding regions (Smolle, Venkatesh et al.

2012). Moreover, Ioc4's recruitment to gene coding regions was found to depend on the Set2 methyltransferase. Indeed, Ioc4 exhibits a preference for binding trimethylated H3K36 nucleosomes, and deletion of *SET2* disrupts Ioc4 localization to coding regions (Smolle, Venkatesh et al. 2012, Li, Bergmann et al. 2022).

Previous work from our lab, such as *in vitro* binding assays have provided compelling evidence confirming ISW1a's preference for H2A.Z-containing mononucleosomes (Bergmann 2021). Furthermore, our lab has also revealed that ISW1a selectively binds H2A.Z-containing nucleosomes over canonical H2A-containing ones, and repositions H2A.Z-containing nucleosomes faster when compared to canonical nucleosomes (Bergmann 2021). The specificity of ISW1a's interaction with H2A.Z-containing nucleosomes is attributed to the Ioc3 subunit, as evidenced by *in vitro* studies where ISW1b's binding affinity for the different nucleosome substrates remains unchanged (Bergmann 2021). Interestingly, experiments with Ioc3 constructs suggest that the N-terminal region of Ioc3 is crucial for mediating ISW1a's preference for H2A.Z-containing nucleosomes (Bergmann 2021). Consequently, it is plausible to propose that the presence of H2A.Z, commonly incorporated at the +1 nucleosome, might influence ISW1a's recruitment to the start of genes.

Overall, distinct experimental approaches have revealed that Isw1 remodelers occupy different regions of genes: while ISW1a targets the ends of genes, ISW1b is recruited to the coding regions. However, the precise mechanisms underlying ISW1a the *in vivo* recruitment onto chromatin remain elusive.

1.6.8 Role of ISW1a Complex in Transcriptional Fidelity

While the role of ISW1b in suppressing cryptic transcription at the mid-3′ end of genes has been previously documented, the involvement of ISW1a in this process remains unexplored. Unpublished preliminary findings from northern blot analysis suggest that ISW1a may also play a role in preventing the accumulation of intragenic cryptic transcripts (Figure 1.6.4 A). Given the overlapping functions of Isw1 and Chd1 within gene bodies, cryptic transcription levels were assessed in

cells with a *chd1Δ* background. Further investigations are needed to delineate the individual contributions of these chromatin remodelers to the cryptic phenotype.

Studies examining histone turnover levels in the absence of Ioc3 have also been conducted but not yet published. In yeast, the histone acetyltransferase Rtt109 exclusively targets soluble histones. The depletion of H3K56ac significantly diminishes RNAPII occupancy near the transcription start sites, reflecting the pivotal role of H3K56ac in promoting nucleosome turnover in promoter-proximal regions (Topal, Vasseur et al. 2019). Evaluation of H3K56ac occupancy using tiling arrays can therefore provide valuable insights regarding the incorporation of "new" histones. Loss of ISW1a leads to a modest increase in histone turnover specifically at the 5′ end of genes, which intriguingly contrasts with the observed pattern in *isw1Δ* cells (Figure 1.6.4 B). This difference may be due to a more prominent role of ISW1b in orchestrating histone turnover dynamics. Deleting of I*SW1* and *IOC4* prompts a nucleosome shift toward gene promoters, potentially leading to unresolved dinucleosomes at the 5′ end of genes which might negatively impact histone turnover in that region (Yen, Vinayachandran et al. 2012, Eriksson and Clark 2021). Conversely, deletion of *IOC3* leads to a nucleosome shift toward the 3′ end, which could expose longer stretches of DNA at the 5′ end of genes, fostering an environment that might favor histone turnover (Bhardwaj, Hailu et al. 2020). Further studies are needed to elucidate the full extent of the cryptic phenotype suppressed by ISW1a and underlying mechanism.

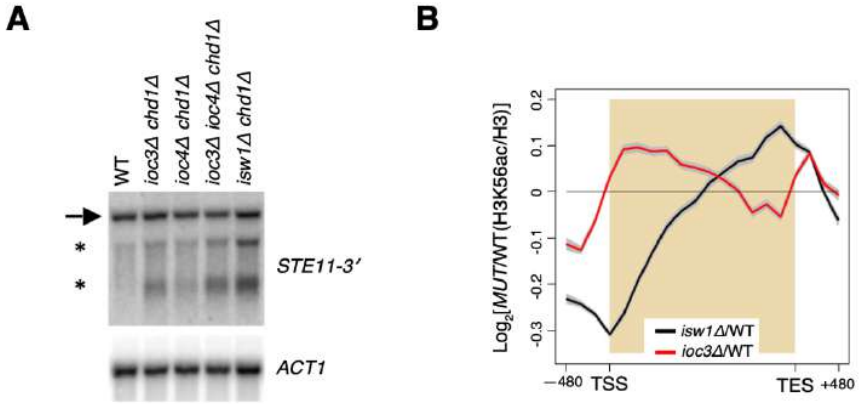

Figure 1.6.4 Loss of *IOC3* derepresses cryptic transcription and histone turnover. (A) Northern blot analysis targeting the 3′ end of *STE11*; *ACT1* served as a loading control. Full-length (→) and cryptic (*) transcripts are shown. (B) Histone turnover metagene profiles based on H3K56ac/H3 occupancy ratios (IP/input) in mutant versus wild-type yeast. Data are represented as mean ± standard error of mean (SEM; in grey) of three independent experiments. Flanking regions are 480 bp around TSS and TES. ChIP-chip experiments were performed using yeast genomic tiling arrays, as previously described (Smolle, Venkatesh et al. 2012).

1.7 Aims of this thesis

In this thesis, I investigated two main research questions: the impact of ISW1a on cryptic transcription, and how ISW1a suppresses this phenomenon *in vivo*.

Due to the overlapping functions of Isw1 and Chd1 remodelers, previous research of Isw1's impact on cryptic transcription has been conducted in cells lacking both *ISW1* and *CHD1* genes. Previous work has reported an additive cryptic phenotype in cells lacking both Isw1 and Chd1 ATPases via microarray analysis or northern blot analysis for specific genes (Smolle, Venkatesh et al. 2012). To characterize the transcriptional phenotype of the double mutant *isw1Δ chd1Δ* at a higher resolution, I used high-throughput sequencing techniques, namely strand-specific RNA-seq and 5′cap-seq. While RNA-seq allows the identification of differentially expressed genes and cryptic antisense RNAs, 5′cap-seq maps TSSs genome-wide, allowing to discriminate between sense cryptic transcription and gene expression - a limitation of the former technique.

Next, I employed the same two techniques in single mutants to identify the individual contributions of Isw1 and Chd1 in suppressing cryptic transcription.

However, deleting ISW1 prevents the formation of both ISW1b and ISW1a, which may obscure the individual effects of the two complexes on cryptic transcription. Previous studies have described the role of ISW1b in repressing cryptic transcription, but the role of ISW1a remains unexplored (Smolle, Venkatesh et al. 2012, Li, Bergmann et al. 2022). To unveil the distinct contributions of ISW1a and CHD1 in suppressing cryptic transcription, I employed both RNA-seq and 5′cap-seq in cells lacking ISW1a complex and CHD1, or both. Finally, since cryptic transcripts are usually rapidly degraded, I questioned whether the extent of Isw1a-repressed cryptic transcription is masked by the presence of a fully functional nuclear exosome. To answer this, I have also mapped the TSSs in cells lacking the Isw1a's subunit, Ioc3, and the catalytic subunit of the nuclear exosome, Rrp6.

While ISW1b acts at mid-3' end of genes, ISW1a localizes at the ends of genes (Smolle, Venkatesh et al. 2012, Yen, Vinayachandran et al. 2012). Because the yeast genome is highly dense, the occupancy of Isw1a at the 3′ of genes could potentially correspond to the 5′ of an adjacent gene, suggesting a role for ISW1a in transcription initiation. Chromatin signatures characteristic of active transcription at the 5′ end of genes include a well-positioned +1 H2A.Z-containing nucleosome as well as an accumulation in H3K4me3 histone mark. To explore the mechanisms of ISW1a-mediated suppression of cryptic transcription, three approaches were implemented. To see whether ISW1a affects the occupancy of H2A.Z and H3K4me3 genome-wide, ChIP-seq against H2A-Z and H3K4me3 was performed in cells lacking ISW1a. To gain insights regarding changes in the H2A-Z and H3K4me3, I compared the ChIP-seq datasets with the ones from RNA-seq and 5′cap-seq. Another approach, was to measure multiple antisense transcripts in various Ioc3-, Htz1-, Swr1-, Set1- and Set3-mutants using multiplexed strand-specific RT-qPCR. And finally, to further elucidate ISW1a-mediated cryptic transcription suppression, I investigated how Isw1a is recruited to the ends of genes, as this remains unclear. Given that the *in vitro* findings from our lab support the idea that Isw1a's recruitment is promoted by the histone variant H2A.Z, I tested this hypothesis *in vivo* using CUT&RUN and ChIP-qPCR (Bergmann 2021).

2 Methods

2.1 Molecular biology methods

2.1.1 Yeast strains

All yeast strains used in this study are listed in Table 2.1.1. Gene deletions were achieved through homologous recombination with a marker gene. Primers used for genomic deletions are indicated in Table 2.1.2. Deletion cassettes were amplified using oligos containing target gene overhangs and designed to anneal to the plasmid containing the marker gene. PCR amplification of the cassettes was carried out with Fusion High Fidelity DNA polymerase (NEB, #M0530L), 0.25 µM of each deletion primer and plasmid DNA. PCR conditions were as follows: initial denaturation at 98°C for 60 seconds; 5 cycles of 10 seconds at 98°C, 30 seconds at 58°C, and 1.30 minutes at 72°C; another denaturation step at 98°C for 30 seconds; 25 cycles of 10 seconds at 98°C, 30 seconds at 72°C, and final extension at 72°C for 1.30 minutes. PCR products were verified for the correct size on a 1.5% agarose electrophoresis gel and subsequently column-purified using a PCR cleanup kit (Metabion, #mi-PCR250). Cells were set up at optical density at 600 nm (OD_{600}) of 0.2 and grown in YPD at 30°C until reaching an OD_{600} of 1.6-1.8. PEG at a final concentration of 33%, 100 mM LiAc, and 2 µg/µl single-stranded carrier DNA were added to cells for transformation. Lastly, 3-5 µg of the deletion cassettes DNA were added. Transformation reactions were incubated for 30 minutes at 30°C and 1000 rpm, immediately followed by 22 minutes of heat shock at 42°C. Subsequently, cells were allowed to grow at 30°C on selective plates. DNA was extracted from transformed clones using the Yeast DNA Extraction Kit (ThermoScientific, #78870). Transformation efficiency was assessed by PCR amplification of external and internal target gene products using Fusion High Fidelity DNA polymerase with 0.5 µM of each primer, 200 µM

dNTPs, and 3% DMSO. PCR was conducted for external and internal primer sets of the deleted genes. Fragment sizes from the external and internal PCR products were checked by 1.5% agarose gel electrophoresis. Transformed clones were inoculated overnight in YPD and glycerol stocks were prepared the next day with 30% glycerol.

Table 2.1.1 All strains used in this study.

Strain	Parental	Genotype	Source	Experiment
BY4741		*MATa his3Δ1 leu2Δ0 met15Δ0 ura3Δ0*	Open Biosystems	All except CUT&RUN and ChIP-seq
YMS033	BY4741	*MATa his3Δ1 leu2Δ0 met15Δ0 ura3Δ0 isw1Δ::KanMX*	Open Biosystems (Smolle, Venkatesh et al. 2012)	RNA-seq
YMS034	BY4741	*MATa his3Δ1 leu2Δ0 met15Δ0 ura3Δ0 chd1Δ::KanMX*	Open Biosystems (Smolle, Venkatesh et al. 2012)	RNA-seq; 5′cap-seq
YMS038	BY4741	*MATa his3Δ1 leu2Δ0 met15Δ0 ura3Δ0 ioc3Δ::KanMX*	Open Biosystems	RNA-seq; 5′cap-seq
YMS067	YMS033	*MATa his3Δ1 leu2Δ0 met15Δ0 ura3Δ0 isw1Δ::KanMX chd1Δ::HIS3*	Michaela Smolle	RNA-seq; 5′cap-seq
YMS137	YMS034	*MATa his3Δ1 leu2Δ0 met15Δ0 ura3Δ0 chd1Δ::KanMX ioc3Δ::HYG*	Michaela Smolle (Smolle, Venkatesh et al. 2012)	RNA-seq
YAS013	BY4741	*MATa his3Δ1 leu2Δ0 met15Δ0 ura3Δ0 rrp6Δ::HIS3*	Andreia Almeida	5′cap-seq
YAS014	YMS038	*MATa his3Δ1 leu2Δ0 met15Δ0 ura3Δ0 ioc3Δ::KanMX rrp6Δ::HIS3*	Andreia Almeida	5′cap-seq
YMS039	BY4741	*MATa his3Δ1 leu2Δ0 met15Δ0 ura3Δ0 ioc4Δ::KanMX*	Open Biosystems	Multiplexed strand-specific RT-qPCR
YLS019	BY4741	*MATa his3Δ1 leu2Δ0 met15Δ0 ura3Δ0 htz1Δ::HIS*	Lisa Schuster	Multiplexed strand-specific RT-qPCR
YLS020	YMS033	*Mat a his3Δ1 leu2Δ0 met15Δ0 ura3Δ0 isw1Δ::KanMX htz1Δ::HIS*	Lisa Schuster	Multiplexed strand-specific RT-qPCR
YMS319	YMS038	*MATa his3Δ1 leu2Δ0 met15Δ0 ura3Δ0 ioc3Δ::KanMX htz1Δ::HIS3*	Ina Koeva	Multiplexed strand-specific RT-qPCR
YMS225	BY4741	*MATa his3Δ1 leu2Δ0 met15Δ0 ura3Δ0 set1Δ::URA*	Michaela Smolle	Multiplexed strand-specific RT-qPCR
YLS018	YMS225	*Mat a his3Δ1 leu2Δ0 met15Δ0 ura3Δ0 set1Δ::URA isw1Δ::HIS*	Lisa Schuster	Multiplexed strand-specific RT-qPCR
YLS006	YMS225	*Mat a his3Δ1 leu2Δ0 met15Δ0 ura3Δ0 set1Δ::URA ioc3Δ::HIS5*	Lisa Schuster	Multiplexed strand-specific RT-qPCR
YMS198	BY4741	*MATa his3Δ1 leu2Δ0 met15Δ0 ura3Δ0 set3Δ::KanMX*	Open Biosystems	Multiplexed strand-specific RT-qPCR
YMS209	YMS198	*MATa his3Δ1 leu2Δ0 met15Δ0 ura3Δ0 set3Δ::KanMX isw1Δ::URA3*	Michaela Smolle	Multiplexed strand-specific RT-qPCR
YMS210	YMS198	*MATa his3Δ1 leu2Δ0 met15Δ0 ura3Δ0 set3Δ::KanMX ioc3Δ::HYG*	Michaela Smolle	Multiplexed strand-specific RT-qPCR
YMS201	BY4741	*MATa his3Δ1 leu2Δ0 met15Δ0 ura3Δ0 rad6Δ::KanMX*	Open Biosystems	Multiplexed strand-specific RT-qPCR
YMS215	YMS201	*MATa his3Δ1 leu2Δ0 met15Δ0 ura3Δ0 rad6Δ::KanMX isw1Δ::URA3*	Michaela Smolle	Multiplexed strand-specific RT-qPCR

YLS005	YMS201	*Mat a his3Δ1 leu2Δ0 met15Δ0 ura3Δ0 rad6Δ::KanMX ioc3Δ::HIS5*	Lisa Schuster	Multiplexed strand-specific RT-qPCR
YLL036	BY4741	*MATa his3Δ1 leu2Δ0 met15Δ0 ura3Δ0 swr1Δ::URA3*	Lingling Yang	Multiplexed strand-specific RT-qPCR
YLL037	YLL036	*MATa his3Δ1 leu2Δ0 met15Δ0 ura3Δ0 swr1Δ::URA3 isw1Δ::LEU2*	Lingling Yang	Multiplexed strand-specific RT-qPCR
YLL038	YMS038	*MATa his3Δ1 leu2Δ0 met15Δ0 ura3Δ0 ioc3Δ::KanMX swr1Δ::URA3*	Lingling Yang	Multiplexed strand-specific RT-qPCR
YLL039	YMS039	*MATa his3Δ1 leu2Δ0 met15Δ0 ura3Δ0 ioc4Δ::KanMX swr1Δ::URA3*	Lingling Yang	Multiplexed strand-specific RT-qPCR
YMS099	YMS081	*MATa his3Δ1 leu2Δ0 met15Δ0 ura3Δ0 IOC3-3xFlag::loxP*	Michaela Smolle (Smolle, Venkatesh et al. 2012)	CUT&RUN; ChIP-qPCR
YAS009	YMS099	*MATa his3Δ1 leu2Δ0 met15Δ0 ura3Δ0 IOC3-3xFlag::loxP htz1Δ::HIS3*	Andreia Almeida	ChIP-qPCR
YAS011	YMS099	*MATa his3Δ1 leu2Δ0 met15Δ0 ura3Δ0 IOC3-3xFlag::loxP gcn5Δ::HIS3*	Andreia Almeida	ChIP-qPCR
YAM013	YMS078	*MATa his3Δ1 leu2Δ0 met15Δ0 ura3Δ0 ISW1-3xFlag IOC3-13xmyc::KanR*	André Marschall	Western blotting
YAM015	YMS078	*MATa his3Δ1 leu2Δ0 met15Δ0 ura3Δ0 ISW1-3xFlag IOC4-13xmyc::KanR*	André Marschall	Western blotting
YAM016	YAM013	*MATa his3Δ1 leu2Δ0 met15Δ0 ura3Δ0 ISW1-3xFlag IOC3-13xmyc::KanR ioc4Δ::HIS3*	André Marschall	Western blotting
YAM031	YAM015	*MATa his3Δ1 leu2Δ0 met15Δ0 ura3Δ0 ISW1-3xFlag IOC4-13xmyc:KanR ioc3Δ::HIS3*	André Marschall	Western blotting
YMS123	BY4741	*MATa his3Δ1 leu2Δ0 met15Δ0 ura3Δ0 bar1Δ::LEU2*	Swaminathan Venkatesh (Venkatesh, Smolle et al. 2012)	ChIP-seq
YMS124	YMS033	*MATa his3Δ1 leu2Δ0 met15Δ0 ura3Δ0 isw1Δ::KanMX bar1Δ::LEU2*	Michaela Smolle (Smolle, Venkatesh et al. 2012)	ChIP-seq
YMS206	YMS038	*MATa his3Δ1 leu2Δ0 met15Δ0 ura3Δ0 ioc3Δ::KanMX bar1Δ::LEU2*	Michaela Smolle	ChIP-seq

Table 2.1.2 Oligos used for genomic deletions.

Name	Description	Sequence (5′-3′)
*HTZ1*_del_F	Forward; *htz1Δ::HIS3* pFA6a-280	AATTTCGCACTATAGCCGCACGTAAAAATAACTTAACATAcggatccccgggttaattaa
*HTZ1*_del_R	Reverse, *htz1Δ::HIS3* pFA6a-280	AGGGAGAATTACGGGAAATGGGAAAGAAAAACTATTCTTCgaattcgagctcgtttaaac
*HTZ1*_ext_F	Forward; ORF external	AATTTCGCACTATAGCCGCAC
*HTZ1*_ext_R	Reverse; ORF external	TCGGGTACGGAGAGACAAATT
*HTZ1*_int_F	Forward; ORF internal	AAGCGTTACCTGAAAAGGCA
*HTZ1*_int_R	Reverse, ORF internal	CAAAACACCACCTGAAGCAA
*RRP6*_del_F	Forward; *rrp6Δ::HIS3* pFA6a-280	AGGAACAACAAACAGCTTATAAGCACCCAATAAGTGCGTTcggatccccgggttaatta
*RRP6*_del_R	Reverse; *rrp6Δ::HIS3* pFA6a-280	CCATAATTTATAAATAAAAAAATACGCTTGTTTTACATAAgaattcgagctcgtttaa
*RRP6*_ext_F	Forward; ORF external	CAAAAATATGAGGGCATCG
*RRP6*_ext_R	Reverse; ORF external	GGAGCCATAACTCCATGA
*RRP6*_int_F	Forward; ORF internal	CTTGCGGATATGGCGAAT
*RRP6*_int_R	Reverse, ORF internal	ATTATCAATCTCAGGCGAGT

2.1.2 Total RNA extraction

Total RNA was isolated via phenol-chloroform extraction followed by ethanol precipitation. Cell pellets were thawed on ice and resuspended in AE buffer (50 mM Sodium acetate pH 5.2, 10 mM EDTA). Cell lysis was achieved using 10% SDS and acidic phenol pH 4.5 (Roth, #A980.1), followed by incubation at 65°C, 1200 rpm for four minutes at room temperature. Phase separation was conducted by chloroform treatment in 2 mL Phase Lock Gel tubes (QuantaBio, #2302830). The upper aqueous phase containing the RNA was mixed with 0.1 volume of 3M NaAc and 2.5 volume of 100% ethanol and incubated for 1 hour at -80°C. After centrifugation for 30 minutes at 15,000 x g and 4°C, samples were washed with 70% ethanol. The RNA precipitate was dried at room temperature and subsequently resuspended in RNase-free water (ThermoScientific, #10977035) and stored at -80°C until further use. The concentration of total RNA was determined using Nanodrop, and its integrity was confirmed through 1% agarose gel electrophoresis. The integrity of total RNA used for library preparations is depicted in Figure 2.1.1. Genomic DNA removal from total RNA

was achieved using the TURBO DNA-free Kit (ThermoScientific, #AM1907) as per the manufacturer's instructions.

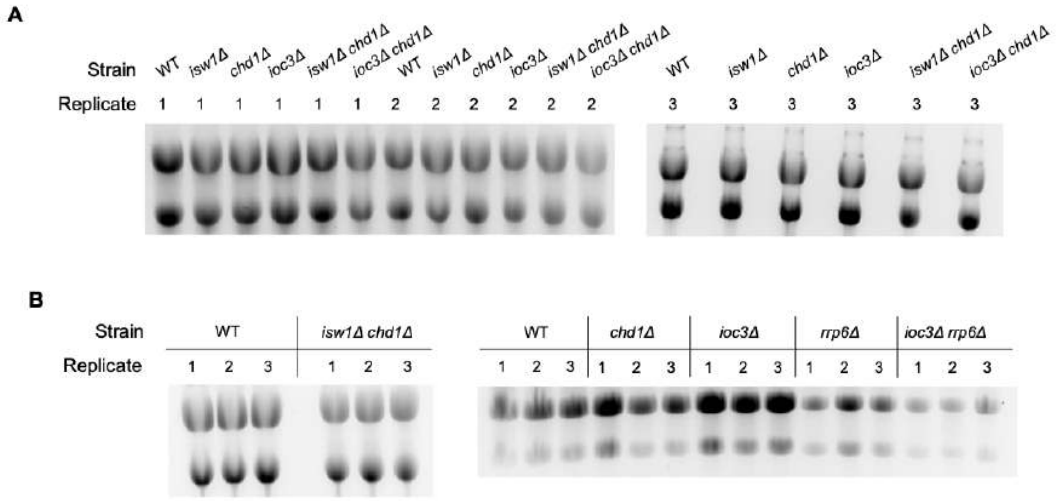

Figure 2.1.1 RNA integrity (25S and 18S rRNA) prior to library preparation. (A, B) Total RNA used for RNA-seq libraries (A) and 5′cap-seq libraries (B).

2.1.3 Strand-specific RNA-seq libraries

Yeast cells were grown in YPD medium at 30°C with a starting OD_{600} of 0.2 until reaching an OD_{600} of ~ 0.7. Three biological replicates were subjected to processing in this experiment. DNase-treated RNA was enriched for polyadenylated molecules using the NEBNext Poly(A) mRNA Magnetic Isolation Module (NEB, #E7490S) and proceeded directly to library preparation according to the instructions stipulated by the NEBNext Ultra II Directional RNA Library Prep Kit for Illumina (NEB, #E7760L) manual. Oligo(dT) beads were combined with 1 µg of DNase-treated RNA. Denaturation occurred at 65°C for 5 minutes, followed by a 5-minute incubation at room temperature to allow the RNA to bind to the beads. The RNA-beads mixtures were washed twice to eliminate any unbound RNA. Poly(A) RNA was eluted in Tris buffer at 80°C for 2 minutes. Then RNA binding buffer was added to the mixture to enable the RNA to re-bind to

the same beads for 5 minutes at room temperature. After another washing step, poly(A) RNA was eluted and fragmented in First Strand Synthesis Reaction Buffer and Random Primer Mix at 94°C for 15 minutes. The fragmented RNA was separated from the beads and transferred to the first strand cDNA reaction (10 minutes at 25°C, 50 minutes at 42°C, 15 minutes at 70°C). Second strand synthesis reaction was conducted for 1 hour at 16°C. Purification of double-stranded cDNA was achieved using AMPure beads (Beckman Coulter, #A63882). DNA was resuspended in 0.1X TE buffer and stored at -20°C. The next day, end prep was carried out at 20°C for 30 minutes followed by 30 minutes at 65°C. End prepped DNA was mixed with a 1:5 adaptor dilution and subjected to a 15-minute incubation at 20°C. USER enzyme was added to the ligation mixture, followed by 15 minutes at 37°C. Adaptor ligated DNA was purified using AMPure beads and proceeded immediately to PCR enrichment using the NEBNext Multiplex Oligos for Illumina (Index Primers Set 1, NEB, #E7335S). The PCR conditions were as follows: initial denaturation at 98°C for 30 seconds, 9 cycles of denaturation at 98°C for 10 seconds and annealing/extension at 65°C for 75 seconds, and a final extension at 65°C for 5 minutes). Two AMPure beads washing steps were performed to purify the PCR reaction and to eliminate adaptor and PCR oligos excess. cDNA libraries were quantified and quality-checked with the DNA high sensitivity Kit (Agilent, #5067-4626) for the 2100 Bioanalyzer (Agilent, #G2939BA), revealing an average fragment size of approximately 400 bps and an average of 13 ng/ul concentration. Sequencing was performed in an Illumina HiSeq 1500 instrument with a sequencing depth of 30 million reads per sample and a single-end 50 bp read.

2.1.4 5′cap-seq library preparation

Yeast cells were grown in YPD medium at 30°C with a starting OD_{600} of 0.2 until reaching an OD_{600} of ~ 0.8-0.9. Three biological replicates were considered in this experiment. Two strain sets were processed independently: one set with *isw1Δ chd1Δ* and wild-type strains, and another set composed of *chd1Δ*, *ioc3Δ*, *rrp6Δ*,

ioc3Δ rrp6Δ and wild-type strains. The 5′ cap library preparation followed the methodology outlined by Pelechano et al., maintaining consistency with the specified oligos (Table 2.1.3) (Pelechano, Wei et al.). DNase treatment was carried out on 50 µg of total RNA, followed by the removal of 5′P from fragmented and non-capped RNA at 37°C for 30 minutes, using 30 U of calf intestinal alkaline phosphatase (CIP), Quick CIP (NEB, #M0525S) for the *isw1Δ chd1Δ* double mutant set of strains, and CIP (NEB, #M0290S) for the remaining strain set. Samples were treated twice with phenol to eliminate any remaining CIP and once with Phenol/Chloroform/Isoamyl alcohol (Sigma-Aldrich, #P3803-100ML) as previously recommended (Pelechano, Wei et al.). Ethanol precipitation followed and capped RNA was resuspended in RNase-free water. Decapping was conducted at 37°C for 1 hour using 5 U of Cap-Clip (Biozyme, #C-CC15011H), exposing a 5′P in previously capped molecules. RNA purification through phenol-chloroform-isoamyl alcohol and ethanol precipitation followed. Unique molecular identifier (UMI) ligation occurred for 16 hours at 16°C using a DNA/RNA oligo rP5_RND and 20 U of T4 RNA ligase I (NEB, #M0204S). The oligo excess from the UMI ligation step was removed using 1.8X AMPure beads. Poly(A) RNA isolation was accomplished with Dynabeads Oligo(dT) 25 (ThermoScientific, #61002), while adhering to the manufacturer's instructions. Polyadenylated RNA underwent fragmentation at 80°C for 5 minutes. Denaturation with random primers (ThermoScientific, #48190011) and dNTPs occurred at 65°C for 5 minutes. First strand synthesis was performed using 400 U of the SuperScript III Reverse Transcriptase (ThermoScientific, #18080093) under the conditions: 5 minutes at 25°C, 50 minutes at 50°C, and 15 minutes at 70°C. After purification with AMPure beads, second-strand cDNA synthesis was performed with biotinylated oligo BioNotI-P5-PET, followed by another AMPure beads clean-up and streptavidin-based purification using streptavidin-coated magnetic beads (ThermoScientific, #11205D). DNA end repair was carried out at 20°C for 30 minutes using the NEBNext End repair module (NEB, #E6050S). A protruding adenine was added to the DNA fragments by adding 7.5 U of Klenow fragment exonuclease (NEB, #M0212S) and dA tailing buffer (NEB, #B7002S).

Following a 30-minute incubation at 37°C, the RNA-beads complexes were washed with bind and wash buffer (5 mM Tris-Cl pH 7.5, 0.5 mM EDTA pH 8.0, and 1 M NaCl) and eluted in elution buffer (ThermoScientific, #A33566). The ligation of a common adaptor was conducted with 2.5 µM of P7MPX annealed adapter and 4000 U of T4 DNA ligase followed by 16 hours at 16°C. RNA-beads complexes were then subjected to PCR enrichment using the Phusion High-Fidelity PCR Master Mix with HF Buffer (NEB, #M0531S) and PE2_MPX oligos. PCR conditions applied for the *isw1Δ chd1Δ* double mutant and wild-type strains were as follows: initial denaturation at 98°C for 30 seconds, 7 cycles of denaturation-annealing-extension, and a final extension at 72°C for 5 minutes. For the other set of strains, the PCR program conditions remained similar, however with 9 cycles. Fragments between 300 and 500 bps were enriched with AMPure beads and assessed using the DNA high sensitivity Kit (Agilent, #5067-4626) on the 2100 Bioanalyzer (Agilent, #G2939BA), revealing an average concentration of 2.6 ng/µl. Sequencing was performed in an Illumina HiSeq 1500 instrument with a sequencing depth of 10 million reads per sample and single-end 50 bp reads.

Table 2.1.3 Oligos used for 5′cap-seq.

Name	Description	Sequence (5′-3′)
rP5_RND	RNA-DNA oligo	[dC][dT][dT][dT][dC][dC][dC][dT][dA][dC][dA][dC][dG][dA][dC][dG][dC][dT][dC][dT][dT][dC][dC][dG][dA][dT]CUNNNNNNNN
BioNotI-P5-PET	Biotinylated oligo	[Btn]TATAGCGGCCGCAATGATACGGCGACCACCGAGATCTACACTCTTTCCCTACACGACGCTCTTCCGATCT
P7MPX_linker_for	adaptor forward	GTGACTGGAGTTCAGACGTGTGCTCTTCCGATC*T
P7MPX_linker_rev	adaptor reverse	[Phos]GATCGGAAGAGCACACGTCTGAACTCCAGTCAC[AmC7]
PE1.0	common index	ATGATACGGCGACCACCGAGATCTACACTCTTTCCCTACACGACGCTCTTCCGATC*T
PE2_MPX_01	index 1	CAAGCAGAAGACGGCATACGAGATCGTGATGTGACTGGAGTTCAGACGTGTGCTCTTCCGATC*T
PE2_MPX_02	index 2	CAAGCAGAAGACGGCATACGAGATACATCGGTGACTGGAGTTCAGACGTGTGCTCTTCCGATC*T
PE2_MPX_03	index 3	CAAGCAGAAGACGGCATACGAGATGCCTAAGTGACTGGAGTTCAGACGTGTGCTCTTCCGATC*T
PE2_MPX_04	index 4	CAAGCAGAAGACGGCATACGAGATTGGTCAGTGACTGGAGTTCAGACGTGTGCTCTTCCGATC*T
PE2_MPX_05	index 5	CAAGCAGAAGACGGCATACGAGATCACTGTGTGACTGGAGTTCAGACGTGTGCTCTTCCGATC*T

PE2_MPX_06	index 6	CAAGCAGAAGACGGCATACGAGATATTGGCGTGACTGGAGTTCAGACGTGTG CTCTTCCGATC*T
PE2_MPX_07	index 7	CAAGCAGAAGACGGCATACGAGATGATCTGGTGACTGGAGTTCAGACGTGTG CTCTTCCGATC*T

2.1.5 Multiplexed strand-specific RT-qPCR

Yeast cells were grown in YPD medium at 30°C with a starting OD_{600} of 0.2 until reaching an optical density OD_{600} of ~ 0.7. To amplify antisense transcripts, a multiplexed reverse transcription (RT) reaction was prepared with eight antisense-specific primers targeting cryptic transcripts overlapping with the genes *AIM23*, *DCV1*, *FAA2*, *FLO10*, *HXT10*, *RAD30*, *SPR28*, and *YER187W*. These genes were selected based on RNA-seq analysis from *ioc3Δ* and *isw1Δ* versus wild-type. Additionally, one sense-specific primer was used for the endogenous control *ACT1*. In the first step of cDNA synthesis, approximately 4 µg of DNase-treated RNA were mixed with a 10 mM dNTP mix and a primer mix containing the specified primers at 2 pmol each. Annealing was conducted at 70°C for 10 minutes, followed by 10 minutes on ice. To minimize antisense cDNA artifacts, 0.3 µg of actinomycin D were added after the denaturation step. First-strand synthesis was performed using 60 U of SuperScript III Reverse Transcriptase. Reverse transcription was conducted at 55°C for one hour, followed by heat inactivation at 70°C for 15 minutes. For results in Figure 3.8.3, SuperScript IV Reverse Transcriptase (ThermoScientific, #18090200) was used instead of SuperScript III. Annealing was conducted at 65°C for 5 minutes and cDNA synthesis was performed at 55°C for 15 minutes followed by inactivation at 80°C for 10 minutes. All samples were quantitated by qPCR using PowerTrack SYBR Green Master Mix (ThermoScientific, #A46109) and a QuantStudio 5 Real-Time PCR System (ThermoScientific, #A28575). cDNA was appropriately diluted before being added to the qPCR reaction, with a 1:10 dilution for reactions targeting antisense transcripts and a 1:800 dilution for the *ACT1* reaction. qPCR probes concentration was 200 nM, ensuring an efficiency between 95-104% across primer sets. The qPCR program was based on the "Fast cycling mode" PowerUp SYBR Green Master Mix manual (UDG activation at 50 °C for 2

minutes, DNA polymerase activation at 95 °C for 2 minutes; 40 cycles of denaturation at 95 °C for 1 second followed by annealing and extension at 60 °C for 30 seconds; finalizing with a melt curve stage of 95 °C for 15 seconds, 60 °C for 1 minute, and 95 °C for 15 seconds). Target regions were first normalized to *ACT1* for all samples. Subsequently, results for mutant yeast strains were referenced against the mean values for wild-type yeast using the comparative CT (ΔΔCT) method. Three biological replicates were considered, as well as two technical replicates for the qPCR. Potential cross RT primer-dimers were checked using Multiple Primer Analyzer from Thermo Scientific Web Tools (www.thermofisher.com/de). Additionally, RT reactions lacking reverse transcriptase were included in the analysis to confirm the absence of cross primer-dimers during cDNA synthesis. All primers used in this experiment are listed in Table 2.1.4.

Table 2.1.4 Oligos used for multiplexed strand-specific RT-qPCR.

Name	Description	Sequence (5′-3′)
*ACT1*_1	Sense RT and qPCR oligo	CAAGGTATCATGGTCGGTATGG
ACT1_2	qPCR oligo	CGTGTTCAATTGGGTAACGTAAAG
*AIM23*_1	Antisense RT and qPCR oligo	CGAGCTAAAGAGGCAGCTAAT
AIM23_2	qPCR oligo	TGCTTCAATTCGGTGGGTAG
*DCV1*_1	Antisense RT and qPCR oligo	CCTGCTCTCGAGTACGTTTAAT
DCV1_2	qPCR oligo	CTTAGGACTCAGCCACCAAC
*FAA2*_1	Antisense RT and qPCR oligo	TCTTGTGGTGCCATAGGTATTT
FAA2_2	qPCR oligo	CCACGAATTTGCAGTTCACC
*FLO10*_1	Antisense RT and qPCR oligo	CACTCCATATGCAACCTCATCT
FLO10_2	qPCR oligo	GAAACGGTTGTGTCTGTTTGG
*HXT10*_1	Antisense RT and qPCR oligo	CTGTCTGATGATTGCCTTTGG
HXT10_2	qPCR oligo	GTAACTCACCAAACCTTCTCTTG
*RAD30*_1	Antisense RT and qPCR oligo	CGAGTCCTCCTTAGCATGTATC
RAD30_2	qPCR oligo	GCAGACTACCGGATCTTCTTT
*SPR28*_1	Antisense RT and qPCR oligo	CAATCTGTGCGGTCAGGATA
SPR28_2	qPCR oligo	CTTCGATGGCGTTTCCATTT
*YER187W*_1	Antisense RT and qPCR oligo	AGTGACAATTCTGGAACACTGTAT
YER187W_2	qPCR oligo	GCTGCTATTCATGTCGTCTGT

2.1.6 CUT&RUN and library preparation

Two biological replicates were considered. Yeast cells were grown in 250 ml YPD medium at 30°C with a starting OD_{600} of 0.2 until reaching an OD_{600} of ~ 0.7-0.9. Cells were resuspended in Resuspension Buffer (1.2 M sorbitol, 100 mM potassium phosphate pH 7.5, 0.5 mM $CaCl_2$, 0.5 mM beta-mercaptoethanol) at a concentration of 10 OD/mL and incubated for 30 minutes at 30°C in a water bath. Subsequently, zymolyase was added to a final concentration of 2 U/ml, and incubation continued for 30 minutes at 35°C. Spheroblast formation progress was monitored by measuring OD_{600} every 10 minutes until completion, with OD_{600} reaching around 10-20% of the initial value. Following two washes with SPC buffer (1M sorbitol, 20 mM PIPES pH 6.3, 0.1 mM CaCl2), cells were mixed with Ficoll buffer (20 mM PIPES pH 6.3, 0.5 mM CaCl2, 9% Ficoll 400). Pellets were washed and mixed with Ficoll buffer again. Nuclei constituting approximately $5x10^8$, were aliquoted to 25 OD_{600} and stored at -80°C. Nuclei from approximately $125x10^6$ cells were mixed with ConA-coated magnetic beads and incubated at room temperature for 5 minutes with rotation. Following this, samples were subjected to two washes with Dig-Wash buffer (20 mM HEPES pH 7.5, 150 mM NaCl, 0.5 mM Spermidine and 0.05% digitonin). Nuclei-beads were resuspended in antibody buffer (Dig-Wash buffer with 2 mM EDTA) and divided into aliquots for negative control and test samples. While the test samples were incubated with 1:400 mouse monoclonal anti-FLAG M2 antibody (Sigma-Aldrich, #F1804-1MG), the negative control samples were incubated with mouse IgG isotype control antibody (Cell Signaling, #5415). Both test and control samples were incubated overnight at 4°C with rotation. The next day samples were incubated with the secondary antibody (1:200 of rabbit anti-mouse IgG, Abcam, #ab46540) for 1 hour at 4°C, maintaining rotation. After nuclei-beads were washed with Dig-Wash buffer, 135 ng of pAG-MNase were added, followed by a 1-hour incubation at 4°C. After two additional washes with Dig-Wash buffer, beads were resuspended in incubation buffer (Dig-Wash buffer with 10mM CaCl2). Chromatin digestion was performed at 0°C in ice/water bath for 5 minutes. The

digestion was halted by adding STOP buffer (150 mM NaCl, 20 nM EDTA, 4 mM EGTA, 50 µg/ml RNase A, 40 µg/ml glycogen), followed by a 30-minute incubation at 37°C. The released CUT&RUN fragments were separated from the beads and subjected to a phenol-chloroform extraction using phase lock tubes. DNA was resuspended 0.1X TE buffer and quantified using Qubit. The digestion yielded on average of 12 ng of DNA. The NEBNext Ultra II DNA Library Prep Kit for Illumina (NEB, #E7645) manual was followed with some adjustments. End preparation was conducted at 50°C. Adaptor ligation was followed by a 1.75X AMPure bead purification. For the PCR reaction, the total reaction volume was reduced to 30 µL, and the PCR program included 14 cycles with 10 seconds of annealing/extension. NEBNext Multiplex Oligos for Illumina (Index Primers Set 4, NEB, #E7730S) were employed for PCR enrichment. Size selection for fragments between 150-350 bps was achieved using AMPure beads. cDNA libraries were quantified and quality-checked using the DNA high sensitivity Kit (Agilent, #5067-4626) on the 2100 Bioanalyzer (Agilent, #G2939BA). Sequencing was performed in an Illumina HiSeq 1500 instrument with a sequencing depth of 20 million reads per sample with single-end 50 bp reads.

2.1.7 Chromatin immunoprecipitation followed by quantitative PCR (ChIP-qPCR)

Yeast cells were grown in 100 ml YPD medium at 30°C with a starting OD_{600} of 0.15 until reaching an OD_{600} of ~0.7, ensuring two cell divisions. Cross-linking was achieved by exposing the cultures to 1% formaldehyde for 15 minutes at room temperature with gentle shaking (250 rpm). Quenching of the cross-linking process was done with glycine at a final concentration of 0.125 M for 10 minutes, maintaining gentle shaking at room temperature. Subsequent centrifugation and washing steps were performed and cell pellets were stored in screw-cap tubes at -80°C. Cell pellets were resuspended in 150 FA SDS lysis buffer (50 mM HEPES-KOH pH 7.5, 150 mM NaCl, 1 mM EDTA, 1% triton-X 100, 0.1% Na-deoxycholate, and 0.2% SDS), as well as protease inhibitors leupeptin, pepsin

A, PMSF, and protease inhibitor cocktail (Sigma-Aldrich, #P8215). Additionally, 250 µl of 0.5 mm diameter zirconia beads (BioSpec, #11079105z) were added. Cell lysis was carried out using a Precellys 24 homogenizer (Bertin Technologies) under specific conditions: 6800 rpm for 30 seconds per cycle, with 5 minutes on ice between each cycle, repeated for a total of 9 cycles. Chromatin fragmentation was performed at 4°C for 20 minutes, with cycles of 30 seconds on and off, and at 90% amplitude, utilizing a Q800R1 sonicator (QSonica). Chromatin equivalent to 6 OD_{600} was isolated for input DNA purification. The input chromatin underwent treatment with 10 µg of RNase A (ThermoScientific, #EN0531) and 40 µg of Proteinase K (ThermoScientific, #AM2548), followed by cross-link reversal at 65°C for 16 hours. Input DNA was extracted via phenol/chloroform/isoamyl alcohol (Roth, #A156.1) as well as chloroform/isoamyl alcohol (Sigma-Aldrich, #25666) followed by ethanol precipitation, and resuspension in ultra-pure DNase-free water (ThermoScientific, #10977035). Chromatin fragment sizes ranging from 100 to 500 base pairs were confirmed by 1.5% agarose gel electrophoresis. For the Ioc3-Flag ChIP, chromatin corresponding to 20 OD_{600} was incubated with 2 µg of mouse monoclonal anti-FLAG M2 antibody (Sigma-Aldrich, #F1804-1MG) for 16 hours at 4°C, followed by a 5-hour incubation with protein G dynabeads at 4°C. ChIPs were washed with FA buffers of varying salt concentrations (150 nM and 500 nM), TEL (10 mM Tris-HCl pH 8, 250 mM LiCl, 1 mM EDTA, 1% NP-40, 1% Na-Deoxycolate) and TE buffers. Elution was performed in ChIP elution buffer (10 mM Tris-HCL pH 8, 1 mM EDTA, 250 mM NaCl, 1% SDS) at 95°C and 1400 rpm for 10 minutes, followed by a 16-hour incubation at 65°C. Immunoprecipitated (IP) DNA underwent further treatment with RNase A and Proteinase K, followed by DNA extraction, similarly to input DNA purification. Ioc3-Flag occupancy was quantified by qPCR using PowerTrack SYBR Green Master Mix and a QuantStudio 5 Real-Time PCR System. Primer sets for target regions were designed for amplicon inclusion at the 5′ end of genes (up to 200 bps downstream the TSS) since it is where ISW1a has been reported to localize as well as the +1 H2A.Z-containing nucleosome. For regions where ISW1a is not enriched, primers spanning the mid coding

region of gene *STE3* and an intergenic region in chromosome V (CHRV) were used. Oligos were designed using Integrated DNA Technologies (eu.idtdna.com). qPCR probes concentration was 300 nM, ensuring an efficiency between 92-102% across primer sets. Oligos used for this experiment are listed in Table 2.1.5. Input DNA was diluted 1:2000, while IP DNA samples were diluted 1:5. The qPCR program was as follows: DNA polymerase activation at 95 °C for 2 min; 40 cycles of denaturation at 95 °C for 5 seconds followed by annealing and extension at 60 °C for 30 seconds; and a melt curve stage of 95 °C for 15 seconds, 60 °C for 1 min, and 95 °C for 15 seconds. Two biological replicates were considered. Mean Ct values from both IP and input samples were adjusted for dilution. Adjusted Ct values from IP samples were normalized against input samples for each primer set (Figure 2.1.2). Further normalization involved correcting for variations in target genes by referencing against the mean signals for two control regions, *STE3* and a subtelomeric region on CHRV due to minimal Ioc3 occupancy.

Table 2.1.5 Oligos used for ChIP-qPCR.

Name	**Description**	**Sequence (5′-3′)**
chrV_control_F	Forward; control region	GGCTGTCAGAATATGGGGCCGTAGTA
chrV_control_R	Reverse; control region	CACCCCGAAGCTGCTTTC ACA ATAC
*STE3*_control_F	Forward; control region	GTTCGCAAGGCTGTTGATATTC
*STE3*_control_R	Reverse; control region	GTGTCCTTCTACCTGCTGTAAA
*ADH1*_target_F	Forward; target region	CTTCTACGAATCCCACGGTAAG
*ADH1*_target_R	Reverse; target region	GTGTGACAGACACCAGAGTATT
*PDC1*_target_F	Forward; target region	TCGAAAGATTAAAGCAAGTCAACG
*PDC1*_target_R	Reverse; target region	GCCCATCTCATACCTTCAACTT
*PMA1*_target_F	Forward; target region	ATGACGCTGCATCTGAATCT
*PMA1*_target_R	Reverse; target region	GGACCATCGTTATCACTGTCTT
*PYK1*_target_F	Forward; target region	CAAAGACCAACAACCCAGAAAC
*PYK1*_target_R	Reverse; target region	GGTATTCGTAAGAACCGTGAGAG

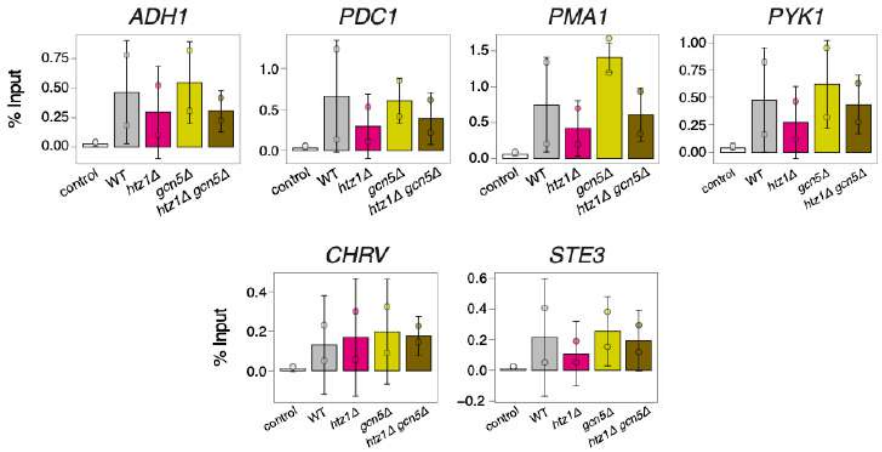

Figure 2.1.2 Ioc3-Flag occupancy expressed in percentage of input. ChIP-qPCR analysis was performed to measure the enrichment of Ioc3-Flag in the start of genes (*ADH1*, *PDC1*, *PMA1* and *PYK1*). Two control regions (*CHRV* and *STE3*) were included. Data represent the percentage of input DNA recovered after immunoprecipitation. The results are expressed as mean ± SEM of two biological replicates. The primer sets used span an amplicon within the first 200 bps of each gene. The colors represent the different yeast strains indicated in the x-axis. A control strain (BY4741) is also included where Ioc3 is not tagged.

2.1.8 Western blotting

Two biological replicates were considered. Day cultures were set up at 0.2 OD_{600} in 20 ml YPD until reaching OD_{600} ~1. The cell pellets were resuspended in FLAG extraction buffer (25 mM HEPES-KOH pH7.5, 350 mM KCl, 2 mM $MgCl_2$, 1 mM EDTA, 10% glycerol and 0.02% NP40) containing proteinase inhibitors, and mixed with glass beads (BioSpec Products, #11079105) in screw-cap tubes. Whole cell extract (WCE) was obtained after cell lysis using the Precellys 24 homogenizer with the following conditions: 7 cycles, each lasting 30 seconds at 6800 rpm, with 5-minute intervals on ice between each cycle. A total of 35 µg of the resulting WCE, assessed using the Bradford method (Bio-Rad Protein Assay Kit I, BIO-RAD, #5000001), was mixed with Laemmli loading buffer and heated at 95°C for 5 minutes. After denaturation, the samples were loaded onto a 7.5% precast polyacrylamide gel (Bio-Rad, #456-1023) alongside a pre-stained protein ladder (ThermoScientific, #26620). Sodium dodecyl sulfate-polyacrylamide gel electrophoresis (SDS-PAGE) was conducted until the bromophenol blue dye migrated out of the gel. The resolved samples were then transferred onto a 0.45

µm polyvinylidene fluoride membrane (Roth, #T830.1) at 300 mA for one hour at 4 °C. To isolate the endogenous control Pgk1 from other proteins of interest, blots were segmented around 55 kB. From then on, the blots were always protected from light. Blocking with TBSTM (5% bovine serum albumin, 1x TBS, and 0.1% Tween 20) was performed overnight at 4 °C. The blot containing the proteins of interest underwent incubation with a 1:500 dilution of mouse monoclonal anti-FLAG M2 antibody (Sigma-Aldrich, #F1804-1MG) overnight at 4 °C while the Pgk1 blot continued blocking for an additional day before being subjected to incubation with a 1:3000 dilution of mouse anti-PGK1 antibody (Abcam, #ab113687) for 2 hours at 4°C. Post-incubation with primary antibody, both blots were washed three times with TBST (1x TBS, and 0.1% Tween 20) for 10 minutes and then exposed to the secondary fluorescent antibody anti-mouse CF770 (Sigma-Aldrich, #SAB4600214-125UL) at a 1:10000 dilution for 1 hour at 4°C. The blot containing the proteins of interest was incubated for 2 hours at 4°C with rabbit anti-MYC antibody (Myc 9E10, Helmholtz Zentrum Munich Core Facility Monoclonal antibodies) at a 1:6000 dilution. The blot was washed and exposed to secondary fluorescent antibody anti-rabbit CF680 (Sigma-Aldrich, #SAB4600200-125UL) at a 1:10000 dilution for 1 hour at 4°C. Before scanning, blots underwent three 5-minute washes with TBST and were dried in the dark between two filter papers. Scanning was performed using the Li-cor Odyssey Infrared Imaging System (Li-cor).

2.1.9 ChIP-seq library preparation

ChIP-seq experimental procedure was performed by Lingling Yang from the Department of Physiology Chemistry. Two biological replicates were considered. Yeast strains were grown in 200 ml of YPD medium at 30°C, and arrested with α-factor at a concentration of 5 µM. Cells were cross-linked and processed for ChIP. G1 arrest of cells was confirmed by fluorescence-activated cell sorting (FACS) analysis of samples collected before and after treatment with α-factor. ChIP lysates were used to immunoprecipitate H3, H2A.Z and H3K4me3 using

histone H3 antibody (Active Motif, #61475), Htz1/H2A.Z antibody (Active Motif, #39647), and histone H3 K4me3 antibody (Abcam, #ab8580), respectively. DNA was extracted and libraries were prepared using NEBNext Multiplex Oligos for Illumina (NEB #E7335S, #E7500S, #E7710S) and NEBNext Ultra II DNA Library Prep Kit for Illumina (NEB, #E7645L), according to the manufacturer's instructions. Sequencing was performed in an Illumina HiSeq 1500 instrument with a sequencing depth of 5 million reads per sample and single-end 50 bp reads.

2.2 Bioinformatics methods

2.2.1 RNA-seq data processing

Processing of RNA-seq data involved a series of steps to ensure accurate and reliable results. Reads were demultiplexed using the indexes incorporated during PCR enrichment, executed with the command line 'je demultiplex-illu' from Je v1.2. Quality assessment of fastq files was performed using FASQC v0.11.7. Single-end reads were mapped to the reference genome (S288C Scer3) using Bowtie2 v2.2.9 with default parameters, resulting in over 80% of uniquely mapped reads. Samtools v1.9 was utilized to convert SAM files into BAM files. BAM files were randomly subsampled to the least abundant number of reads found (31,141,242), derived from *isw1Δ chd1Δ* replicate 3, using BRGenomics (R package). Strand-specific coverage was obtained using GenomicRanges (R package). STAR v2.7.1a aligner was employed to map reads to various features, including the yeast Scer3 annotated transcriptome (https://www.ensembl.org/), as well as other features like SUTs, CUTs, and SRATs (Xu et al, 2009; Venkatesh et al, 2016). The '--quantMode GeneCounts' parameter in the STAR running command was used to quantify reads per feature. STAR results for all samples were combined into two summarized experiment objects using the SummarizedExperiment (R package), creating one for sense counts and another for antisense counts per gene or feature. Differential expression analysis was

conducted from both sense and antisense summarized experiments using DESeq2 (R package). Sample distances between replicates were assessed by principal component analysis (PCA) (Figure 2.2.1). Genes were considered differentially expressed if they had an adjusted p-value<0.05 and a 1.5-fold change. Downstream analysis and plotting focused on SUTs, CUTs, and SRATs, or non-overlapping protein-coding genes, excluding the mitochondrial chromosome. Derepressed antisense differentially expressed genes (asDEGs) and sense differentially expressed genes (sDEGs) were subjected to gene ontology (GO) enrichment analysis with the Database for Annotation, Visualization and Integrated Discovery (DAVID, david.ncifcrf.gov/home.jsp) (Huang da, Sherman et al. 2009, Sherman, Hao et al. 2022).

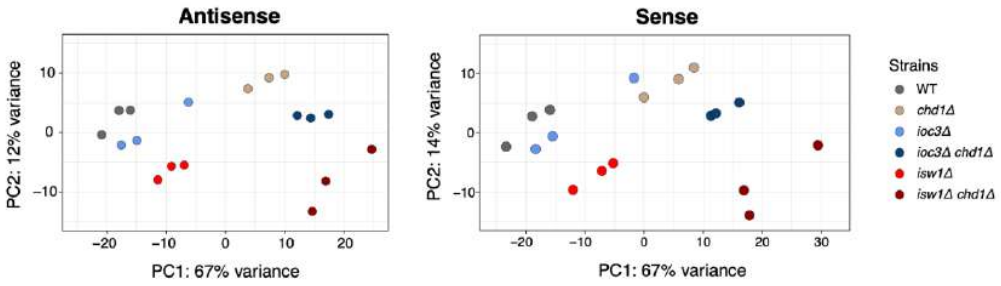

Figure 2.2.1 PCA plot of sense and antisense transcript profiles. Principal component analysis (PCA) was performed on RNA-seq data to compare the expression profiles of sense and antisense transcripts across different strains. Each point represents an individual sample, with clustering indicating distances in transcript patterns. The first two principal components (PC1 and PC2) account for the majority of variance in the data. Three biological replicates per strain are represented.

2.2.2 5′cap-seq data processing

The 5′cap-seq data was processed as recommended by Pelechano et al. (Pelechano, Wei et al.). Reads were demultiplexed as previously described. UMI extraction was performed using the UMI-tools (Python package). The first 8 nucleotides, representing the UMI, were extracted from sequences and appended to the read name lines from the fastq files using the ‘extract’ function

with specific parameters: '--extract-method=regex —bc-pattern='.*(?P<umi_1>.{8})$''. Quality assessment of fastq files was performed as before mentioned. For alignment to the reference genome (S288C Scer3), Novoalign v3.09.00 was employed with default parameters, reporting over 67 or 80% uniquely mapped reads across samples. Aligned reads containing the same UMI in the read name and mapping to the exact same 5′ end were collapsed using the 'dedup' function from UMI-tools, generating BAM files containing only deduplicated reads. Only the start coordinate of the reads was considered, representing the TSS tag: the first nucleotide of the RNA molecule. This was done using the 'resize' function from GenomicRanges (R package) with the parameter 'fix="start"'. For downstream analysis, only TSS tags present in at least two biological replicates were retained using the 'intersect' function from GenomicRanges (R package). Final library sizes for each strain set were documented (Table 2.2.1 and Table 2.2.2). Distances between replicates was assessed by correlation of tag counts per TSS (Figure 2.2.2). TSS tags from replicates were merged and normalized via CAGEr's common reference power-law distribution. TSS tags within 60 bps distance were clustered using the 'clusterCTSS' function from CAGEr (R package). Singletons were ignored. TSS clusters (TCs) information regarding their genomic location or corresponding gene was retrieved using the 'assignTxType' and 'assignGeneID' functions, respectively (CAGEfightR, R package). Specifically, TCs had to overlap with a region of 250 bps upstream the gene up to 1 bp downstream in order to be assign to a gene ID. Heatmaps were produced in R. Although a minority, sense intragenic TCs above 200 bps were filtered out, since these corresponded to elevated background noise from highly expressed genes. For promoter, sense intragenic, and antisense intragenic TCs, only those from non-overlapping protein-coding genes were considered. Matrices were created from the normalized coverage from bigWig files aligned to the TC centroids using the 'coverageWindowsCenteredStranded' function from tsTools (R package). Matrix values were summed into 20 bps per bin. Heatmaps were plotted with 200 bps up and downstream the TC centroid. De novo motif discovery on TSS clusters

was performed using XSTREME tool from MEME suite (meme-suite.org/meme/index.html), and with Homer v4.9. TCs were extended 250 bps upstream and 50 bps downstream. Sequences underlying the extended TCs were retrieved using Bedtools v2.28.0 with the 'getfasta' command. Motif discovery analysis with XSTREME was performed with default parameters, and the target sequences were shuffled and used as background. Homer de novo motif search was performed with the 'findMotifs.pl' command. Herein, two analyses were performed, each with different background sequences. One where the background sequence was the *Saccharomyces cerevisiae* genome (Saccharomyces_cerevisiae.R64-1-1.dna.toplevel.fa), and the other where only promoter regions of protein-coding genes were considered. For the latter one, promoter regions were defined as the DNA sequence spanning the TSS of protein-coding genes up until 250 bps upstream.

Table 2.2.1 Final library sizes for the first 5′cap-seq experiment.

Strains	**Replicate 1**	**Replicate 2**	**Replicate 3**
WT	250 687	236 390	365 117
isw1Δ chd1Δ	322 227	326 208	424 040

Table 2.2.2 Final library sizes for the second 5′cap-seq experiment.

Strains	**Replicate 1**	**Replicate 2**	**Replicate 3**
WT	990 120	849 327	681 745
chd1Δ	883 636	773 617	780 830
ioc3Δ	1 008 087	869 035	690 511
rrp6Δ	996 823	575 840	808 532
ioc3Δ rrp6Δ	735 032	803 720	948 609

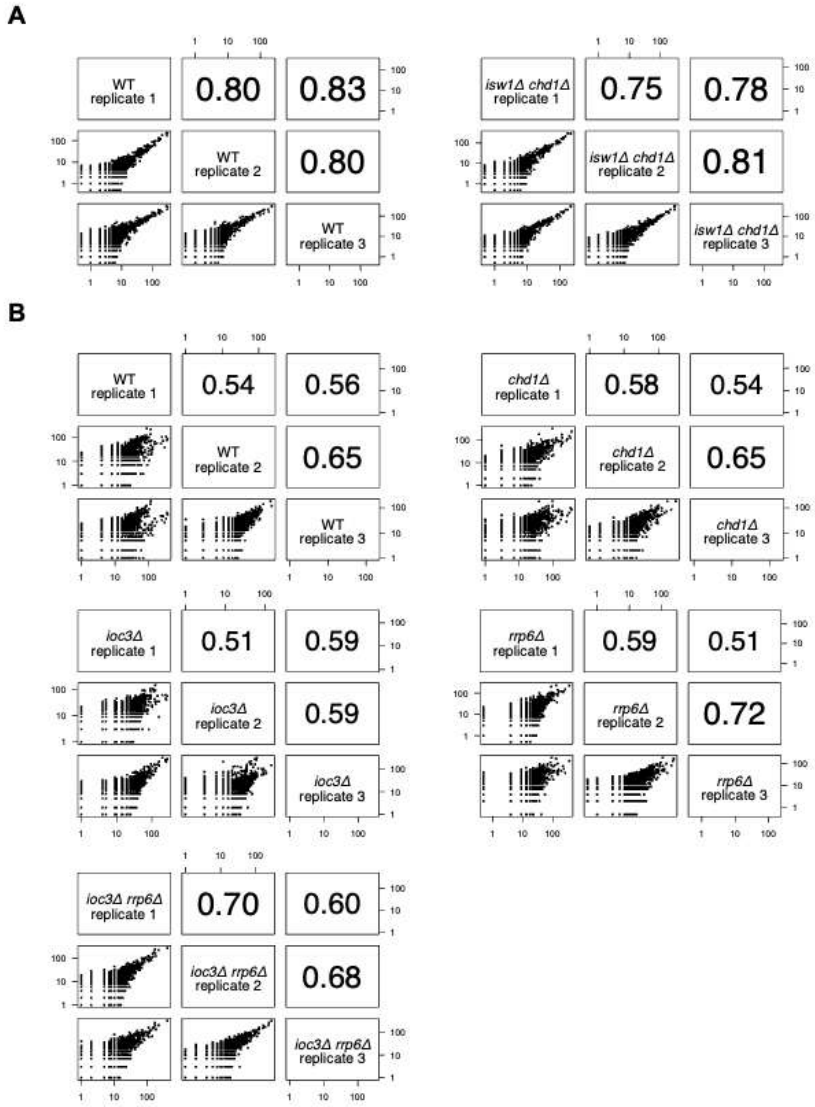

Figure 2.2.2 Sample distances from the first (A) and second (B) 5′cap-seq experiments. Pairwise scatterplots depict the correlation of raw CAGE tag counts per transcription start site (TSS) – TSS tags - across all replicates. Each scatterplot shows the relationship between expression scores in two samples, plotted on a logarithmic scale. Pearson correlation coefficients are displayed for each sample pair.

2.2.3 Annotation and Validation of Isw1 and Chd1-Repressed Antisense Transcripts (ICRATs)

The annotation of antisense transcripts dependent on the *isw1Δ chd1Δ* double deletion was achieved mostly using GenomicRanges (R package), and by combining RNA-seq and 5′cap-seq data from *isw1Δ chd1Δ* and wild-type yeast. To ensure uniform coverage, RNA-seq bam files from *isw1Δ chd1Δ* double mutant and wild-type biological replicates were merged and reads were extended by 200 bps from the start. RNA coverage for both strains was normalized through random subsampling as previously described. Using GenomicRanges (R package), a score threshold of 15 was applied to segment coverage in *isw1Δ chd1Δ*, determined by visual inspection on Integrative Genomics Viewer (IGV). This threshold covered approximately 100% of total coverage (Figure 2.2.3 A). The resulting bed file was exported, and genes, SUTs, and CUTs were subtracted using Bedtools2 v2.28.0. Only antisense features overlapping with asDEGs found in the *isw1Δ chd1Δ*/WT context were retained, with a minimum overlap of 100 bps, to avoid false antisense features representing the end of an adjacent gene. To solve annotation fragmentation, neighboring features were joined based on criteria considering whether a feature contained an antisense TSS cluster at its 5′ end. For this purpose, a less stringent TSS clustering with CAGEr, where singletons were not removed. TCs were extended 250 bps downstream, and the overlap between features and TCs was assessed as follows. If a TC overlapped with the first 100 bps of a feature, this feature would be considered to possess a TC near its 5′ end (Figure 2.2.3 B). Features overlapping containing a TC near the 5′ end were extended 100 bps downstream, while those not overlapping were extended 100 bps on both sides (Figure 2.2.3 C). Overlapping extended features were joined using the reduce function from GenomicRanges (R package), and ends were trimmed back to their original sites (Figure 2.2.3 C). This resize-reduce-trim (RRT) strategy integrating 5′cap-seq data successfully improved the precision of the annotation by reducing the number of features that did not contain a TC around the 5′ end

(Figure 2.2.3 D and E). The annotation was further refined by estimating the differential expression of features using DESeq2 (R package) after STAR alignment against Scer3 transcriptome including the newly annotated features. Potential ICRATs with an adjusted p-value<0.05 and a 1.5-fold expression increase relative to wild-type were visually inspected on IGV and manually curated if necessary. Another differential expression analysis was performed after STAR alignment against Scer3 transcriptome including the manually curated ICRATs. It was again employed a cutoff at 1.5-fold increase in the abundance of the transcripts in the double mutant over the wild-type, to select the final ICRATs. These parameters resulted in the identification of 1918 ICRATs, consisting of transcripts or regions with increased antisense transcription over loss of Isw1 and Chd1 remodelers. To compare ICRAT expression in other remodeler mutants versus wild-type, single mutants *ioc3Δ*, *chd1Δ*, *isw1Δ*, and *ioc3Δ chd1Δ* were subjected to STAR alignment against Scer3 transcriptome, including the final 1918 ICRATs, followed by differential expression analysis. To determine overlapping ORF regions, distinct ORF regions from asDEGs in the *isw1Δ chd1Δ*/WT context were defined based on start = 25%, mid = 25-75%, end = 75-100% of the gene width. If an ICRAT overlapped with both start and mid, it would be considered to overlap with the start of the ORF. The same rationale was applied to "end". If an ICRAT overlapped with start, mid and end parts of the ORF, it would be considered to overlap with all the ORF. Stranded RNA-seq bigWig files from diverse chaperone mutants were retrieved from GEO dataset series GSE110004 and used to visualize their normalized coverage over ICRATs (Wu, Patel et al.).

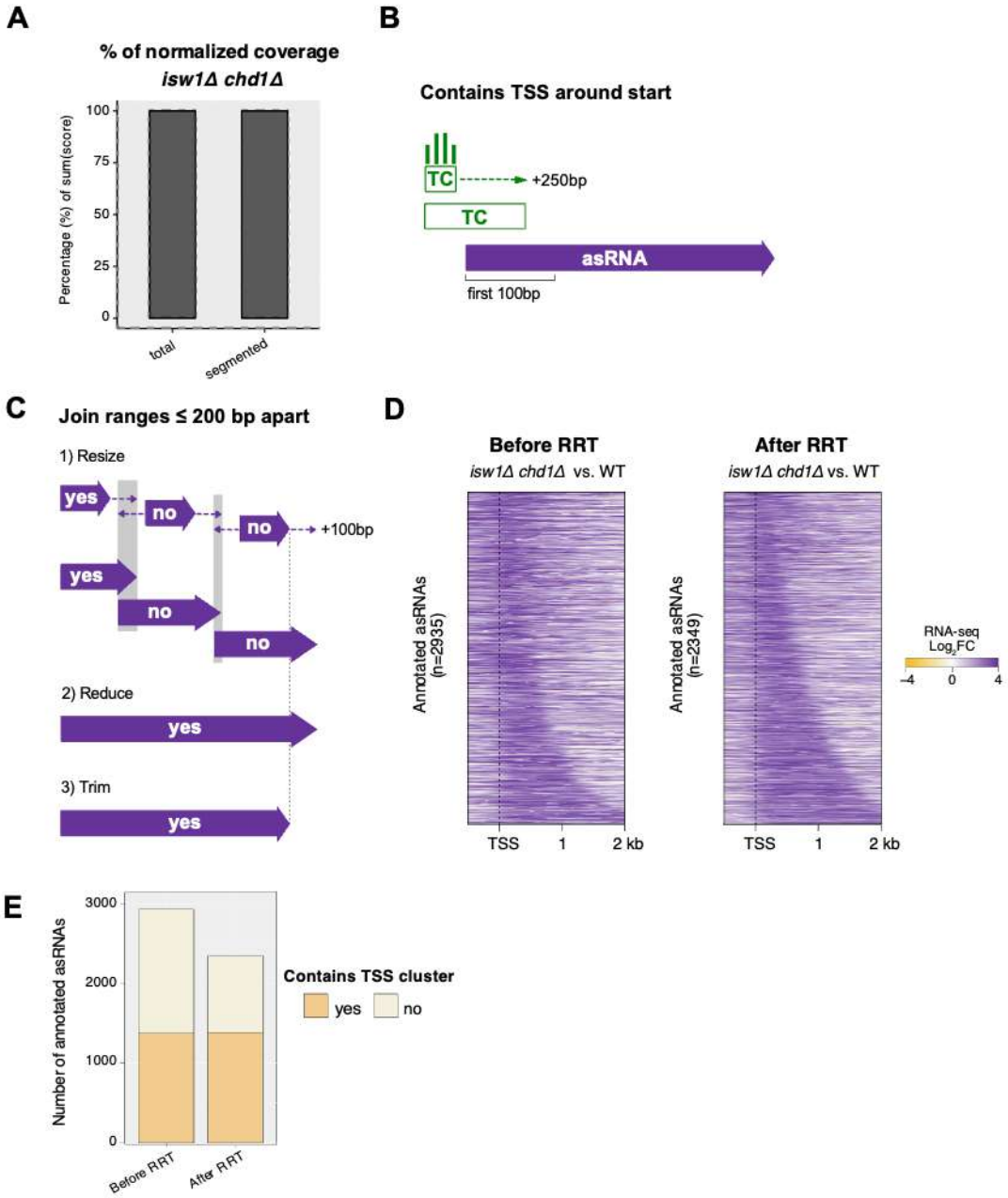

Figure 2.2.3 The Resize-Reduce-Trim method successfully improved the annotation of potential ICRATs. (A) Percentage of score expression before and after coverage segmentation. (B, C) Overview of the Resize-Reduce-Trim (RRT) method: (B) Illustration depicting the consideration of overlapping annotated antisense ranges with a TSS cluster near their 5′ end. (C) Criteria for merging annotated ranges less than 200 base pairs apart. (D) Heatmaps showing RNA-seq normalized signal in *isw1Δ chd1Δ* relative to wild-type over annotated ranges before and after applying the RRT method. The transcripts are aligned by their annotated start coordinate (TSS) and sorted by length. Data is derived from the mean of normalized RNA-seq coverage in 10-nucleotide bins, averaged across three biological replicates. (E) Comparison of the number of annotated ranges containing a TSS cluster near their 5′ end before and after applying the RRT method.

2.2.4 CUT&RUN data processing

Reads were demultiplexed using the indexes incorporated during PCR enrichment, as previously mentioned. Illumina adapters were trimmed using Cutadapt v1.9.1, ensuring reads shorter than 10 bps after adapter removal were discarded. Quality assessment of fastq files was performed using FASQC v0.11.7 before and after trimming. Single-end trimmed reads were mapped to the reference genome (S288C Scer3) using Bowtie2 with parameters suggested in the CUT&RUNTools pipeline: '--local --very-sensitive-local —no-unal', ensuring a more sensitive algorithm for local alignment and leaving out unaligned reads from the output SAM files (Zhu, Liu et al.). Most samples showed over 70% uniquely mapped reads. SAM files were converted to BAM files as previously described. Counts Per Million (CPM) normalization was applied to obtain normalized coverage using Deeptools v3.5.0 and the 'bamCoverage' command with the parameters '--effectiveGenomeSize 12157105 --binSize 10 --normalizeUsing CPM'. Peak calling was performed with MACS2 v2.1.2 using the narrowPeak setting and specific parameters '-g 12000000 --keep-dup all -q 0.0001 --mfold 1 50 --min-length 50 --max-gap 170'. All duplicate reads were retained in the final MACS2 analysis, following the recommendation in CUT&RUNTools due to potential bias introduced by pAG-MNase cleavage. De novo motif discovery was conducted on the top peaks from a test sample, "FLAG_Ioc3-Flag_R1," using MEME suite. The top 600 peaks with higher fold-change were selected. Sequences underlying the selected peaks were retrieved using Bedtools v2.28.0 as before mentioned. XSTREME option was selected to find de novo and enriched motifs with default parameters. Common peaks between replicates and peak classification based on genomic location were assessed and plotted using the ChIPpeakAnno (R package). Heatmaps for peaks aligned to Rap1 or Reb1 motifs were generated in R, recurring to Rap1 and Reb1 binding sites previously reported (Rhee and Pugh).

2.2.5 ChIP-seq data processing

The pre-processing and coverage normalization was conducted by Lingling Yang from the Department of Physiology Chemistry. All immunoprecipitated DNA samples were first normalized to their corresponding input. H2A.Z/input and H3K4me3/input samples were then normalized to histone H3/input data.

3 Results

3.1 Isw1 and Chd1 prevent cryptic initiation at thousands of genes

The cryptic phenotype observed in yeast cells lacking Chd1 and Isw1 catalytic subunits has been demonstrated through microarray and northern blot analyses targeting specific genes (Smolle, Venkatesh et al. 2012). Microarray expression profiling in *isw1Δ chd1Δ* compared to wild-type cells revealed the accumulation of sense intragenic transcription predominantly over the 3′ end of 646 genes, as well as antisense transcription particularly over the 5′ end of 962 genes (Smolle, Venkatesh et al. 2012).

In order to overcome the constrained sensitivity associated with microarray data and to gain a more comprehensive understanding of the influence of Isw1 and Chd1 on cryptic transcription, I performed strand-specific RNA-seq on *isw1Δ chd1Δ* and wild-type cells (Draghici, Khatri et al. 2006). To get an overview of transcription phenotypes caused by deletion of Isw1 and Chd1 ATPases, I compared the changes in RNA-seq normalized coverage of both sense and antisense strands of protein-coding genes in *isw1Δ chd1Δ* versus wild-type. I observed that the majority of genes exhibiting increased levels of antisense transcription did not show significantly altered sense expression levels in the double mutant compared to wild-type (Figure 3.1.1 A, n=2582). This indicates that, generally, the increase in asRNA production in the double mutant does not seem to negatively interfere with the mRNA production, as these mRNA levels tend to remain unchanged. However, I could observe a second largest subset of genes with increased levels of both sense and antisense transcription (Figure 3.1.1 A, n=1238). Overall, deleting Isw1 and Chd1 seems to trigger a transcriptional derepression phenotype that is more prevalent in the antisense direction.

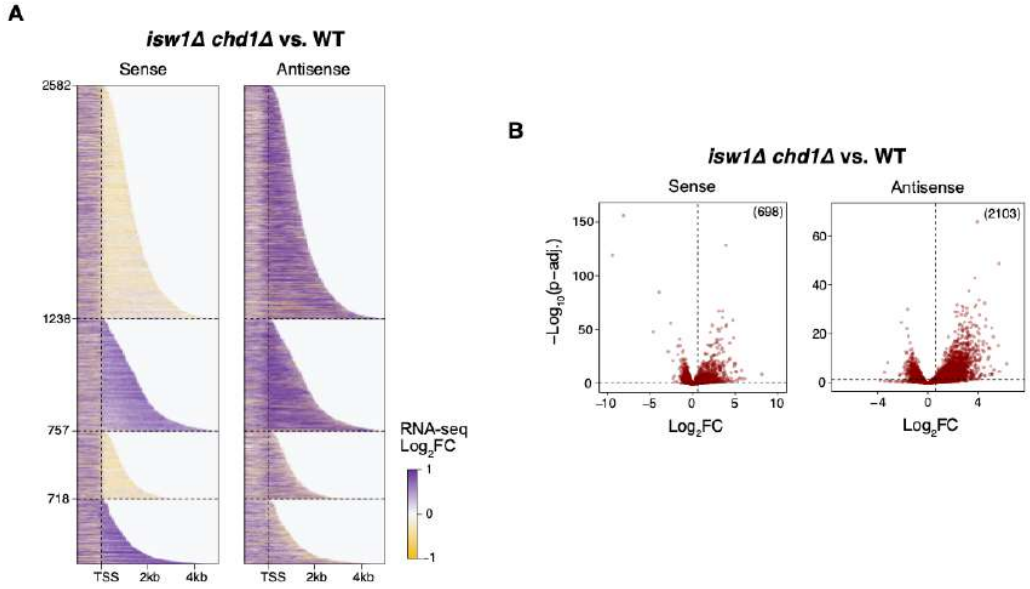

Figure 3.1.1 Deleting Isw1 and Chd1 leads to transcription derepression at thousands of genes. (A) Gene expression clustering. Heatmaps show transcriptional changes in *isw1Δ chd1Δ* compared to wild-type for 5173 protein-coding genes. Genes are sorted into four clusters based on changes in antisense and sense expression and ordered by length. The clustering was determined using the logarithm base 2 of fold-change (log_2FC) calculated by DESeq2 for *isw1Δ chd1Δ* versus wild-type. From top to bottom, clusters are organized as (1) sense $log_2FC < 0$ and antisense $log_2FC > 0$ (n=2582), (2) both sense and antisense $log_2FC > 0$ (n=1238), (3) both sense and antisense $log_2FC < 0$ (n=757), and (4) sense $log_2FC > 0$ and antisense $log_2FC < 0$ (n=718). RNA-seq values represent the mean of normalized coverage in 10-bp bins, averaged over three biological replicates. (B) Results of sense and antisense differential expression analysis performed on *isw1Δ chd1Δ* versus wild-type yeast. The dashed line represents significance (adjusted p-value of 0.05). Red indicates upregulated genes, and blue indicates downregulated genes (1.5-fold-change). The number of upregulated or derepressed genes is indicated.

Differential gene expression analysis (adjusted p-value ≤ 0.05 and a ≥1.5-fold-change) confirmed this transcriptional derepression phenotype, revealing 698 genes with increased sense expression and approximately 35% of yeast genes with increased antisense expression (n=2103) (Figure 3.1.1 B). Only a few genes were down-regulated (n=72) while 215 genes showed down-regulated antisense levels (Figure 3.1.1 B). Upon visual inspection of the RNA-seq coverage tracks, I observed that the most of the down-regulated asRNAs corresponded to reads coming from

the end of nearby genes or to small (< 100 bps) overlapping dubious ORFs, while other down-regulated asRNAs corresponded to previously identified ncRNAs.

While strand-specific RNA-seq easily enables the identification of antisense RNA levels, it also prevents an easy discrimination between mRNA levels and sense cryptic RNA expression. Through visual exploration of RNA-seq tracks on the integrative genomics viewer (IGV), I noticed that the derepressed sense differentially expressed genes (sDEGs) seemed to accumulate cryptic intragenic sense RNAs in the double mutant. To discern between increased mRNA levels and sense intragenic transcripts, I employed 5′cap-seq to map the transcription start sites (TSSs) genome-wide. This technique provides knowledge on the promoter exposure and expression levels of the start site of capped RNA molecules (Pelechano, Wei et al. 2016). For each strain, the number of TSS reads per unique capped molecule at a specific genomic position were collapsed, forming a TSS tag. Subsequently, TSS clusters (TC) were defined as a region in the genome containing multiple TSS tags up to 60 bps apart. While the number of sense and antisense intragenic TCs was remarkably increased in the double mutant compared to wild-type (Figure 3.1.2 C, E, F), the abundance and expression of gene promoter TCs remained similar (Figure 3.1.2 C and D). These findings strongly suggest that the sense derepression observed in RNA-seq derives from sense intragenic cryptic transcripts rather than mRNAs.

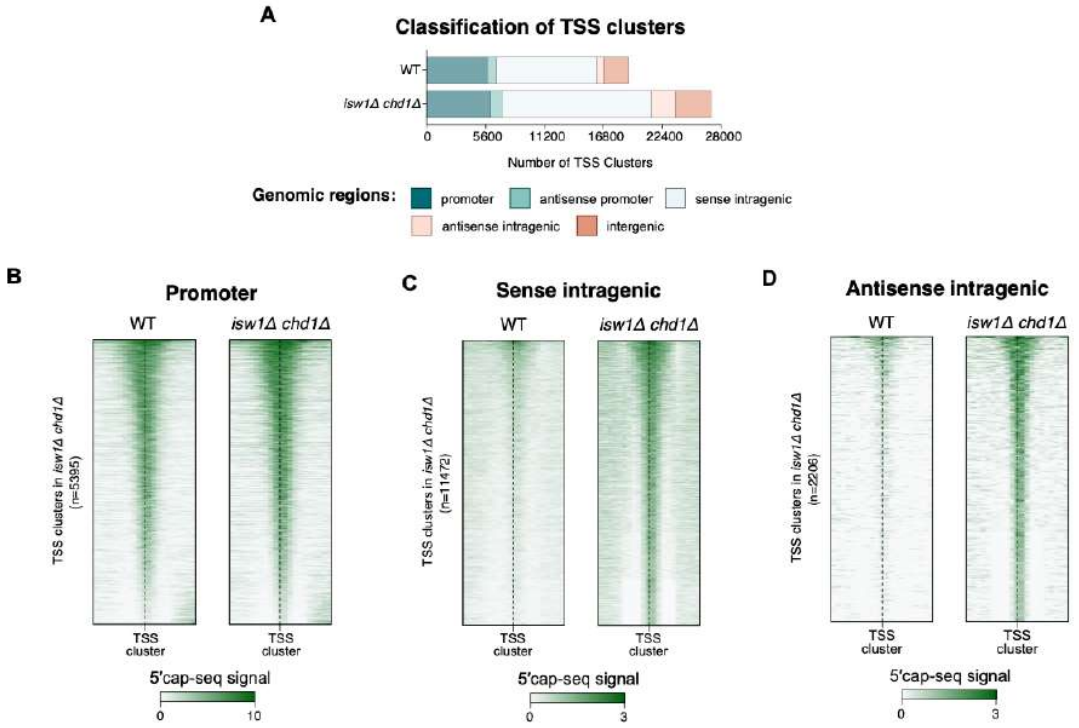

Figure 3.1.2 Loss of both ISW1 and CHD1 leads to exposure of thousands of intragenic promoters. (A) Classification of TSS clusters (TCs) in wild-type and *isw1Δ chd1Δ* double mutant based on genomic location. (B-D) Normalized 5′cap-seq signal in wild-type and *isw1Δ chd1Δ* strains surrounding gene promoter TCs (B), sense intragenic TCs (C) and antisense intragenic TCs (D). Heatmaps display a 200 bp window flanking the TC centroid. Values represent the sum of normalized coverage in 20-bp bins, merged from three biological replicates.

Previously published Northern blot analyses have showed a strong cryptic phenotype for *isw1Δ chd1Δ* compared to wild-type in specific genes, including *PCA1* (Smolle, Venkatesh et al. 2012). In one of these northern blots, where probes were directed against the 3′ end of the *PCA1* gene, at least three derepressed sense cryptic transcripts were revealed in *isw1Δ chd1Δ* cells. Overlapping 5′cap-seq and RNA-seq normalized coverage data, allowed me to detect the presence of intragenic TSS tags marking the start of *PCA1* sense cryptic transcripts in *isw1Δ chd1Δ* cells (Figure 3.1.3, Supplementary Figure 3.10.1 A). Furthermore, overlapping 5′cap-seq and RNA-seq normalized signals also suggested that some intragenic cryptic promoters may also be bidirectional, given the presence of both

sense and antisense increased transcript levels and corresponding TCs in the double mutant (Figure 3.1.3).

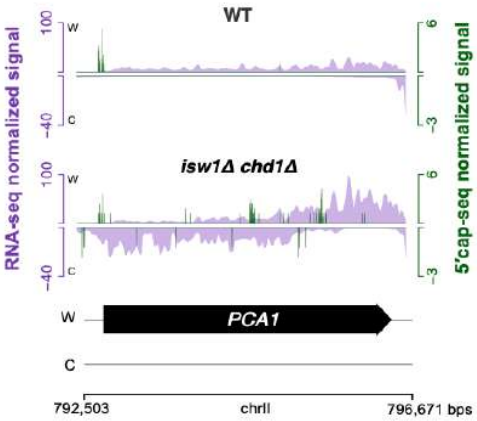

Figure 3.1.3 Representative gene *PCA1* shows increased sense and antisense TSS and RNA expression in *isw1Δ chd1Δ* compared to wild-type. RNA-seq (purple) and 5′cap-seq (green) normalized coverage are presented. RNA-seq values are the mean of normalized coverage in 10-bp bins, averaged over three biological replicates. 5′cap-seq values are the normalized coverage merged from three biological replicates. Watson (W) and Crick (C) strands are indicated, as well as genomic coordinates.

Next, I wanted to determine whether a specific region within the gene body was more susceptible to the exposure of a cryptic promoter in *isw1Δ chd1Δ* cells. To do this, I first divided ORF regions of protein-coding genes into start, mid, and end regions, where start represents the first 25% of gene width, mid represents the region from 25-75% of gene width and end represents the last 25%. Then I overlapped the sense and antisense intragenic TCs with these regions, assigning each TC to a gene region. In both wild-type and double mutant, intragenic TCs are more prominent at mid-3′ end of genes. Compared to sense intragenic TCs, antisense intragenic TCs are substantially more abundant in the double mutant relatively to wild-type, which may suggest that sense intragenic transcription may be more tightly regulated than the antisense one (Figure 3.1.4).

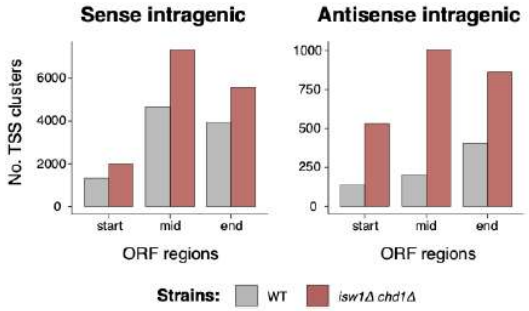

Figure 3.1.4 Distribution of intragenic TSS clusters across gene regions in wild-type and *isw1Δ chd1Δ* yeast. Open reading frame regions are divided into three regions based on percentage of gene width: start=25%, mid=25-75%, and end=75%-100%.

Overall, the application of high-throughput sequencing methodologies has substantially improved the detection of cryptic transcripts and their respective TSSs, providing a more detailed characterization of the additive cryptic phenotype seen in the *isw1Δ chd1Δ* double mutant. Consequently, this highlights the significant role of Isw1 and Chd1 remodelers in maintaining chromatin structure during RNAPII elongation by preventing the exposure of numerous intragenic promoters.

3.2 Characterization of Isw1 and Chd1-repressed antisense transcripts

Various groups of cryptic transcripts have been annotated in yeast. As mentioned before, stable unannotated transcripts (SUTs), a group of non-coding RNA species can be found in wild-type cells (Xu, Wei et al. 2009). Deleting *RRP6*, the catalytic subunit of the nuclear exosome, reveals the accumulation of cryptic unstable transcripts (CUTs) (Xu, Wei et al. 2009). In yeast lacking the H3K36 methyltransferase Set2, a group of antisense RNA species has been identified and referred to Set2-repressed antisense transcripts (SRATs) (Venkatesh, Li et al. 2016). The identification of these ncRNAs has allowed follow-up studies on their regulatory functions.

I decided to annotate Isw1 and Chd1-dependent antisense ncRNAs in order to (1) gain biological insights when investigating the individual contributions of Isw1 and Chd1 remodelers, (2) to compare with published RNA-seq data from other factors crucial to maintaining chromatin structure, and (3) to constitute a valuable resource for follow-up studies, particularly in the chromatin organization and non-coding transcription research communities. To annotate these cryptic transcripts, I primarily used the RNA-seq data from the double mutant, which is also why sense intragenic transcripts were not included, given that their expression signal is obscured by the coverage signal emanating from mRNA. Isw1 and Chd1-Repressed Antisense Transcripts (ICRATs) were annotated to encompass the antisense differentially expressed genes (asDEGs) identified in the *isw1Δ chd1Δ* versus wild-type context. A representative example of an asDEG, *FLO10*, with the overlapping ICRAT is depicted in Figure 3.2.1 A (Supplementary Figure 3.10.1 B). The annotation and validation process I conducted, as described in the Methods section 2.2.3, successfully covered 80% of asDEGs, resulting in the identification of 1918 ICRATs (Figure 3.2.1 B and C). The remaining 20% of asDEGs exhibited minimal coverage on the antisense strand, leading to their exclusion during the annotation process. While some asDEGs contained two or more ICRATs, the majority of asDEGs contain a single ICRAT (Figure 3.2.1 D). Additionally, there was a modest correlation between the length of the asDEGs and the number of overlapping ICRATs, with longer genes being more prone to having multiple asRNAs (Figure 3.2.1 E).

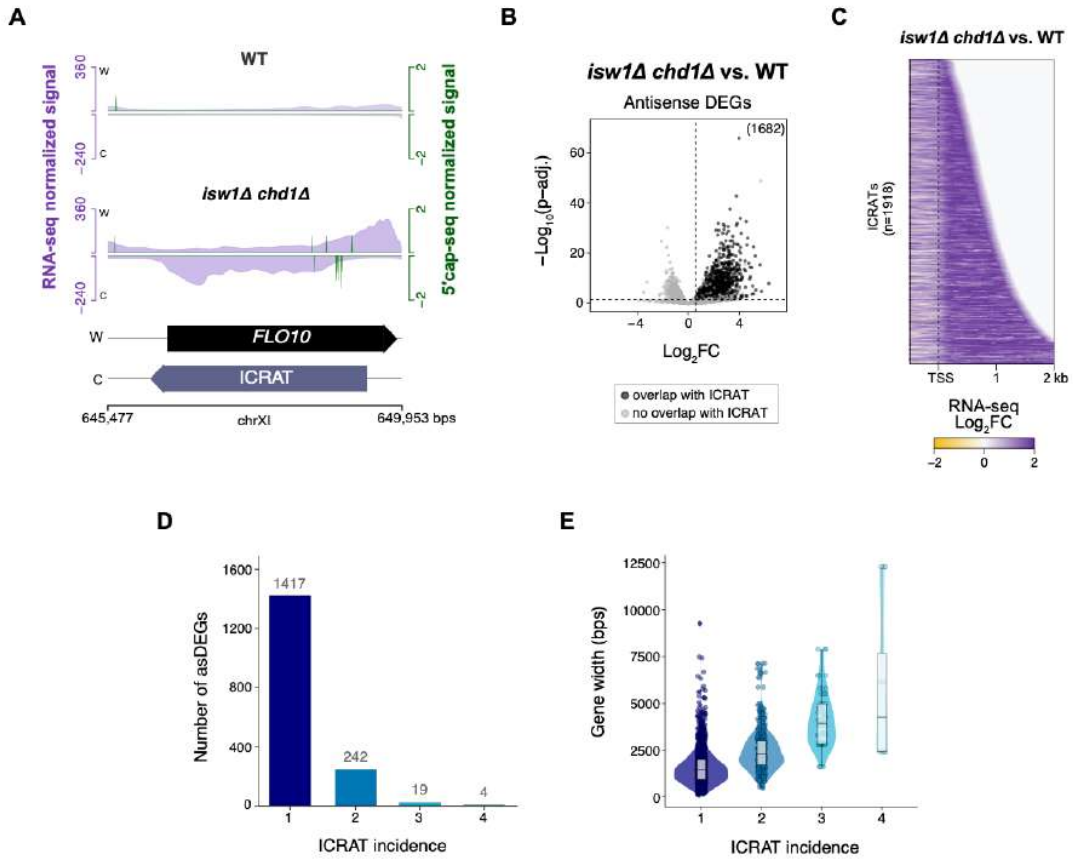

Figure 3.2.1 Annotated Isw1 and Chd1-repressed antisense transcripts (ICRATs). (A) Representative ICRAT overlapping with *FLO10*. RNA-seq (purple) and 5′cap-seq (green) normalized coverage are presented. RNA-seq values are the mean of normalized coverage in 10-bp bins, averaged over three biological replicates. 5′cap-seq values are the normalized coverage merged from three biological replicates. Watson (W) and Crick (C) strands are indicated, as well as genomic coordinates. (B) Derepressed asDEGs containing ICRATs (n=1682). Significance and fold-change thresholds are represented with dashed lines. (C) Heatmap of ICRATs expression. The heatmap displays the log_2FC of the RNA-seq normalized coverage in *isw1Δ chd1Δ* over wild-type for 1918 ICRATs. Transcripts were aligned by their annotated start coordinate and ordered by their length. Data was obtained from the mean of normalized RNA-seq coverage in 10-bp bins, averaged over three biological replicates. (D) Number of derepressed asDEGs genes that overlap with one or more ICRATs. (E) Width of derepressed asDEGs genes that overlap with one or more ICRATs.

To further characterize ICRATs, I looked into RNA features that confer molecular stability and protection against degradation such as capping and poly-adenylation. Both 5′cap-seq and RNA-seq techniques target polyadenylated transcripts, but while uncapped RNA levels can be identified with RNA-seq, only capped molecules are detected through 5′cap-seq. To test how many ICRATs are

capped, I determined the TCs that are located near the start of ICRATs by extending TCs 250 bps downstream and crossing them against the first 100 bps of ICRATs. The majority of the annotated cryptic transcripts are capped, with a cumulative count of 1275 ICRATs featuring a TSS cluster in close proximity to the 5′ end (Figure 3.2.2 A and B). These findings imply that a substantial proportion of ICRATs are capped polyadenylated transcripts. Since capping and polyadenylation are essential for RNA maturation and resilience against degradation, the accumulation of ICRATs in *isw1Δ chd1Δ* cells could result from RNA stability or from an excess of asRNA production resulting in a slower degradation (Ramanathan, Robb et al. 2016, Passmore and Coller 2022). However, like other lncRNAs, ICRATs display lower expression levels compared to mRNAs.

Identifying and understanding the presence of DNA regulatory elements in the promoter region of ICRATs could help elucidating the mechanism of their transcription initiation and functional relevance. To gain insight into possible sequence determinants of ICRATs transcription initiation, I examined the promoter-proximal regions of these transcripts for enriched sequence elements by de novo motif analysis. In *S.cerevisiae*, TATA boxes can be found 40 to 120 bps upstream the TSS (Hahn, Hoar et al. 1985). I defined the TSS clusters of the capped ICRATs with an extension of 250 bps upstream and 50 bps downstream as the promoter-proximal regions for de novo motif analysis with two different tools. MEME suite tool (https://meme-suite.org/meme/index.html), brought up TATA in the context of an extended dinucleotide repeat sequence over 235 sites (Figure 3.2.2 C). While this could suggest that a fraction of cryptic promoters might bear TATA box (TATAWAWR) elements, it could also be a consequence of MEME's high sensitivity for dinucleotide repeat sequences. To explore the consistency of MEME's findings, I performed de novo motif search using HOMER. This analysis also identified a single significant motif (TATATWWTATWW), bringing up TATA as MEME did (Supplementary Figure 3.10.2 A). However, HOMER interpreted this motif as A/T sequence bias, likely deriving from a systematic bias between the target (ICRATs' TSS clusters) and background sequences (all protein-coding yeast gene promoters). When using the entire genome of *S. cerevisiae* as the background

sequence, HOMER did not detect any significant motifs (Supplementary Figure 3.10.2 B). These findings suggest that the cryptic promoters within ICRATs may lack discernible DNA regulatory elements.

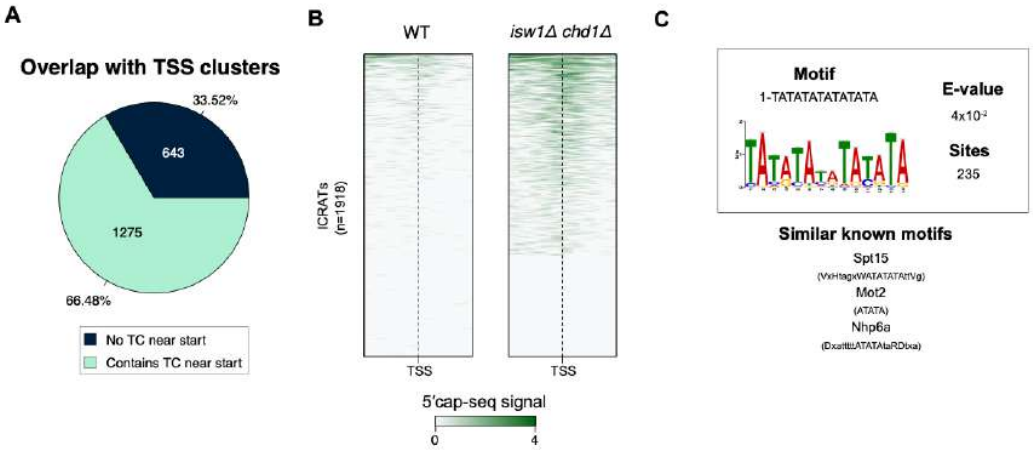

Figure 3.2.2 Capped ICRATs and promoter motif analysis. (A) Proportion of capped and uncapped ICRATs. (B) Normalized 5′cap-seq coverage in wild-type and *isw1Δ chd1Δ* strains surrounding the start of ICRATs. ICRATs were aligned by their start coordinate and ordered by signal strength in the *isw1Δ chd1Δ* double mutant. Data shown for 0.2 kb around ICRATs start site. Values represent the sum of normalized coverage in 20-bp bins, merged from three biological replicates. (C) De novo motif analysis by MEME suite, performed on extended TSS clusters from capped ICRATs. MEME suite identified one motif with e-value < 0.05 and identified similar known motifs.

Differential expression analysis of previously identified non-coding transcripts (SRATs, SUTs and CUTs) revealed an evident increase in SRAT expression in *isw1Δ chd1Δ* relatively to wild type (Figure 3.2.3 A). While annotating ICRATs, I filtered out those overlapping with SUTs and CUTs but not SRATs. As I mentioned before, SRATs are antisense transcripts expressed in the absence of histone methyltransferase Set2 (Venkatesh, Li et al. 2016). When I evaluated the overlap between ICRATs and SRATs, I observed that only approximately 9% of ICRATs displayed an equal overlap with SRATs, while the majority of ICRATs either did not overlap or demonstrated an irregular overlap with SRATs (26%) (Figure 3.2.3 B). I considered an identical or even overlap if 80% of the width of both transcripts overlapped. An uneven or irregular overlap was considered if both transcripts

overlapped but with less than 80% of their length. The majority of ICRATs did not overlap with SRATs at all (Figure 3.2.3 B). Given that these observations point to a significant lack of similarity regarding genomic locations, I decided to not filter out SRATs from the final ICRATs. This also suggests that the suppression of antisense transcripts by Isw1 and Chd1 may involve a mechanism distinct from that associated with Set2.

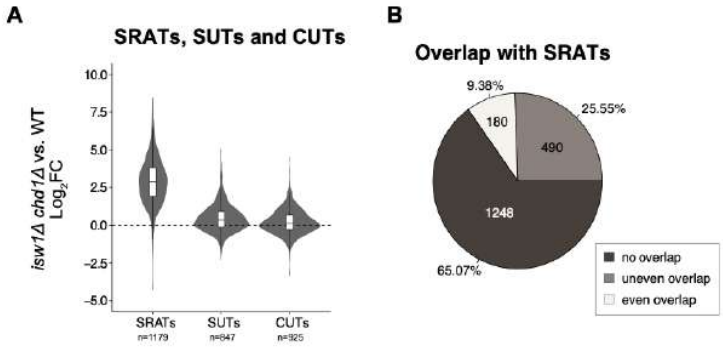

Figure 3.2.3 SRATs are the most derepressed group of annotated ncRNAs in yeast, yet they show poor overlap with ICRATs. (A) Changes in expression levels for three groups of annotated non-coding RNAs (ncRNAs; SRATs, SUTs and CUTs), as determined by differential expression analysis on *isw1Δ chd1Δ* versus wild-type. The total number of ncRNAs in each group is indicated. (B) Results of overlap analysis show the number and percentage of ICRATs overlapping with SRATs. Types of overlap categorized as "even" or "uneven" were determined based on a threshold of 80% of the length of both ICRAT and SRAT or any type of overlap, respectively.

Similar to Set2, Spt21, Spt10, Spt6, and FACT are essential factors for maintaining chromatin structure integrity and have been shown to suppress cryptic transcription in yeast (Wu, Patel et al. 2018). Without either Spt10 or Spt21, the mRNAs from genes encoding one of the two copies of the canonical histones H2B (*HTB2*) and H4 (*HHF2*) are either not detectable or drastically reduced (Dollard, Ricupero-Hovasse et al. 1994). Histone chaperones Spt6 and FACT participate in the reassembly of nucleosomes in the wake of RNAPII passage (Duina 2011). To investigate whether these factors also suppress ICRATs, I retrieved RNA-seq normalized coverage data from GEO for yeast cells depleted of Spt10 or Spt21, or impaired in Spt6 or the FACT component Spt16, and examined ICRAT expression

levels. On a general level, the RNA-seq data from these cells revealed transcriptional derepression over the ICRATs compared to their respective wild-type, with FACT-impaired cells showing the most pronounced derepression phenotype (Figure 3.2.4 A and B). When comparing Figure 3.2.1 C and Figure 3.2.4 A, I notice that the initiation sites of many of these asRNAs may differ. These findings suggest that Isw1 and Chd1 are not the sole contributors for suppressing the expression of these asRNAs in yeast. However, a differential expression analysis would elucidate with more accuracy how many ICRATs are significantly derepressed in these GEO datasets.

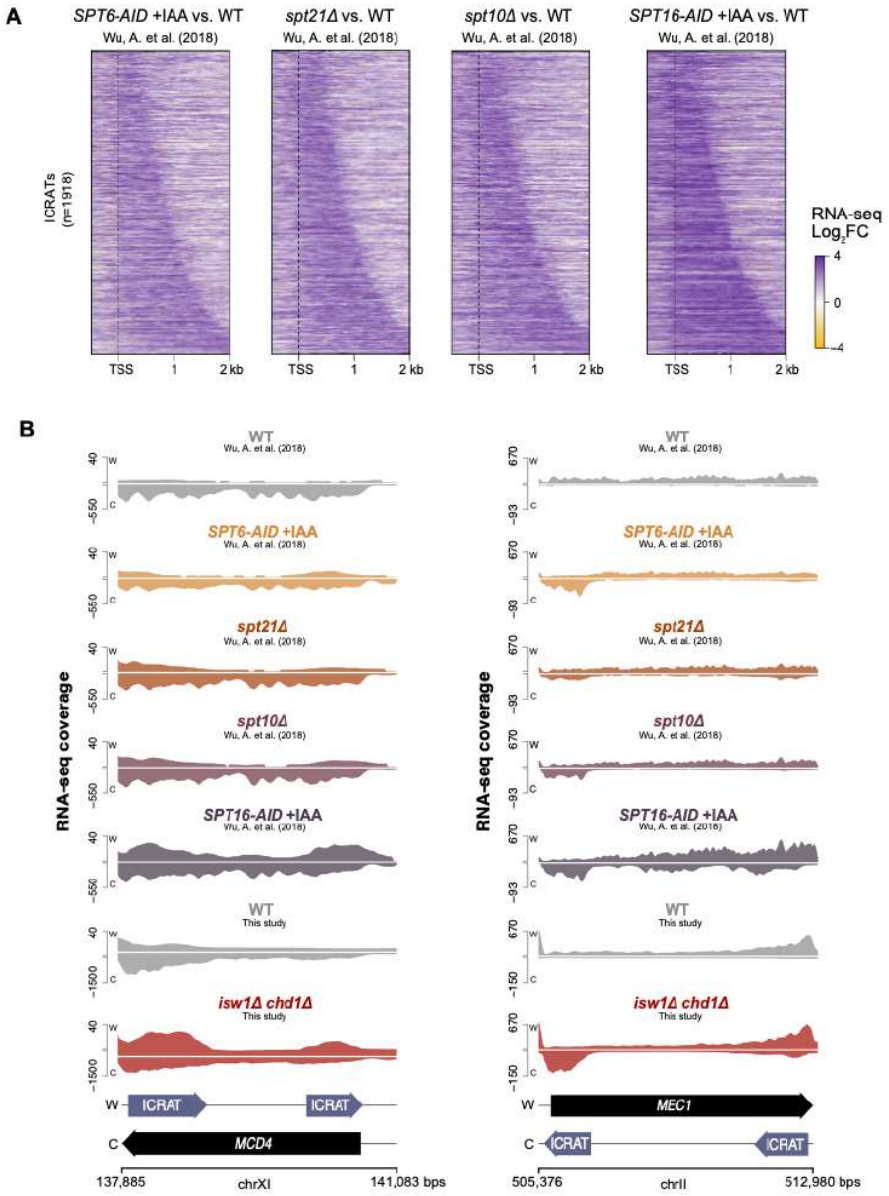

Figure 3.2.4 The FACT complex, among other factors involved in chromatin structure, may also regulate ICRAT expression. (A) Heatmaps display the log_2FC of the RNA-seq normalized coverage over 1918 ICRATs in Spt6-deficient, *spt21Δ*, *spt20Δ*, and Spt16-deficient cells versus wild-type. Transcripts were aligned by their annotated start coordinate and ordered by their length. Data was obtained from the mean of normalized RNA-seq coverage in 10-bp bins, averaged over two biological replicates. (B) Representative ICRATs overlapping with MCD4 and MEC1. RNA-seq normalized coverage are presented for the chromatin mutants and respective wild-type, as well as for *isw1Δ chd1Δ* and wild-type strains used in this study. RNA-seq values are the mean of normalized coverage in 10-bp bins, averaged over two biological replicates for the retrieved data and three biological replicates for the data in this study. Watson (W) and Crick (C) strands are indicated. (A, B) RNA-seq coverage values from chaperone mutant strains and respective wild-type yeast were retrieved from published data (Wu, Patel et al. 2018).

3.3 Individual contributions of Isw1 and Chd1 chromatin remodelers to suppressing cryptic transcription

In yeast, the Isw1 ATPase exists in two chromatin remodeling complexes known as ISW1a (Isw1/Ioc3) and ISW1b (Isw1/Ioc2/Ioc4) (Tsukiyama, Palmer et al. 1999, Vary, Gangaraju et al. 2003). Deleting *ISW1* abolishes both ISW1a and ISW1b, whereas deleting any *IOC3* or *IOC4* additional subunits prevents the formation of ISW1a or ISW1b, respectively. Western blot analysis of *ioc3Δ* cells showed no influence in both Isw1 and Ioc4 protein levels (Figure 3.3.1). Similarly, deleting *IOC4* did not change overall Isw1 and Ioc3 protein levels (Figure 3.3.1). This suggests that the absence of Ioc3 does not prompt the formation of additional ISW1b complexes and vice-versa.

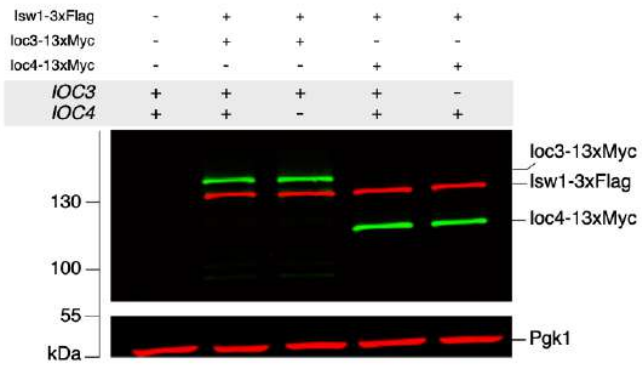

Figure 3.3.1 *IOC3* deletion does not influence the overall levels of Ioc4 protein in cells, and vice-versa. Western blot results of Isw1-3xFlag (134 kDa), Ioc3-13xMyc (110 kDa), and Ioc4-13xMyc (95 kDa) protein expression levels in the presence and absence of *IOC3* or *IOC4*. Pgk1 (44 kDa) was used as loading control. Representative gel from one of three independent experiments.

While ISW1b has been reported to suppress cryptic transcription together with Chd1 over mid-3′ end of genes, the role of ISW1a in regulating cryptic transcription has not been described (Smolle, Venkatesh et al. 2012, Li, Bergmann et al. 2022). Preliminary northern blot analysis suggests that ISW1a may also play a role with Chd1 in regulating cryptic transcription (Figure 1.6.4). Therefore, following the characterization of the cryptic transcriptional phenotype in the *isw1Δ chd1Δ*

double mutant, I explored the individual contributions of Chd1 and Isw1 remodelers, particularly ISW1a. To this end, I performed RNA-seq in the single mutants *ioc3Δ, isw1Δ and chd1Δ* as well as in *ioc3Δ chd1Δ* yeast cells.

First, I evaluated the Pearson correlation coefficient of pairwise comparisons between *isw1Δ chd1Δ* and single mutants *isw1Δ and chd1Δ* for both sense and antisense expression differences. Notably, there was a substantial correlation between the double mutant and single mutants (Figure 3.3.2 A and B). Pairwise comparisons between *isw1Δ* and *chd1Δ* single mutants resulted in a reduced correlation coefficient and indicated that in some genes, Isw1 is the main remodeler responsible for transcription derepression, whereas in other genes Chd1 is the main suppressor of transcription (Figure 3.3.2 A and B, far right).

To see how many derepressed differentially expressed genes (DEGs, adjusted p-value ≤ 0.05 and a ≥1.5-fold-change) are shared or unique between these mutants, I crossed the DEGs between all three mutants (*isw1Δ, chd1Δ,* and *isw1Δ chd1Δ)*. I observed a large number of genes with derepressed sense and antisense transcription in the double mutant, suggesting that these genes are dependent on the functions of both Isw1 and Chd1 remodelers to prevent cryptic transcription, and highlighting the additive cryptic phenotype of the double mutant (Figure 3.3.2 D). This cross-examination also pointed to Chd1 as the primary suppressor of sense and antisense transcription, as the overlap of sense and antisense DEGs was larger between the double mutant and *chd1Δ* than *isw1Δ* single mutant (Figure 3.3.2 D).

The role of Chd1 remodeler as primary suppressor of sense and antisense transcription is strikingly evident when I assessed the Pearson correlation of pairwise comparisons and cross-examination of derepressed asDEGs between *ioc3Δ chd1Δ* double mutant and *ioc3Δ* and *chd1Δ* single mutants (Figure 3.3.3 A, B and C). Additionally, 471 derepressed asDEGs are exclusively detected in the *ioc3Δ chd1Δ* double mutant, suggesting a critical interplay between ISW1a and Chd1 in preventing antisense transcription in these genes (Figure 3.3.3 C and D).

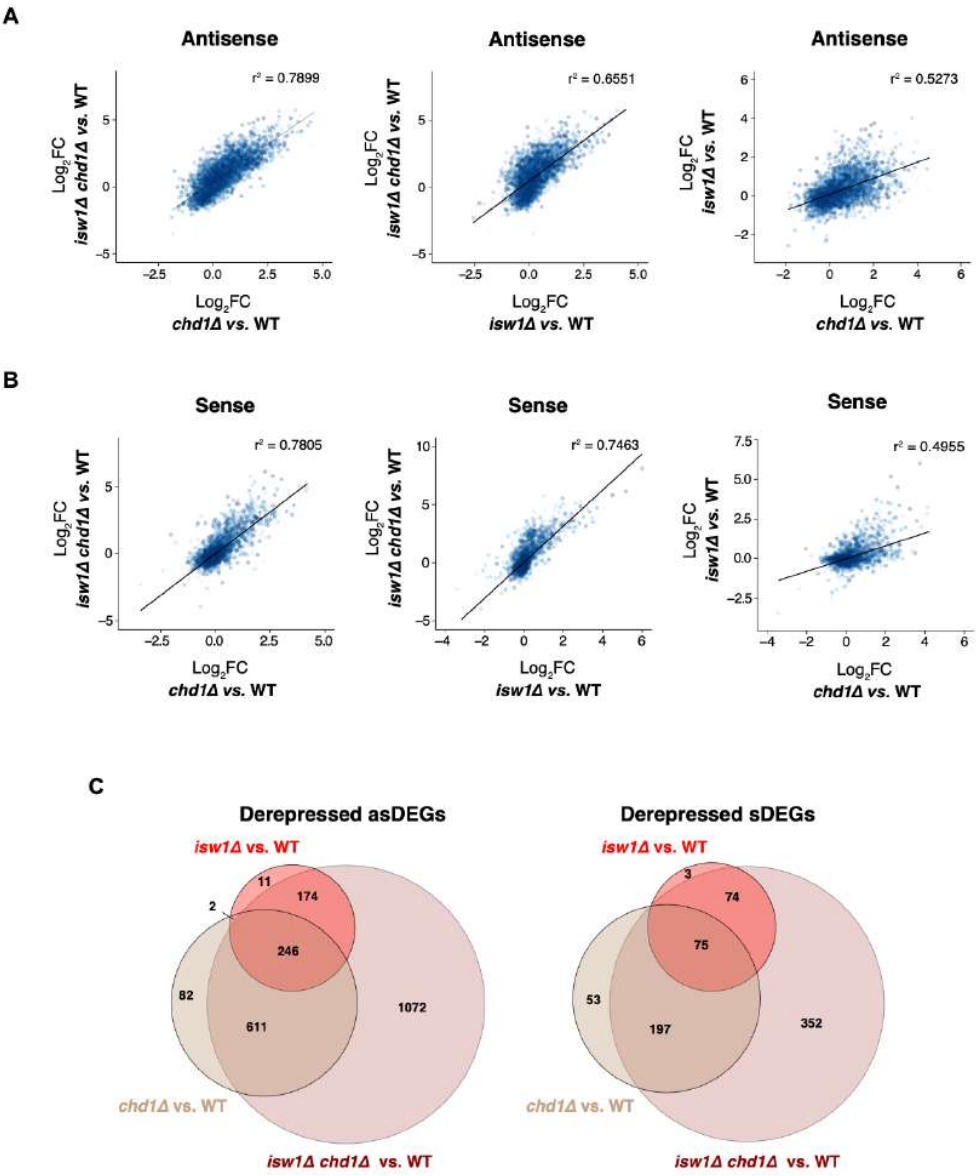

Figure 3.3.2 Relationships between *isw1Δ chd1Δ* and/or single remodeler mutants compared to wild-type yeast. (A, B) Pairwise comparisons of antisense (A) and sense (B) expression levels between distinct *MUT*/WT contexts. Pearson correlation coefficient values are indicated. Only non-overlapping protein-coding genes were considered. (C) Overlap between sense or antisense derepressed genes, as determined by differential expression analysis on *chd1Δ*, *isw1Δ* and *isw1Δ chd1Δ* versus wild-type.

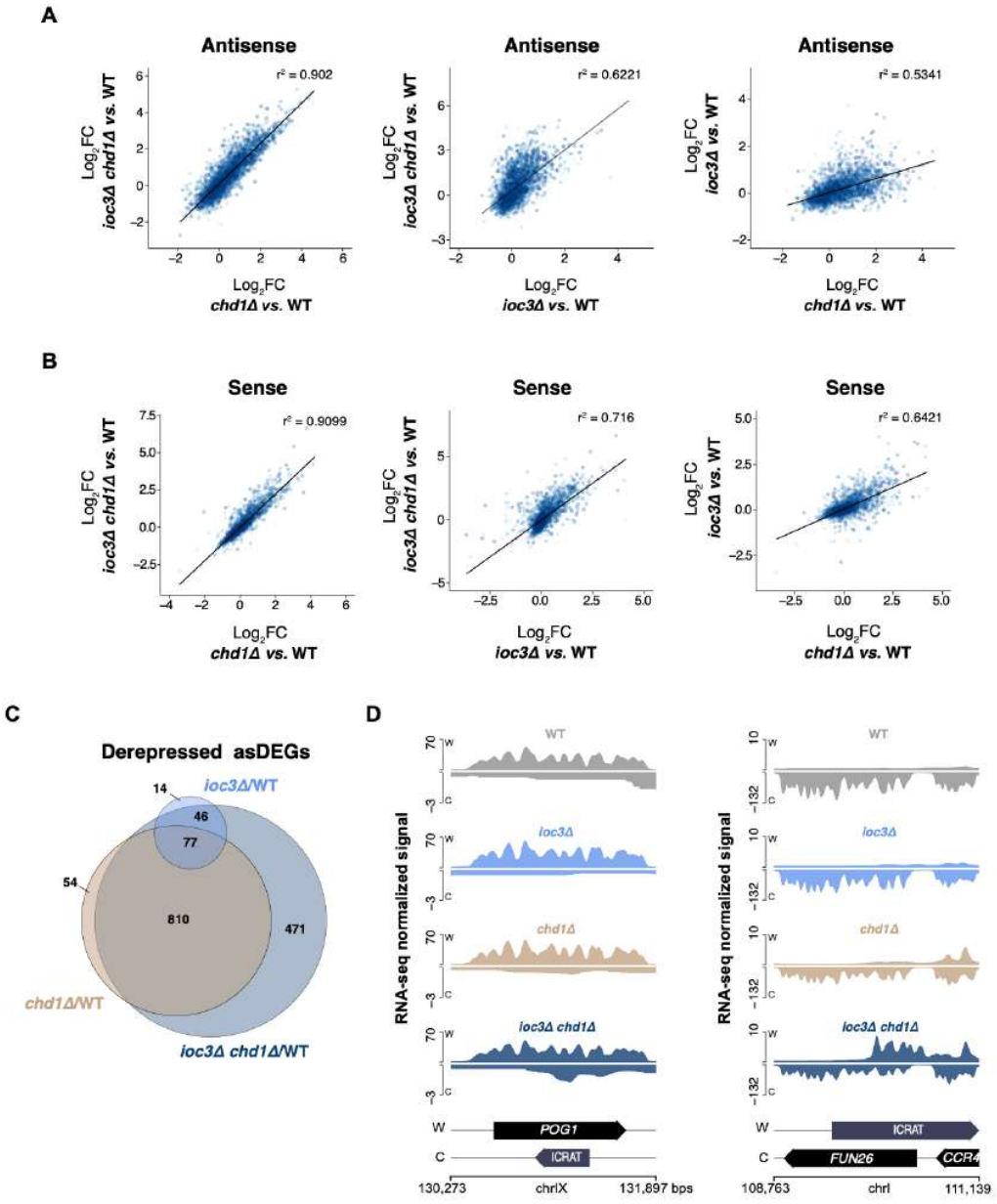

Figure 3.3.3 Chd1 is a major suppressor of cryptic transcription, and cooperates with ISW1a remodeler at hundreds of genes. (A, B) Pairwise comparisons of antisense (A) and sense (B) expression levels between distinct *MUT*/WT contexts. Pearson correlation coefficient values are indicated. Only non-overlapping protein-coding genes were considered. (C) Overlap between sense or antisense derepressed genes, as determined by differential expression analysis on *ioc3Δ*, *chd1Δ* and *ioc3Δ chd1Δ* versus wild-type. (D) RNA-seq normalized coverage over representative genes, *POG1* and *FUN26*, found in the subset of genes in the *ioc3Δ chd1Δ*/WT context that did not overlap with those of the single mutants. Values represent the mean of normalized coverage in 10-bp bins, averaged over three biological replicates. Watson (W) and Crick (C) strands are indicated.

When I assessed the relationship between sense and antisense expression levels in each mutant relatively to wild-type, the majority of genes showed no transcriptional interference *in cis*. In other words, increased antisense RNA levels did not result in down-regulation of the overlapping gene expression (Figure 3.3.4). This observation could indicate that cryptic promoters may not experience prolonged exposure. Instead, it is possible that other chromatin factors compensate to maintain chromatin structure when Isw1 or Chd1 remodelers are absent. Nevertheless, as seen for *isw1Δ chd1Δ* compared to wild-type, I could observe a second trend across all mutants, where both sense and antisense derepression occur in the same gene (Figure 3.3.4).

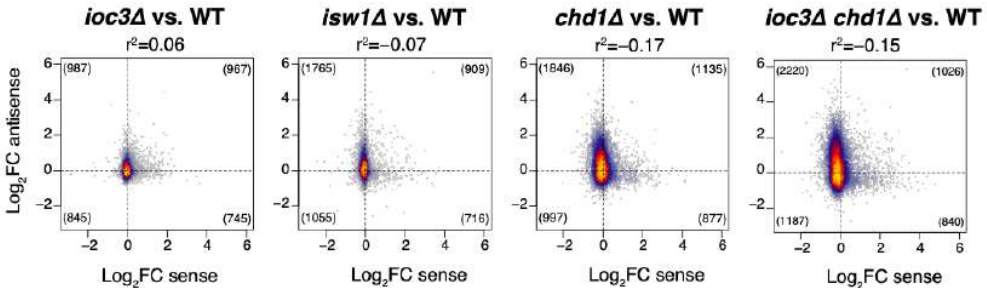

Figure 3.3.4 Increased antisense transcription in the remodeler mutants generally does not result in down-regulation of gene expression *in cis*. Correlation analysis comparing changes in antisense and sense expression levels for each remodeler mutant versus wild type, with yellow indicating higher density of genes. Pearson correlation coefficient values are indicated.

I also investigated the influence of each remodeler regarding ICRATs expression. In order to do this, I performed a differential expression analysis of ICRATs for each single mutant and *ioc3Δ chd1Δ* relatively to wild-type. The number of differentially expressed ICRATs detected covered the majority of increased asDEGs previously identified in each context (Figure 3.3.5).

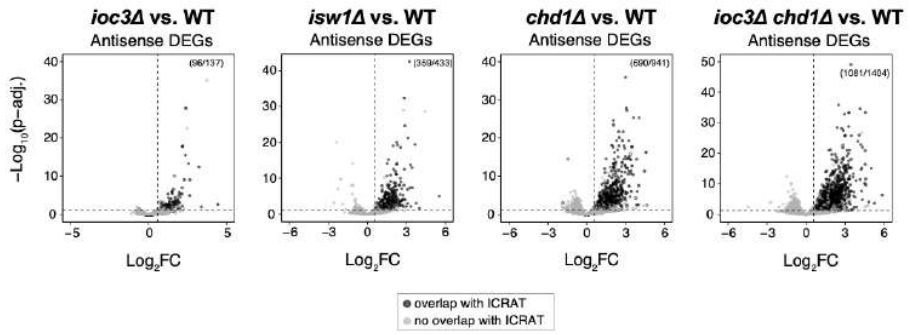

Figure 3.3.5 Derepressed asDEGs containing ICRATs, as determined by differential expression analysis on *ioc3Δ*, *isw1Δ*, *chd1Δ* and *ioc3Δ chd1Δ* mutants versus wild-type. Significance (adjusted p-value of 0.05) and 1.5-fold-change thresholds are represented with dashed lines. The ratio of derepressed antisense differentially expressed genes (asDEGs) containing ICRATs to the total number of derepressed asDEGs is indicated.

ICRATs derepressed in *isw1Δ* cells display a lower degree of derepression in *chd1Δ* cells, and vice versa (Figure 3.3.6 A). Furthermore, RNAPII density levels in *isw1Δ* cells compared to wild-type across ICRATs identified in *chd1Δ* cells are lower compared to RNAPII density levels in *chd1Δ* versus wild-type (Figure 3.3.6 B, left). The opposite is also observed (Figure 3.3.6 B, right). Together these findings indicate that Isw1 and Chd1 suppress different subsets of asRNAs. Then I questioned whether Isw1 and Chd1 remodelers suppress antisense transcription at distinct regions of genes. I assigned each ICRAT to the overlapping intragenic region of the respective asDEG: start, mid, end, or entire open reading frame.

Cells lacking Isw1 or Ioc3 express more ICRATs accumulated at the 5′ end of asDEGs, than at the 3′ end, in contrast to *chd1Δ* cells (Figure 3.3.7 A). To further explore this observation, and because Isw1 and Chd1 have been previously reported to suppress cryptic transcription in longer genes (Smolle, Venkatesh et al. 2012), I looked at antisense expression levels in three groups protein-coding genes, separated according to gene length. I could observe that the longer the genes, the more evident is the influence of ISW1a and Chd1 remodelers in preventing antisense transcription from accumulating at opposite regions of genes (Figure 3.3.7 B, Supplementary Figure 3.10.3).

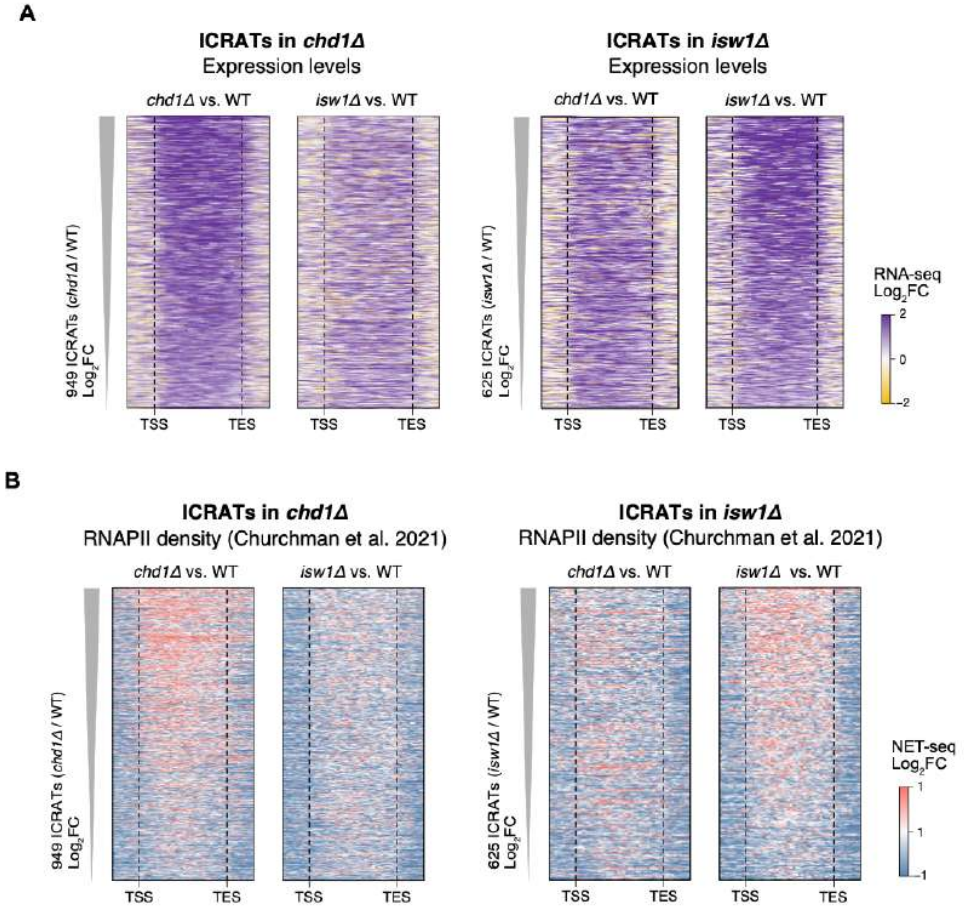

Figure 3.3.6 Isw1 and Chd1 suppress distinct antisense transcripts. (A) Changes in expression levels over ICRATs derepressed in *chd1Δ* (left) and *isw1Δ* (right) compared to wild-type yeast. RNA-seq values are the mean of normalized coverage in 30-bp bins, averaged over three biological replicates. (B) Changes in RNAPII density over ICRATs derepressed in *chd1Δ* (left) and *isw1Δ* (right) compared to wild-type yeast. NET-seq values are the mean of normalized coverage in 30-bp bins, averaged over two biological replicates. (B, C) ICRATs were ordered by decreasing log_2FC values, as determined by differential expression analysis. ICRATs were scaled to 1000 bps, with a 300 bp flanking window.

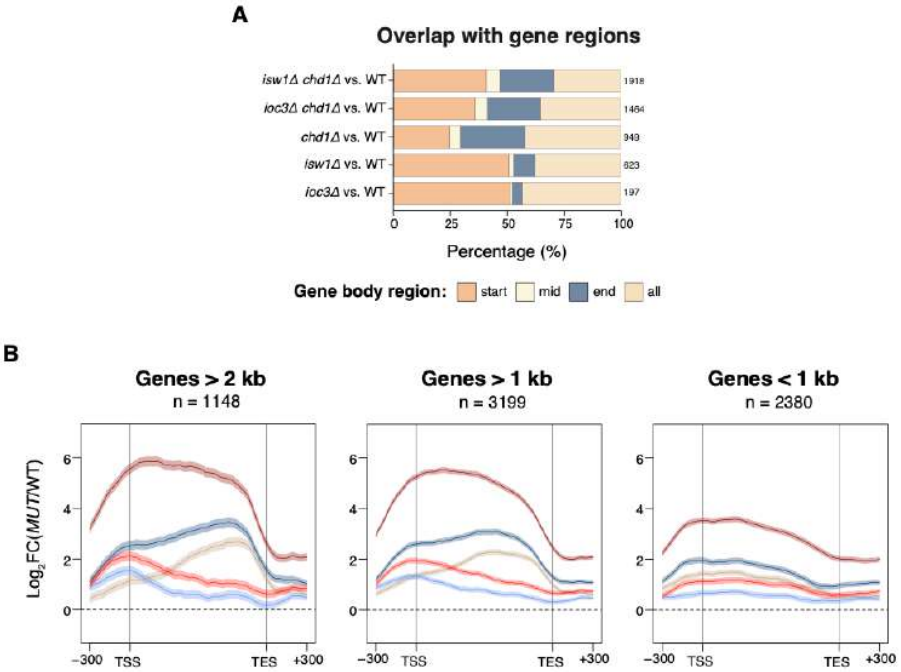

Figure 3.3.7 Isw1 and Chd1 remodelers prevent antisense transcription accumulation at opposite ends of genes. (A) Classification of ICRATs based on the gene regions these overlap with. The number of derepressed ICRATs in each mutant versus wild-type is indicated. (B) Metagene representations of antisense expression levels over genes longer than 2 kb (n = 1148), genes longer than 1 kb (n = 3199), and genes shorter than 1 kb (n = 2380) in various remodeler mutants. The y-axis represents the log2 ratio of normalized antisense RNA-seq coverage for mutant versus wild-type. Data are shown as mean (line) ± SEM (shadow). The TSS and TES are indicated. Gene bodies were scaled to 1000 bp, with a 300 bp flanking window.

3.4 The role of chromatin remodelers Chd1 and ISW1a in preventing the exposure of cryptic promoters

To discriminate between up-regulated gene expression and sense intragenic transcription in *ioc3Δ and chd1Δ*, and to determine the genomic locations where Chd1 and ISW1a prevent exposure of cryptic promoters, I used 5′cap-seq to map the TSSs for each single mutant.

I classified each TSS cluster (TC) according to their location relative to genes: promoter, antisense promoter, sense intragenic, antisense intragenic, and intergenic. The number of TCs in each of these regions was similar in both *ioc3Δ* and wild-type yeast, with a slight increase in antisense intragenic TCs in *ioc3Δ* cells (Figure 3.4.1). Cells lacking Chd1 remodeler showed a higher density of TCs over

intragenic and intergenic regions (Figure 3.4.1). The *chd1Δ*-specific sense intragenic TSS clusters (TCs) are more prominent over mid-3′ regions of genes (Figure 3.4.2 A). Generally, the TSS expression levels over sense intragenic TCs were higher in both *ioc3Δ and chd1Δ* mutants relatively to wild-type (Figure 3.4.2 B).

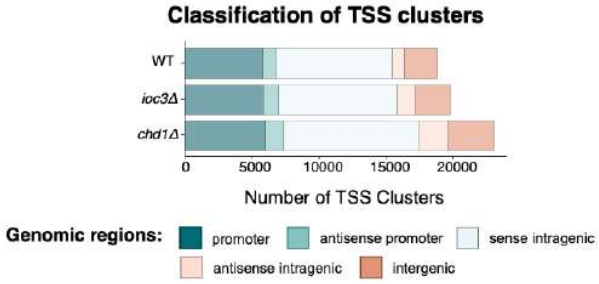

Figure 3.4.1 Deletion of *IOC3* and *CHD1* exposes new promoters. (A) Classification of TSS clusters in wild-type, *ioc3Δ*, and *chd1Δ* mutants based on their genomic location.

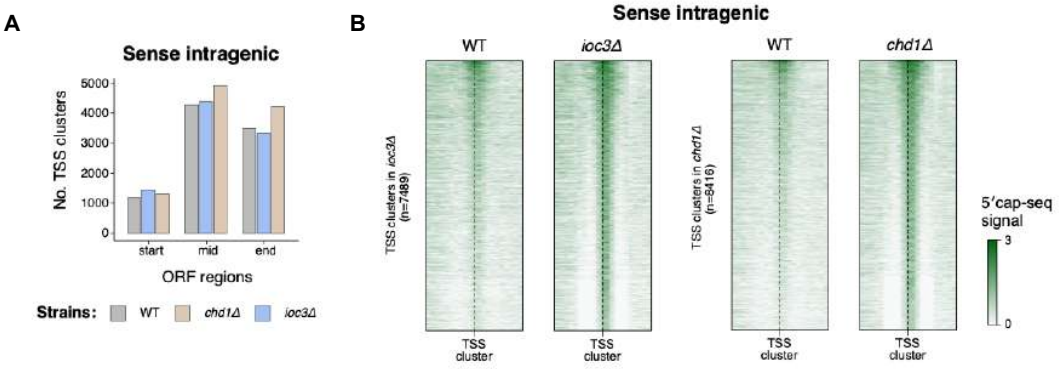

Figure 3.4.2 Density and expression changes of sense intragenic TSS clusters in *ioc3Δ* and *chd1Δ* cells. (A) Distribution of sense intragenic TSS clusters (TCs) across gene regions in wild-type, *ioc3Δ*, and *chd1Δ* yeast. Open reading frame regions were divided into three regions based on percentage of gene width: start=25%, mid=25-75%, and end=75%-100%. (B) Normalized 5′cap-seq signal in wild-type and remodeler mutant strains around sense intragenic TCs. Normalized 5′cap-seq coverage was aligned to each TC centroid ± 200 bp, and ordered by signal strength in the remodeler mutant. Values represent the sum of normalized coverage in 20-bp bins, merged from three biological replicates.

When looking at all protein-coding gene promoter TCs, I could not detect changes in TSS expression in either of the single mutants (Figure 3.4.3 A). However, when I

focused on the sDEGs detected in the RNA-seq analysis for each remodeler mutant, I observed that while the TSS expression at gene promoters in *ioc3Δ* cells was generally unaffected, those in *chd1Δ* cells were mostly derepressed (Figure 3.4.3 B and C, right). In agreement with these results, the RNA expression levels in *ioc3Δ* cells are increased particularly over the end of the sDEGs, whereas in *chd1Δ* cells, the RNA expression levels are increased over the entire gene body (Figure 3.4.3 B and C, left).

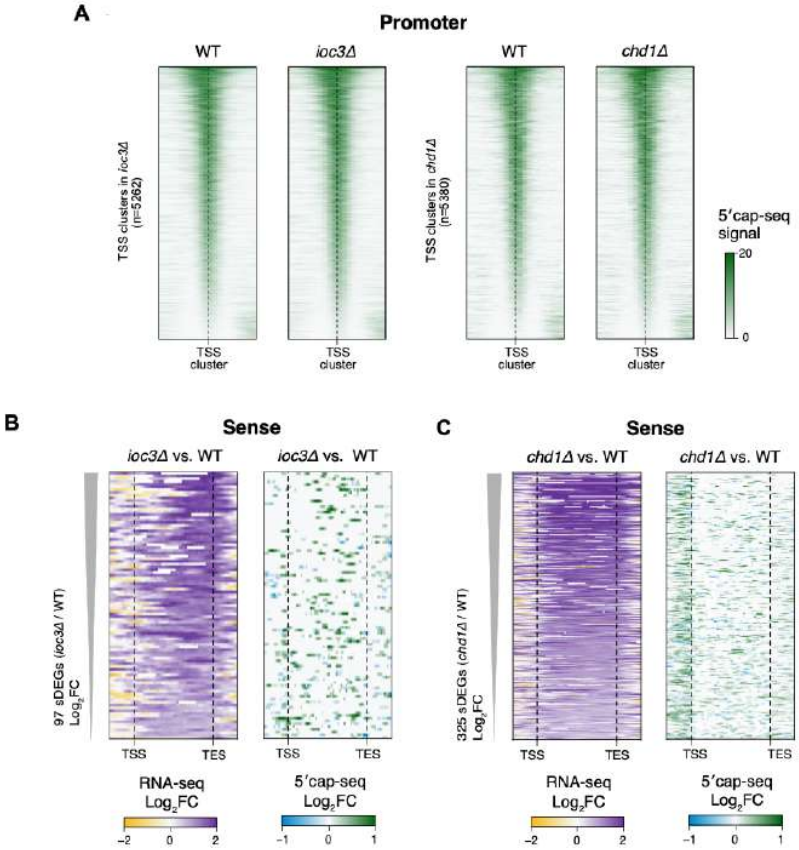

Figure 3.4.3 Genome-wide mapping of TSSs reveals that ISW1a and Chd1 remodelers impact sense transcription in different ways. (A) Normalized 5′cap-seq coverage in wild-type and remodeler mutant strains around sense intragenic TCs. Normalized 5′cap-seq signal was aligned to each TC centroid ± 200 bp, and ordered by signal strength in the remodeler mutant. (B, C) RNA and TSS expression changes over sense differentially expressed genes (sDEGs) in *ioc3Δ* (B) and *chd1Δ* (C) cells versus wild-type. sDEGs were ordered by log_2FC values, as determined by RNA-seq differential expression analysis, and scaled to 1000 bps, with 300 bp flanks. RNA-seq values are the mean of normalized coverage in 20-bp bins, averaged over three biological replicates. (A-C) 5′cap-seq values derive from the sum of normalized coverage in 20-bp bins, merged from three biological replicates.

Regarding antisense intragenic TCs, *ioc3Δ* cells displayed increased TC density over 5′-mid regions of genes compared to wild-type, while in *chd1Δ* cells the number of antisense TCs is higher over mid-3′ regions of genes (Figure 3.4.4 A). Abolishing either ISW1a or Chd1 remodeling complexes notably leads to increased TSS expression levels over antisense intragenic TCs, even if these TCs are also present in wild-type cells (Figure 3.4.4 B). When I focused on the changes in TSS expression over asDEGs in *ioc3Δ* cells, I observed a distinctive increase of TSSs over the 5′ end of genes, marking the initiation sites of the asRNAs that predominantly accumulate over the 5′ end, as shown by RNA-seq (Figure 3.4.4 C). In *chd1Δ* cells, antisense RNAs predominantly accumulate at the 3′ end of asDEGs, likely due to exposure of cryptic promoters both at the 3′ ends of genes and in the intergenic regions downstream of the TES. This is supported by increased TSS expression levels in these regions (Figure 3.4.4 D). Furthermore, the *chd1Δ* single mutant demonstrates a clear increase of intergenic TSSs compared to wild-type (Figure 3.4.5).

Measuring RNA levels and mapping TSSs genome wide, allowed me to uncover a detailed understanding of the individual contributions of ISW1a and Chd1 remodelers in preventing cryptic transcription initiation. And notably, I observed a high degree of consistency between two independently conducted experiments, RNA-seq and 5′cap-seq, each using distinct enzymatic procedures.

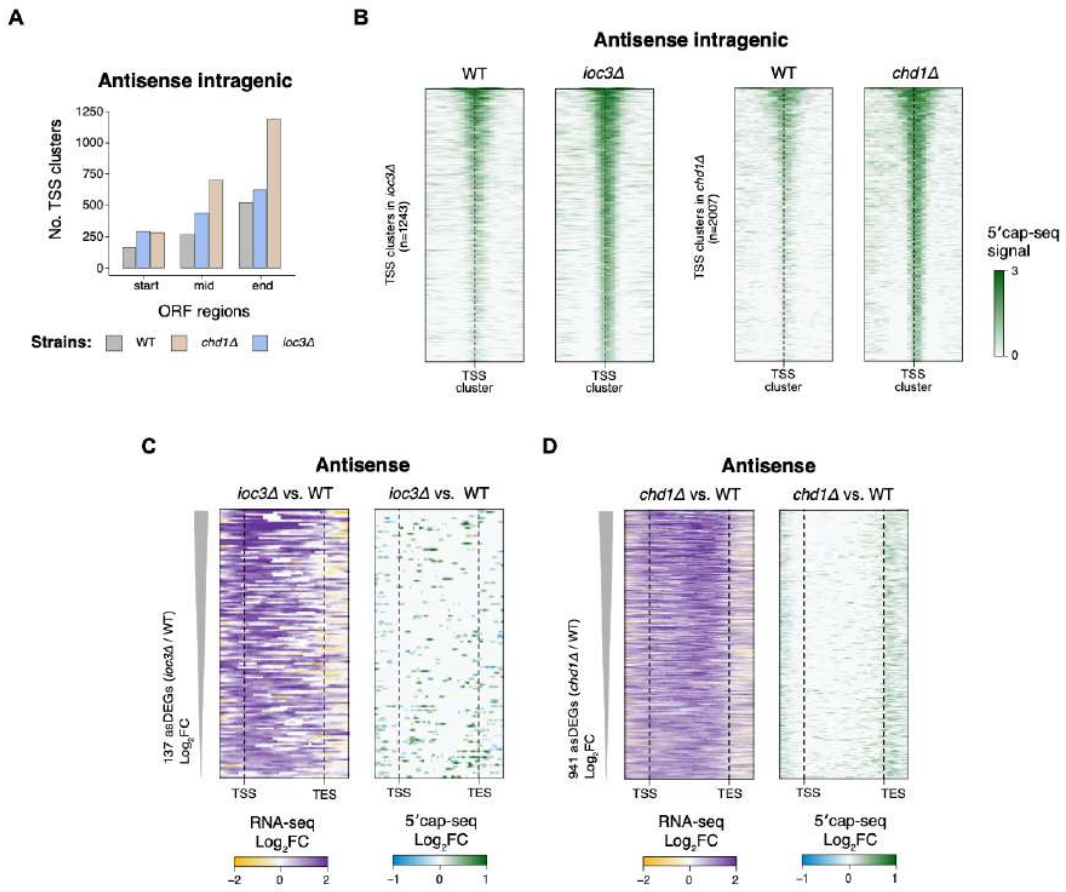

Figure 3.4.4 ISW1a and Chd1 prevent exposure of antisense promoters predominantly at different regions of genes. (A) Distribution of antisense intragenic TSS clusters (TCs) across gene regions in wild-type, *ioc3Δ*, and *chd1Δ* yeast. Open reading frame regions were divided into three regions based on percentage of gene width: start=25%, mid=25-75%, and end=75%-100%. (B) Normalized 5′cap-seq coverage around antisense intragenic TCs in wild-type and remodeler mutants. Normalized 5′cap-seq coverage was aligned to each TC centroid ± 200 bp, and ordered by signal strength in the remodeler mutant. (C, D) RNA and TSS expression changes over antisense differentially expressed genes (asDEGs) in *ioc3Δ* (C) and *chd1Δ* (D) cells versus wild-type. asDEGs were ordered by log_2FC values, as determined by RNA-seq differential expression analysis, and scaled to 1000 bps, with 300 bp flanks. RNA-seq values are the mean of normalized coverage in 20-bp bins, averaged over three biological replicates. (B-D) 5′cap-seq values derive from the sum of normalized coverage in 20-bp bins, merged from three biological replicates.

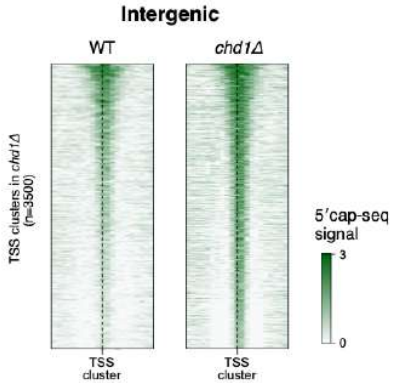

Figure 3.4.5 Chd1 prevents exposure of cryptic promoters at intergenic regions. (B) Normalized 5′cap-seq coverage around intergenic TSS cultures (TCs) in wild-type and *chd1Δ* cells. Normalized 5′cap-seq coverage values were aligned to each TC centroid ± 200 bp, and ordered by descending order of the mutant's values. 5′cap-seq values derive from the sum of normalized coverage in 20-bp bins, merged from three biological replicates.

3.5 Rrp6 masks the cryptic phenotype in cells lacking ISW1a

Previous studies have demonstrated the accumulation of cryptic RNAs, referred to as CUTs, in cells lacking the nuclear exosome subunit Rrp6, along with the widespread of cryptic TSSs, particularly within intergenic regions (Xu, Wei et al. 2009, Wei, Hennig et al. 2019). Given the subtle cryptic transcriptional phenotype observed in cells lacking the ISW1a remodeler, I aimed to determine whether the RNA degradation by the nuclear exosome is masking the extent of the cryptic phenotype in *ioc3Δ* cells. To answer this, I employed 5′cap-seq to assess the cryptic phenotype in cells lacking both ISW1a and the nuclear exosome catalytic subunit Rrp6.

Nucleosome depleted regions are intergenic regions with extended linker DNA, where gene promoters are located. In yeast, CUTs usually initiate from divergent transcription at NDRs (Xu, Wei et al. 2009). 5′cap-seq analysis showed the strongest TSS derepression at intergenic and antisense gene-promoter TCs in *rrp6Δ* cells (Figure 3.5.1 A and B). Antisense promoter TCs are those located near a gene promoter, in the opposite strand while intergenic TCs include those located in more distal intergenic regions. In the *ioc3Δ rrp6Δ* double mutant, TSS expression levels were notably higher at intergenic TCs compared to those in *rrp6Δ* cells alone

(Figure 3.5.1 A). This observation suggests that ISW1a may play a role in suppressing cryptic transcription initiation at intergenic regions as well, potentially including promoters of CUTs. To test whether ISW1a specifically helps suppressing CUTs expression, I looked at TSS changes surrounding the CUTs start site. As expected, both wild-type and *ioc3Δ* cells displayed lower levels of TSS expression relative to *rrp6Δ* cells (Figure 3.5.1 C). Interestingly, *ioc3Δ rrp6Δ* cells exhibited higher levels of TSS expression surrounding the start site of CUTs when compared to *rrp6Δ* cells (Figure 3.5.1 C), supporting my hypothesis that ISW1a may contribute to the suppression of CUTs transcription initiation.

Given that ISW1a prevents the suppression of intragenic transcripts, I evaluated the TSS expression around sense and antisense intragenic TCs. Cells lacking ISW1a and Rrp6 also revealed increased expression levels of intragenic TSSs compared to the single mutants as well as wild-type (Figure 3.5.2 A and B). Particularly at 5′-mid regions of genes, I observed a larger number of antisense intragenic TSS clusters in *ioc3Δ rrp6Δ* relatively to *rrp6Δ* and the remaining strains (Figure 3.5.2 C). These findings indicate that the presence of a nuclear exosome masks the extent of the cryptic phenotype caused by loss of ISW1a complex.

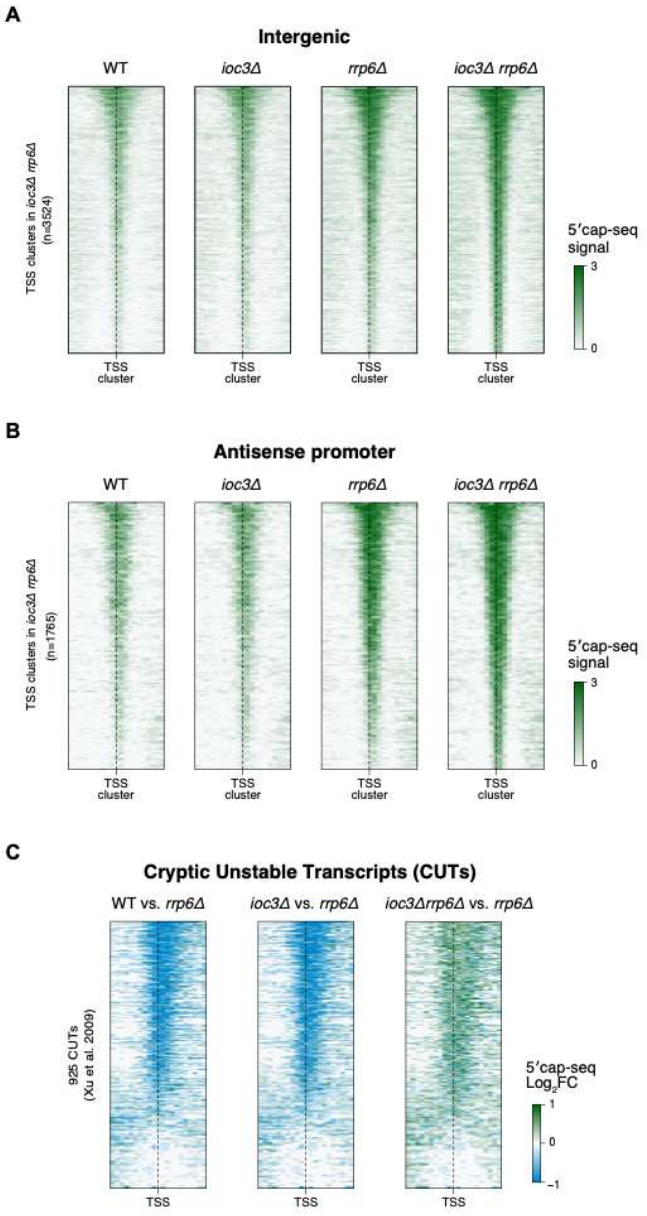

Figure 3.5.1 ISW1a represses intergenic promoters and divergent transcription initiated at gene promoters. (A, B) Normalized 5′cap-seq coverage around intergenic (A) and antisense promoter (B) TSS cultures (TCs) in wild-type, *ioc3Δ*, *rrp6Δ*, and *ioc3Δ rrp6Δ* cells. (C) 5′cap normalized coverage in wild-type, *ioc3Δ*, and *ioc3Δ rrp6Δ* relative to *rrp6Δ* around the TSS of CUTs. (A-C) Normalized 5′cap-seq coverage values were aligned to each TC centroid (A, B) or TSS (C) ± 200 bp, and ordered by descending order of the values of the *ioc3Δ rrp6Δ* double mutant. 5′cap-seq values derive from the sum of normalized coverage in 20-bp bins, merged from three biological replicates.

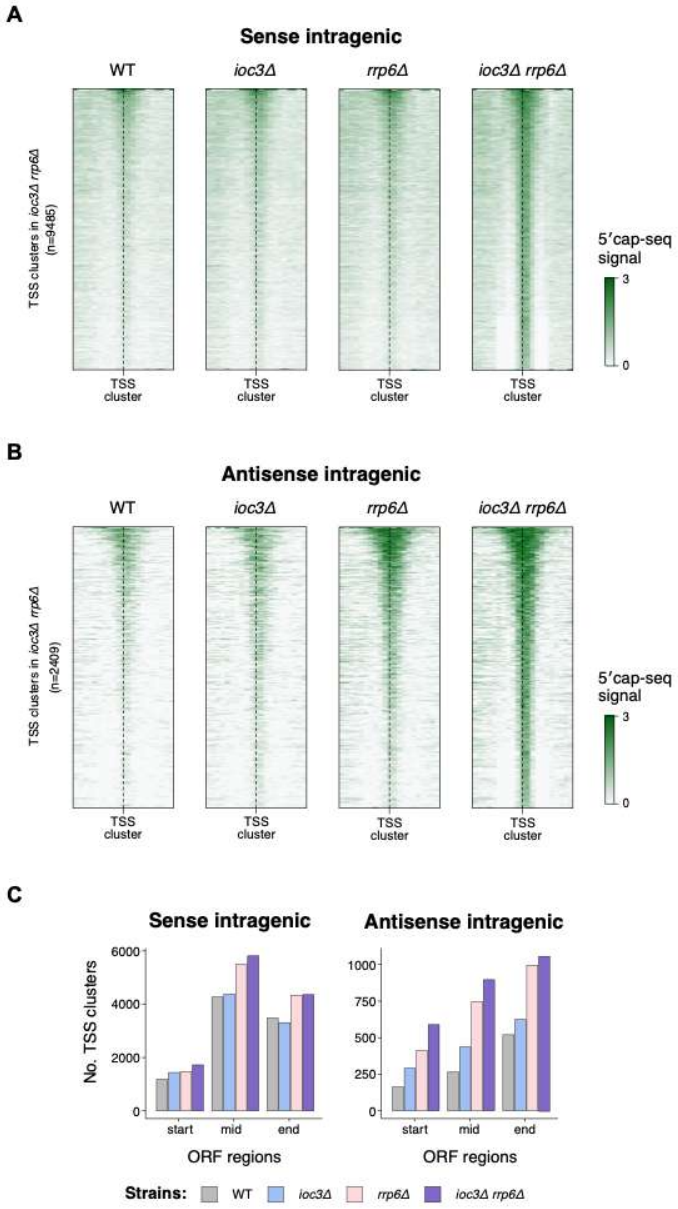

Figure 3.5.2 *IOC3* deletion has heightened cryptic effects on the antisense transcriptome in *rrp6Δ* background compared to wild-type cells. (A, B) Normalized 5′cap-seq coverage around sense (A) and antisense (B) intragenic TSS cultures (TCs) in wild-type, *ioc3Δ*, *rrp6Δ*, and *ioc3Δ rrp6Δ* cells. Normalized 5′cap-seq coverage values were aligned to each TC centroid ± 200 bp, and ordered by descending order of the values of the *ioc3Δ rrp6Δ* double mutant. 5′cap-seq values derive from the sum of normalized coverage in 20-bp bins, merged from three biological replicates. (C) Distribution of sense and antisense intragenic TCs across gene regions in wild-type and mutant strains. Open reading frame regions were divided into three regions based on percentage of gene width: start=25%, mid=25-75%, and end=75%-100%.

3.6 ISW1a and Chd1 remodelers repress cryptic transcription in sporulation and transmembrane transport-related genes

Depleting yeast cells from Isw1 or Chd1 ATPases, or ISW1a complex, resulted in a tendency for transcriptional derepression in both sense and antisense directions. To determine which genes are affected by these remodelers, I submitted the derepressed sense and antisense differentially expressed genes (sDEGs and asDEGs) to gene ontology enrichment analysis (Figure 3.6.1, Supplementary Figure 3.10.4 and Figure 3.10.5). Across all remodeler mutants, derepressed asDEGs showed enrichment for genes involved in transmembrane transport while derepressed sDEGs were notably enriched for genes involved in sporulation and meiotic biological processes (Figure 3.6.1).

In vegetative growing haploid yeast cells, meiotic-specific genes like *IME4*, *IME1*, and *ZIP2* have been reported to be regulated through the generation of non-coding antisense transcripts (Hongay, Grisafi et al. 2006, Chen and Neiman 2011, Gelfand, Mead et al. 2011). In this study, differential expression analysis of RNA-seq data revealed that certain meiotic genes are derepressed in *ioc3Δ*, *isw1Δ*, and *chd1Δ* mutants compared to wild-type yeast (Supplementary Figure 3.10.6 A). Visual exploration of normalized RNA-seq and 5′cap-seq coverage over *ZIP2*, *HFM1*, *IRC18*, *SPO22*, and *HOP1* meiotic genes allowed me to see the presence of intragenic TSS tags as well as their increased expression levels in *ioc3Δ* cells compared to wild-type (Figure 3.6.2, Supplementary Figure 3.10.6 B). This indicates that the heightened sense transcription does not result from an increase in mRNA levels but rather from an augmented production of intragenic sense transcripts. Notably, in certain meiotic genes such as *HFM1* and *SPO22*, the accumulation of sense intragenic transcripts in *ioc3Δ* cells was accompanied by a decrease in antisense RNA levels compared to wild-type cells, suggesting a regulatory role of the respective asRNAs *in cis* (Figure 3.6.2, Supplementary Figure 3.10.6 B). These findings strongly suggest that ISW1a may participate in the regulation of cryptic transcription in meiotic and sporulation-related genes in yeast.

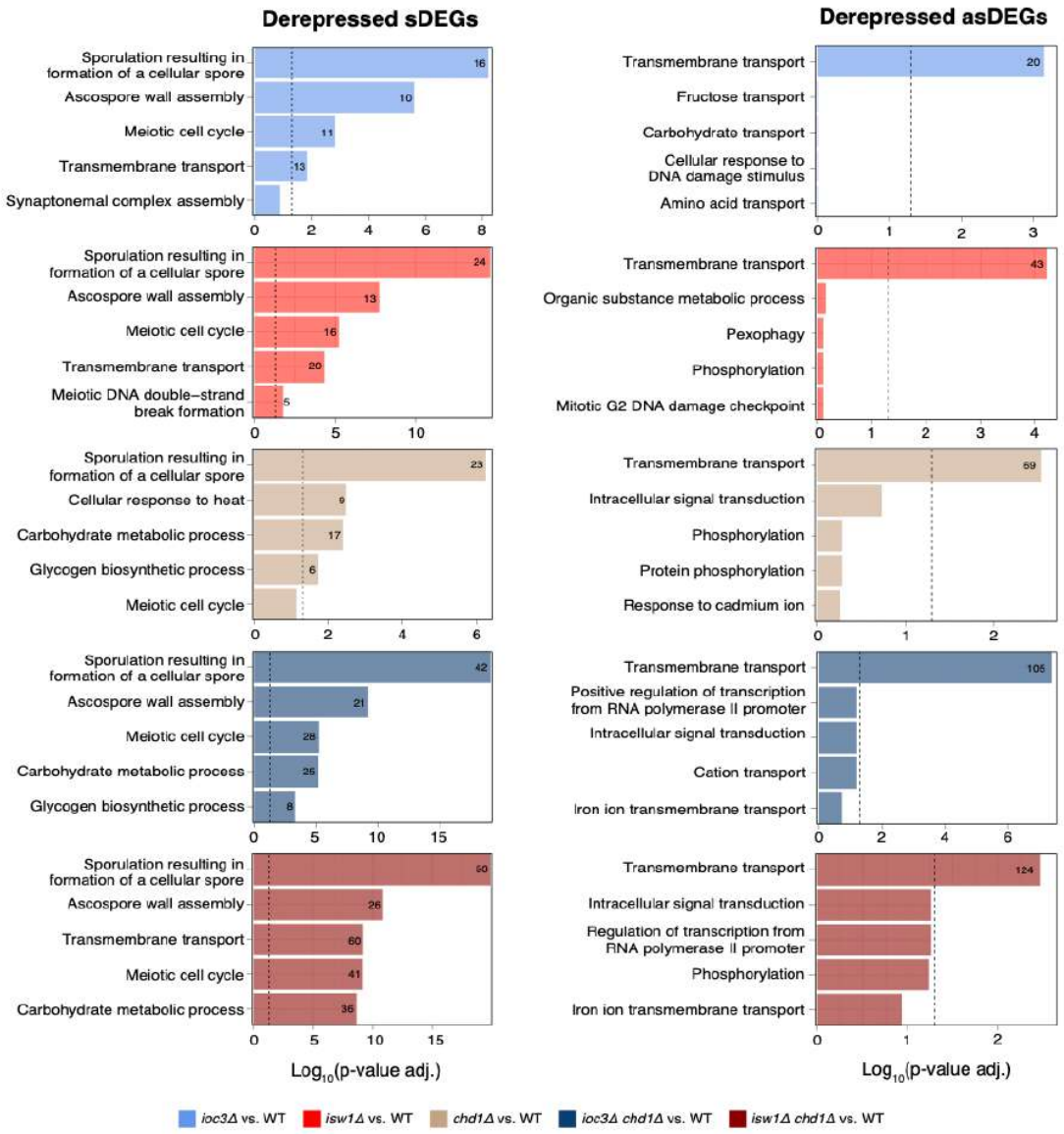

Figure 3.6.1 Gene ontology analysis revealed sporulation and transmembrane transport enrichment in genes with derepressed sense and antisense transcription, respectively. Top five gene ontology enrichment terms of derepressed sense differentially expressed genes (sDEGs; left) and antisense DEGs (asDEGs; right) in each mutant versus wild-type. The y-axis displays biological process terms and the x-axis shows the negative logarithm (base 10) of the Benjamini-Hochberg adjusted p-value. The dashed line marks the adjusted p-value of 0.05. The number of genes found within each biological process term is indicated.

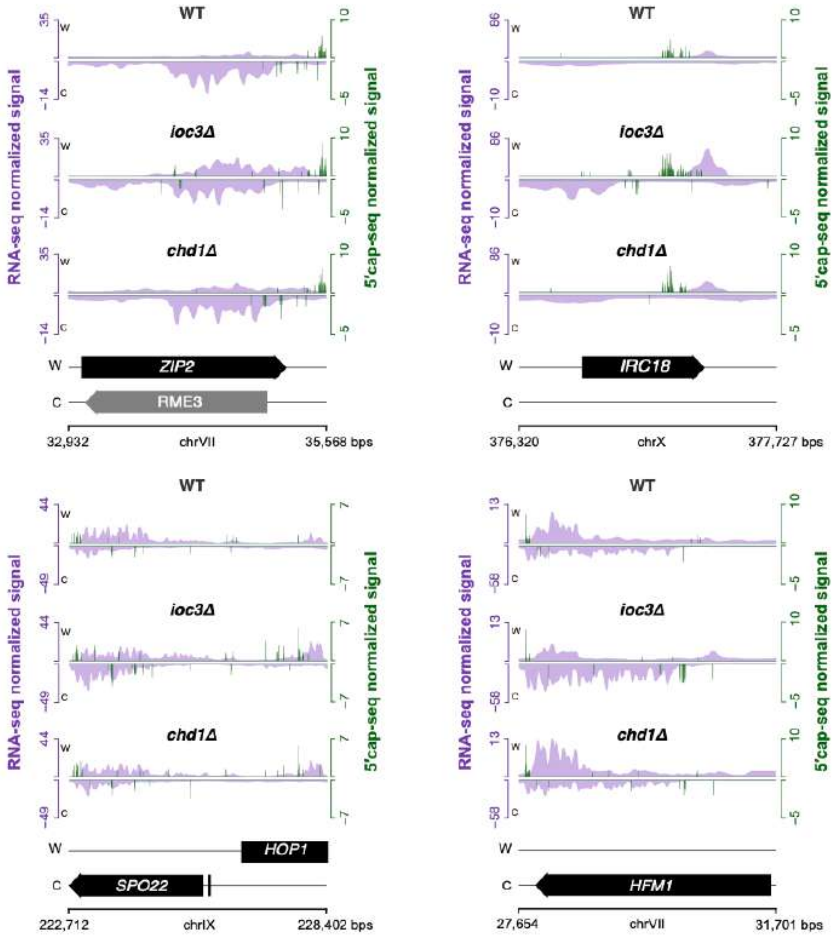

Figure 3.6.2 ISW1a regulates non-coding transcription in sporulation-related genes. RNA-seq (purple) and 5′cap-seq (green) normalized coverage are presented for wild-type, *ioc3Δ*, and *chd1Δ* cells. RNA-seq values are the mean of normalized coverage in 10-bp bins, averaged over three biological replicates. 5′cap-seq values are the normalized coverage merged from three biological replicates. Watson (W) and Crick (C) strands are indicated, as well as genomic coordinates.

The transcriptional repression functions of Isw1 have been previously reported in TATA-containing genes (Morillon, Karabetsou et al. 2003, Morillon, Karabetsou et al. 2005, Lindstrom, Vary et al. 2006). In the *Saccharomyces cerevisiae* genome, the majority of gene promoters are considered TATA-less, with only around 20% of genes containing a canonical TATA box element in their promoter sequence. Genes lacking a TATA box are often associated with "housekeeping" functions, whereas genes containing a TATA box tend to be more tightly regulated, often activated to stimuli such as stress (Yang, Bolotin et al. 2007).

Herein, I assessed whether the differentially derepressed genes found in the remodeler mutants are predominantly TATA-genes, relatively to the ratio of TATA/TATA-less genes in the whole genome. Across all remodeler mutants, derepressed sDEGs showed a higher prevalence of TATA-genes relatively to all *S.cerevisiae* genes (Figure 3.6.3 A). With a subtle exception in *ioc3Δ* cells, asDEGs did not show a higher prevalence of TATA-genes relatively to the *S.cerevisiae* genome (Figure 3.6.3 A). Furthermore, I observed that derepressed sDEGs are primarily less transcribed genes across all remodeler mutants, particularly in *isw1Δ* and *ioc3Δ* single mutants. This is consistent with the higher prevalence of TATA-containing genes and with the enrichment in sporulation-related genes which are usually inactive in haploid wild-type yeast (Figure 3.6.3 B). Additionally, genes with upregulated asRNA levels in *isw1Δ* and *ioc3Δ* cells are predominantly lowly transcribed, whereas in *chd1Δ* cells, the distribution of transcription rates closely resembles that of the overall *S. cerevisiae* protein-coding gene population.

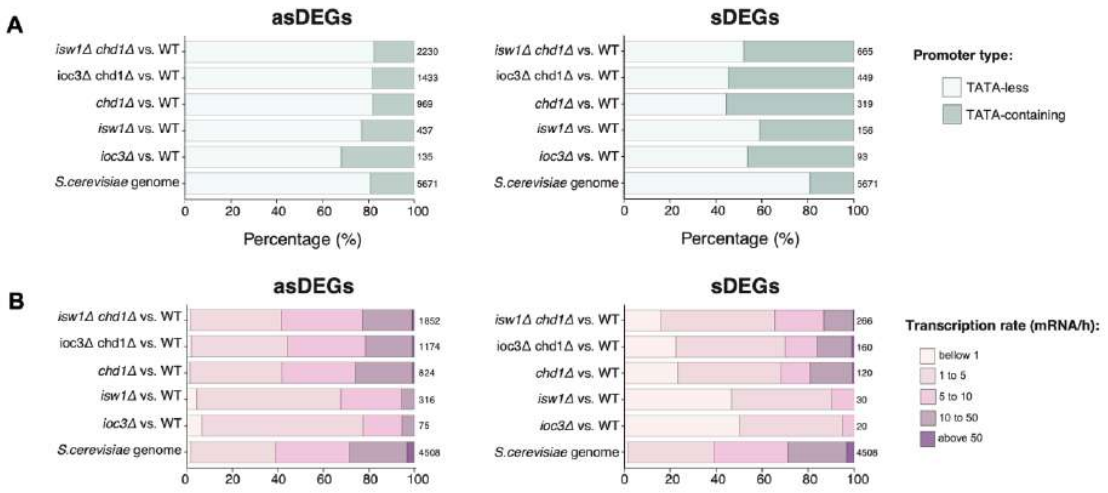

Figure 3.6.3 TATA box and transcription rate analysis of differentially expressed genes in various remodeler mutants and whole *S.cerevisiae* genome. (A) Percentage of TATA-less and TATA-containing genes among asDEGs and sDEGs, based on classification from Basehoar et al. (Basehoar, Zanton et al. 2004). (B) Classification of asDEGs and sDEGs by transcription rate groups, using data from Miller et al. (Miller, Schwalb et al. 2011). Transcription rates were categorized into five groups (mRNA/h). (A, B) The number of differentially expressed genes (DEGs) identified in each analysis is indicated for each context.

3.7 ISW1a prevents incorporation of H2A.Z at intragenic promoters

In the absence of the ISW1a remodeler, intragenic promoters become exposed. This raises the question of whether there are alterations in the chromatin structure in these regions. H2A.Z (Htz1 in yeast) is evolutionarily conserved and enriched at the +1 nucleosome in eukaryotes (Li, Wei et al. 2023). H2A/H2A.Z exchange is mediated by the SWR1 chromatin remodeling complex (Mizuguchi, Shen et al. 2004). The incorporation of variant H2A.Z is crucial for facilitating transcription initiation as it has been shown that it disfavors the DNA-histone binding (Li, Wei et al. 2023). Furthermore, H2A.Z-containing nucleosomes require substantially less energy for DNA unwrapping compared to the H2A-containing nucleosomes (Li, Wei et al. 2023). Gu and colleagues have shown that histone variant H2A.Z accumulates at the 3′ end of 1025 protein-coding genes in wild-type yeast, marking the start site of antisense transcripts observed in *rrp6Δ* cells (Gu, Naiyachit et al. 2015). The same regions were also enriched for other active transcription-associated histone marks, such as H3K4me3 and histone H3 and histone H4 acetylation marks (Gu, Naiyachit et al. 2015).

Our lab explored whether ISW1a affects the occupancy of H2A-Z and H3K4me3 genome-wide, using ChIP-seq against H2A-Z and H3K4me3 in *isw1Δ* and *ioc3Δ* cells. To gain insights on the mechanism of ISW1a-mediated suppression of cryptic transcription, I first compared the changes in H2A.Z occupancy with the TSS expression levels in all intragenic TCs present in 97 sDEGs and 137 asDEGs in *ioc3Δ* cells. Cells lacking ISW1a showed increased H2A.Z occupancy surrounding most of the intragenic TCs (Figure 3.7.1 A). Additionally, I compared the H2A.Z occupancy levels to asRNA expression in *ioc3Δ* and *isw1Δ* cells. The 169 ICRATs accumulated in *ioc3Δ* cells showed increased H2A.Z levels surrounding their TSS when compared to wild-type (Figure 3.7.1 B). Cells lacking Isw1 ATPase revealed a more pronounced H2A.Z accumulation around the TSSs of the 625 ICRATs derepressed in *isw1Δ* mutant (Figure 3.7.1 C). Overall, these findings suggest a positive association between the exposure of cryptic promoters and the pervasive

intragenic incorporation of H2A.Z, which subsequently facilitates the cryptic transcription initiation the absence of ISW1a. Furthermore, since cells lacking Isw1 ATPase revealed a more pronounced H2A.Z accumulation around the TSSs of the 625 ICRATs derepressed in *isw1Δ* mutant (Figure 3.7.1 C), ISW1b complex could also be involved in preventing H2A.Z incorporation at mid-end of genes where it suppresses cryptic transcription (Smolle, Venkatesh et al. 2012, Li, Bergmann et al. 2022).

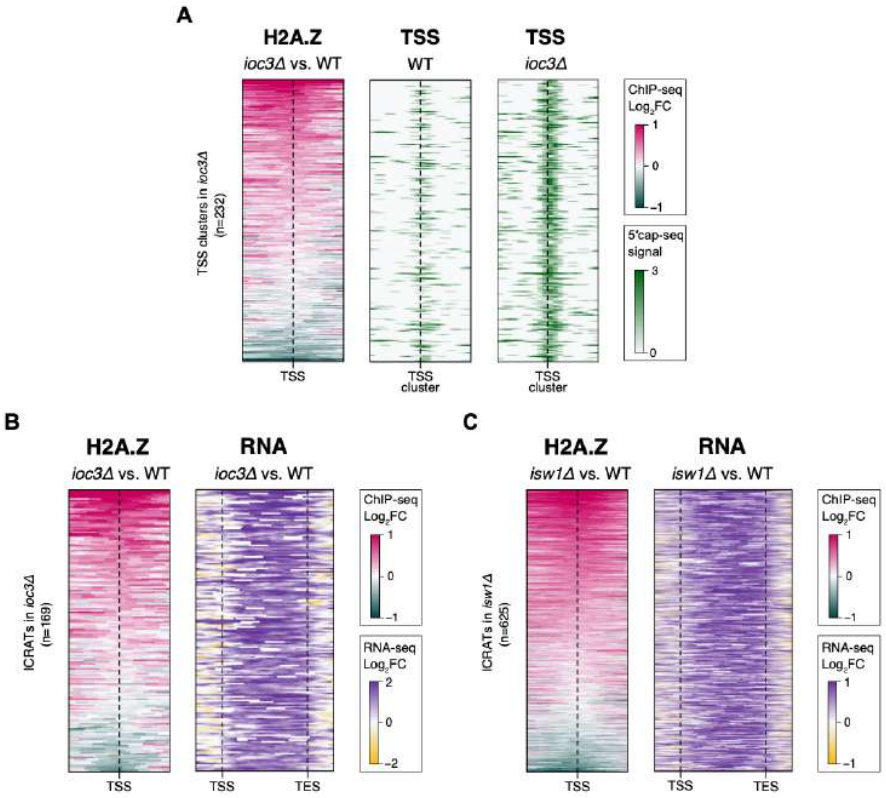

Figure 3.7.1 H2A.Z marks the TSSs of intragenic transcripts in *ioc3Δ* and *isw1Δ* cells. (A) H2A.Z occupancy changes around TSS clusters (TCs) within intragenic regions of significantly derepressed genes in *ioc3Δ*. ChIP-seq and 5′cap-seq normalized coverage values were aligned to TC centroids ± 200 bp. 5′cap-seq values represent the sum of normalized coverage in 20-bp bins from three replicates. (B, C) H2A.Z occupancy changes over ICRATs in *ioc3Δ* (B) and *isw1Δ* (C). Left heatmap shows log2 H2A.Z ChIP-seq ratios (*MUT*/WT) aligned to ICRAT TSSs ± 200 bp; right heatmap shows log2 RNA-seq ratios (*MUT*/WT) over ICRATs scaled to 1000 bp with 300 bp flanks. (A-C) ChIP-seq and RNA-seq values are averaged from two and three replicates, respectively. All heatmaps are ordered by decreasing log2 H2A.Z ChIP-seq (*MUT*/WT).

The Set1-mediated H3K4me3 histone mark is enriched near the TSS of genes and it has been associated to active transcription (Soares, He et al. 2017). This enrichment is followed by the accumulation of H3K4me2 and H3K4me1 further downstream (Soares, He et al. 2017). During transcription elongation, the Set1-Set3C pathway maintains chromatin structure at the 5′ end of genes in a hypoacetylated state (Kim and Buratowski 2009). While RNAPII-recruited Set1 methylates histone H3 tails at lysine K4 residue (H3K4me3, H3K4me2, H3K4me1), Set3 removes histone acetylation marks at 5′ end of genes upon H3K4me2 recognition, maintaining chromatin structure in the wake of RNAPII passage (Kim and Buratowski 2009). When comparing ChIP-seq data against H3K4me3 with asRNA expression levels in *isw1Δ* and *ioc3Δ* cells versus wild-type, I noticed an increase of H3K4me3 within intragenic regions which corresponded to the start of antisense transcripts (Figure 3.7.2). I also observed that the H3K4me3 accumulation at the start of antisense transcripts is accompanied by H2A.Z accumulation (Figure 3.7.2, Supplementary Figure 3.10.7 A).

Next, I tested whether the increased levels of H2A.Z and H3K4me3 in *ioc3Δ* and *isw1Δ* cells were specifically associated to intragenic cryptic transcription or a general effect on chromatin. To do this, I assessed changed in H2A.Z and H3K4me3 occupancy in all protein-coding genes and in derepressed sense and antisense DEGs. In both *ioc3Δ* and *isw1Δ* mutants relatively to wild-type, H2A.Z occupancy was substantially increased at intragenic regions of genes with derepressed sense and antisense transcription compared to 5579 protein-coding genes (Figure 3.7.3, Supplementary Figure 3.10.7 B and C). Additionally, H2A.Z occupancy seems to accumulate closer to the 5′ end of genes in *ioc3Δ* cells, whereas in *isw1Δ* cells the H2A.Z is also distributed to the 3′ end of DEGs (Figure 3.7.3), potentially since ISW1b represses antisense transcription at 3′ end of genes (Smolle, Venkatesh et al. 2012, Li, Bergmann et al. 2022).

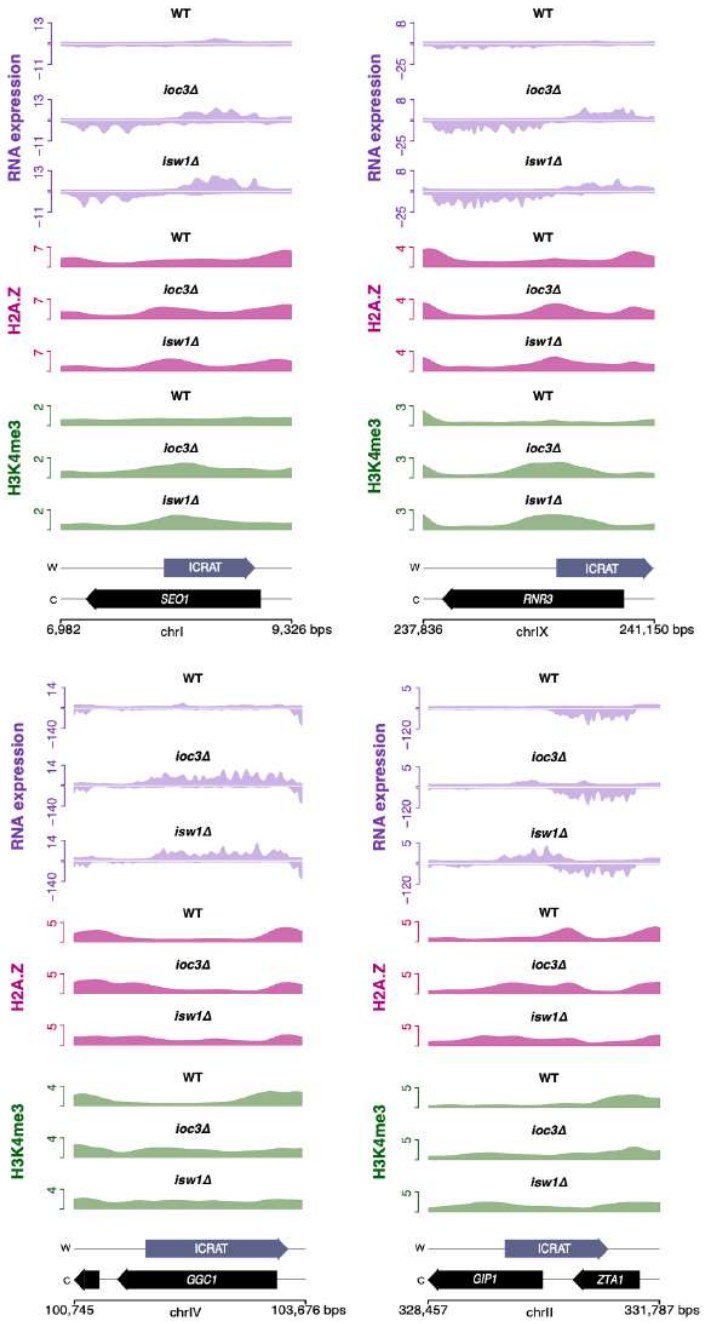

Figure 3.7.2 Representative genes showing increased H2A.Z and H3K4me3 levels near the start of asRNAs. Four genes with overlapping ICRATs are presented with respective RNA expression, H2A.Z and H3K4me3 levels in wild-type, *ioc3Δ*, and *isw1Δ* cells. RNA-seq values represent the mean of normalized coverage in 10-bp bins, averaged over three biological replicates. ChIP-seq values represent the mean of normalized coverage in 10-bp bins, averaged over two biological replicates. Watson (W) and Crick (C) strands are indicated, as well as genomic coordinates.

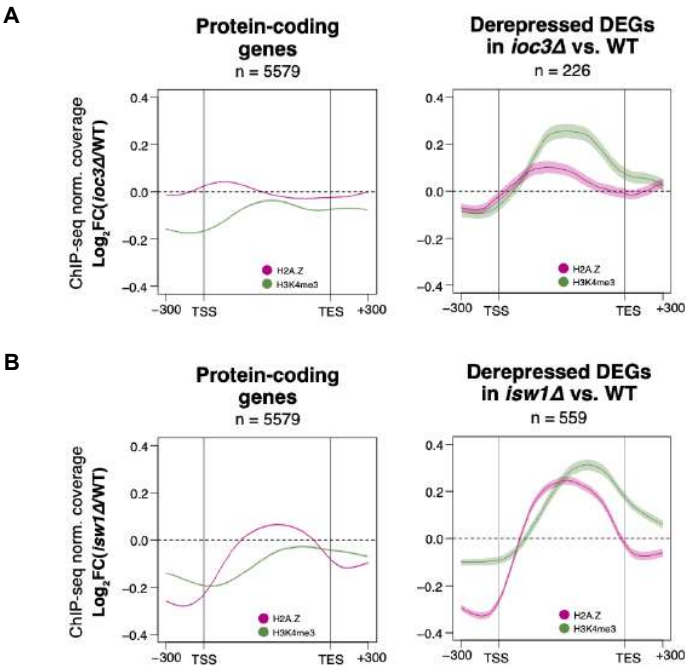

Figure 3.7.3 H2A.Z and H3K4me3 accumulate in the gene bodies of derepressed genes in *isw1Δ* and *ioc3Δ* cells. (A, B) Metagene representations of H2A.Z and H3K4me3 occupancy over protein-coding genes (left) and derepressed DEGs (right). The y-axis represents the log2 ratio of H2A.Z (pink) and H3K4me3 (green) occupancy, as determined using ChIP-seq, in mutant versus wild-type. Data are shown as mean ± SEM. The TSS and TES are indicated. Gene bodies were scaled to 1000 bps, with a 300 bp flanking window.

3.8 H2A.Z facilitates cryptic transcription in *ioc3Δ* and *isw1Δ* cells

The accumulation of both H2A.Z (Htz1 in yeast) and H3K4me3 near the initiation sites of cryptic RNAs in ISW1a-depleted cells prompts the question of their potential role in facilitating cryptic transcription initiation. To explore whether H2A.Z or H3K4me3 accumulation causes cryptic transcription or simply results from it, I used a multiplexed strand-specific RT-qPCR approach to quantify the antisense transcript levels in *isw1Δ, ioc3Δ* and *ioc4Δ* cells, with and without the deletion of *HTZ1* and factors required for H3K4me3 deposition. Figure 3.8.1 provides an overview of the multiplexed strand-specific RT-qPCR approach, highlighting the target genes and their corresponding overlapping antisense transcripts. Primers were specifically designed for cDNA synthesis of these antisense transcripts.

Candidate genes were selected based on RNA-seq data comparing *isw1Δ* mutant to wild-type cells.

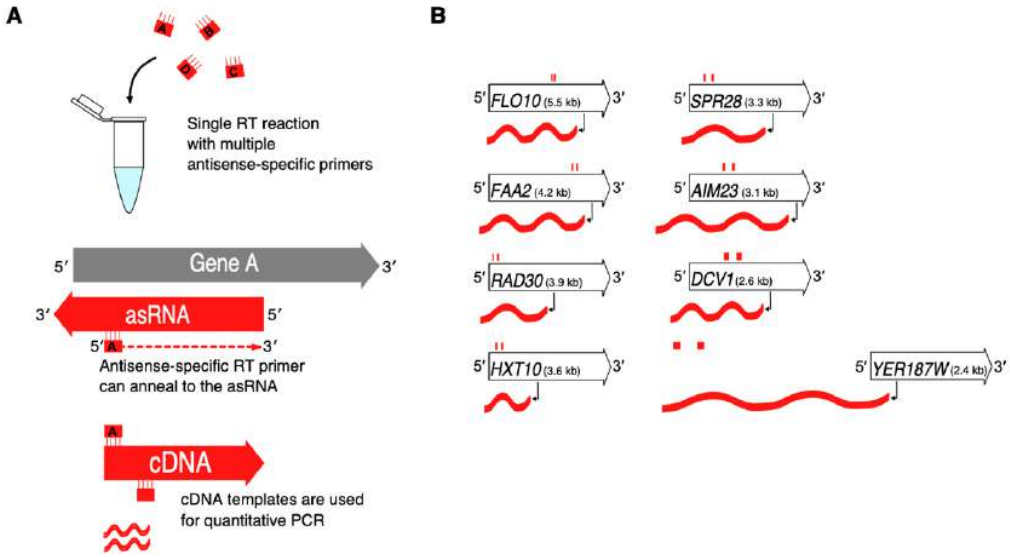

Figure 3.8.1 Multiplexed strand-specific RT-qPCR strategy. (A) Schematic overview of the method. Mixing various antisense-specific primers in a single reaction per sample allows reverse transcription of multiple antisense RNAs. The same primers are also used in the qPCR reaction as forward primers. (B) Scheme showing the selected genes for studying antisense transcription levels, their overlapping antisense RNA (asRNA, red curve), and the qPCR-spanning region of the asRNAs, delimited by representative primers (red rectangles). The gene name and gene length are indicated.

The results demonstrated a significant reduction of asRNA levels in *ioc3Δ* and *isw1Δ* cells with *htz1Δ* background compared without *htz1Δ* background, a pattern consistent across nearly all tested genes (Figure 3.8.2). This observation highlights the crucial role of H2A.Z in facilitating cryptic transcription in the absence of ISW1a. To evaluate the dependency of these results on the activity of the SWR1C complex, responsible for H2A/H2A.Z exchange, I also examined the antisense transcript levels in a *swr1Δ* background (Mizuguchi, Shen et al. 2004). The findings revealed a significant reduction in asRNA expression in *swr1Δ isw1Δ* compared to *isw1Δ* cells for the majority of genes (Figure 3.8.3).

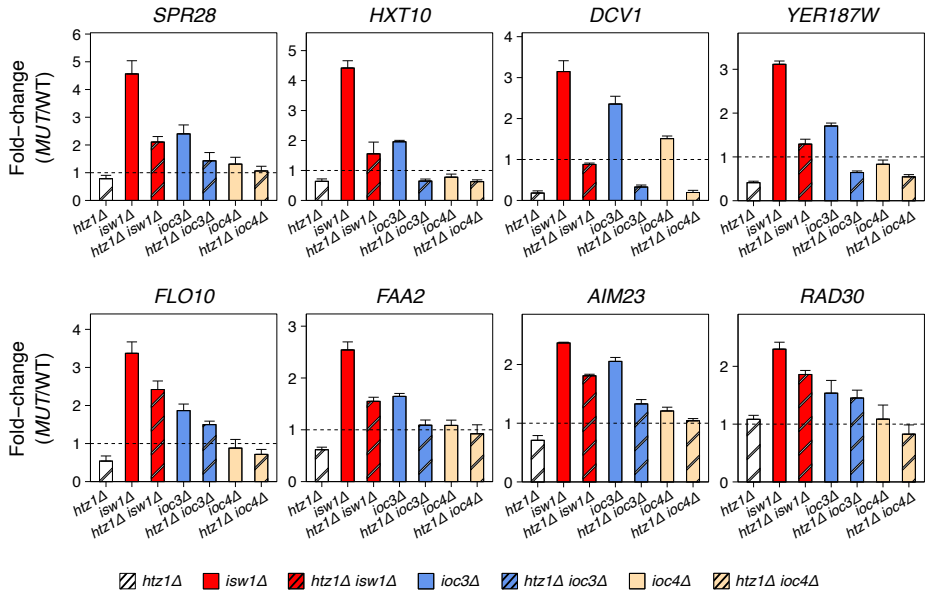

Figure 3.8.2 *HTZ1* deletion suppresses the cryptic phenotype in *isw1Δ* and *ioc3Δ* cells. Strand-specific, multiplexed RT-qPCR analysis of antisense transcription levels in wild-type yeast and Isw1 remodeler mutants with and without the *htz1Δ* background. The dashed line represents antisense expression levels in the wild-type yeast. Three independent experiments were conducted and plotted as mean ± standard error of the mean.

The suppression of asRNA levels in *isw1Δ* cells with *htz1Δ* background was well replicated in a *swr1Δ* background. This suggests that the role of H2A.Z in facilitating cryptic transcription in the absence of the Isw1 may rely on the activity of the SWR1C. Contrastingly, I did not observe the same pattern in *ioc3Δ* cells, except for *SPR28* and *DCV1* genes, where the cryptic phenotype was suppressed by the additional deletion of *SWR1* (Figure 3.8.3). This could suggest that in some genes, SWR1C may not be the factor responsible for depositing intragenic H2A.Z and therefore not participating in H2A.Z-dependent antisense transcription in *ioc3Δ* cells. However, the fact that asRNA expression in *ioc3Δ* is not as pronounced as in *isw1Δ* cells could difficult a notable distinction upon *SWR1* deletion.

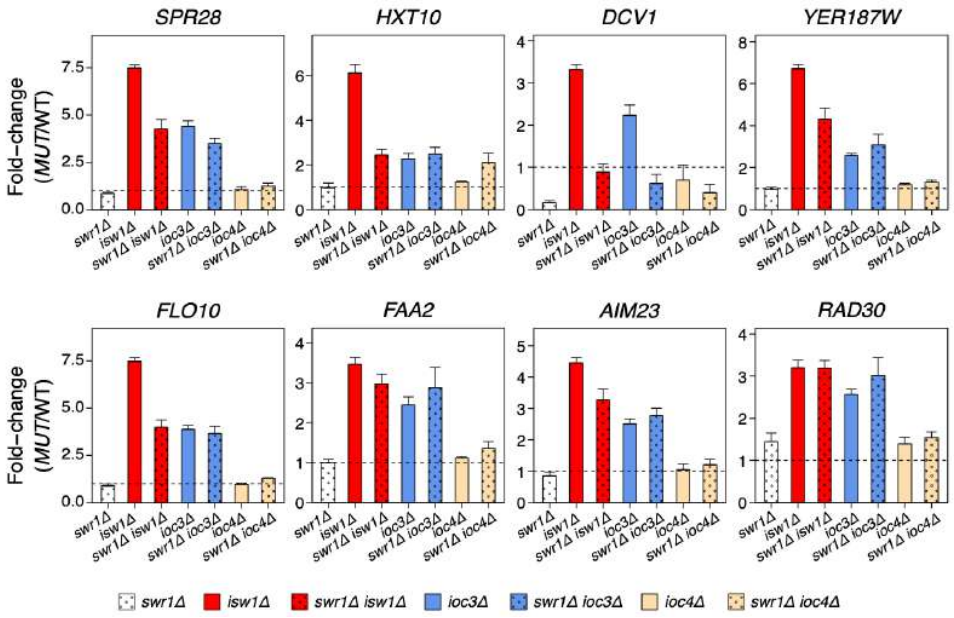

Figure 3.8.3 *SWR1* deletion suppresses the cryptic phenotype in *isw1Δ* cells. Strand-specific multiplexed RT-qPCR analysis of antisense transcription levels in wild-type yeast and Isw1 remodeler mutants with and without the *swr1Δ* background. The dashed line represents antisense expression levels in wild-type yeast. Three independent experiments were conducted and plotted as mean ± SEM.

In yeast, Rad6 together with Bre1 mediate H2B ubiquitination which enables the deposition of H3K4me3 by the Set1 methyltransferase (Sun and Allis 2002, Shahbazian, Zhang et al. 2005). Therefore, I also measured the antisense transcript levels in *isw1Δ, ioc3Δ* and *ioc4Δ* cells, with and without the deletion of *RAD6* or *SET1* genes. The strand-specific RT-qPCR results did not show a predominant pattern among the examined gene candidates (Figure 3.8.4 A and B). In genes where *SET1* single deletion led to increased asRNA levels relative to wild-type, the double mutants *ioc3Δ set1Δ* and *isw1Δ set1Δ* exhibited an additive effect. Otherwise, in genes where *SET1* single deletion showed no impact on asRNA production, the double mutants mirrored the phenotypes of the individual remodeler mutants (Figure 3.8.4 A). Examining the role of Rad6 in cryptic transcription resulted in a variety of phenotypes, where only three genes (*DCV1*, *FAA2* and *RAD30*) showed reduced asRNA levels in the *ioc3Δ rad6Δ* and *isw1Δ rad6Δ* double mutants

compared to the single remodeler mutants (Figure 3.8.4 B). Interestingly, *rad6Δ* cells showed a stronger cryptic phenotype compared to the one from *set1Δ* mutant.

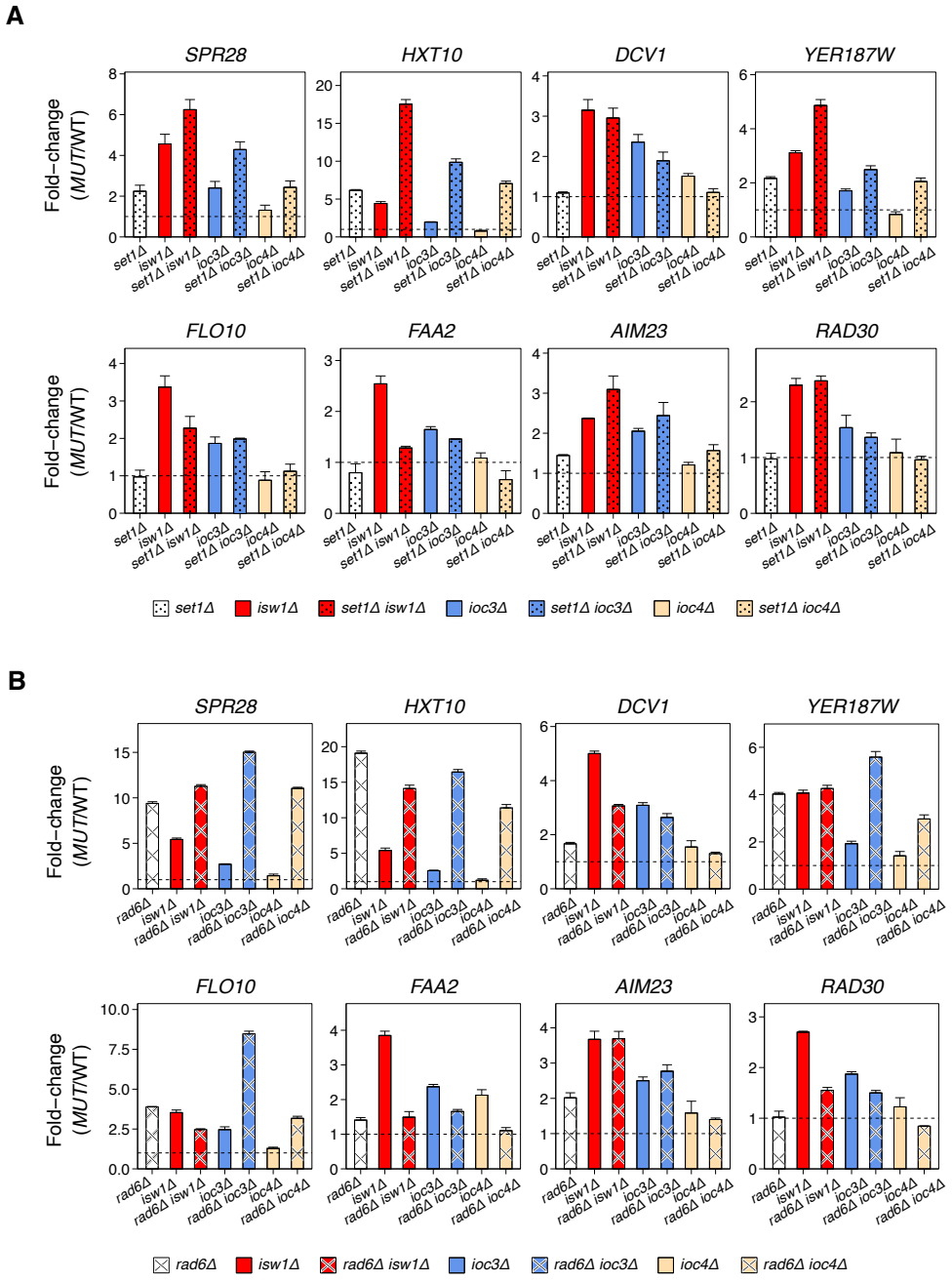

Figure 3.8.4 Impact of *RAD6* and *SET1* deletions on the cryptic transcription phenotype in Isw1 remodeler mutants. Strand-specific multiplexed RT-qPCR analysis of antisense transcription levels in wild-type yeast and Isw1 remodeler mutants with and without the *set1Δ* (A) or *rad6Δ* (B) background. The dashed line represents antisense expression levels in wild-type yeast. Three independent experiments were conducted and plotted as mean ± SEM.

Overall, these findings suggest that H3K4me3 may not be a prerequisite for cryptic transcription activation in ISW1a-depleted cells. H2A.Z, on the other hand, seems to generally contribute to the mechanism of intragenic transcription initiation in the absence of ISW1a. Cells lacking ISW1b complex (*ioc4Δ)* were also included in these experiments. However, the antisense transcript levels were not altered in *ioc4Δ* versus wild-type across nearly all tested genes, indicating that ISW1a is the main contributor for the suppression of the asRNAs examined herein (Figure 3.8.2, Figure 3.8.3, Figure 3.8.4).

3.9 H2A.Z promotes ISW1a recruitment *in vivo*

While recruitment of ISW1b onto mid-3′ regions of genes has been shown to be facilitated by H3K36me3, the mechanisms underlying ISW1a recruitment onto chromatin remain poorly understood (Li, Bergmann et al. 2022). Previous ChIP microarray data uncovered a prominent localization of Ioc3, at the ends of genes (Smolle, Venkatesh et al. 2012). However, because the yeast coding genome is highly dense, the Ioc3 occupancy signal at the 3′ end of genes could correspond to the start of a tandem or divergent adjacent gene. Likewise, a published study involving MNase-ChIP-seq demonstrated a remarkable enrichment of Ioc3 particularly at the +1 nucleosome, which usually contains H2A.Z and other active histone marks such as H3K4me3 and histone acetylation (Yen, Vinayachandran et al. 2012, Kuo, Henry et al. 2015, Soares, He et al. 2017, Bagchi, Battenhouse et al. 2020).

In vitro studies performed by Lena Bergmann, a former PhD student in our lab, have shown that ISW1a complex preferably binds and slides H2A.Z nucleosomes compared to H2A-nucleosomes while no preference has been shown for H3K4me3-nucleosomes versus non-methylated nucleosomes (Bergmann 2021). These *in vitro* assays have also shown a preference for ISW1a binding to highly acetylated nucleosomes (H3K9, K14, K18, K23 and K27ac).

CUT&RUN was attempted to be established in our lab in order to study chromatin remodeler's genomic location *in vivo*. When analyzing the pilot CUT&RUN experiment using Ioc3-Flag and untagged wild-type yeast, I observed that, similarly to previous microarray data, Ioc3-Flag occupancy peaked upstream the TSS and downstream the TES of genes (Figure 3.9.1 A) (Smolle, Venkatesh et al. 2012). However, CUT&RUN revealed a higher Ioc3-Flag occupancy near the TSS than the TES (Figure 3.9.1 A). I identified 2088 Ioc3-Flag peaks shared between two biological replicates, representing the majority of peaks in each replicate (Figure 3.9.1 B). Given the dense nature of the yeast genome and the bidirectionality of yeast promoters, these results could suggest that Ioc3 is recruited to nucleosome depleted regions (NDRs), particularly near the start of genes (Bagchi, Battenhouse et al. 2020).

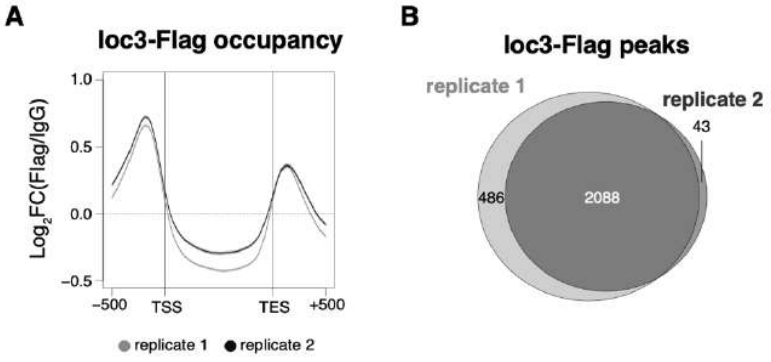

Figure 3.9.1 Ioc3 accumulates at nucleosome-depleted regions in wild-type yeast. (A) Metagene representation of Ioc3-Flag occupancy over protein-coding genes, as determined using CUT&RUN, in wild-type cells. The y-axis represents the log2 ratio of Ioc3-Flag occupancy versus IgG control. Data are shown as mean (line) ± SEM (shadow). Gene bodies were scaled to 1000 bps, with a 500 bp flanking window. (B) Overlap representation of Ioc3-Flag peaks, identified by MACS2, between two biological replicates.

Next, I conducted a motif search analysis using MEME suite to evaluate whether Ioc3 is recruited to a particular DNA regulatory element in the NDRs. For the motif search analysis, I used the top 600 peaks according to their fold-change relatively to the negative control. Whitin these peaks, there was an enrichment for Reb1 and Rap1 consensus motifs (Figure 3.9.2 A and B). Both replicates revealed

a notable occupancy of Ioc3-Flag at the Reb1 and Rap1 binding sites which I retrieved from published data (Figure 3.9.2 C and B) (Rhee and Pugh 2011).

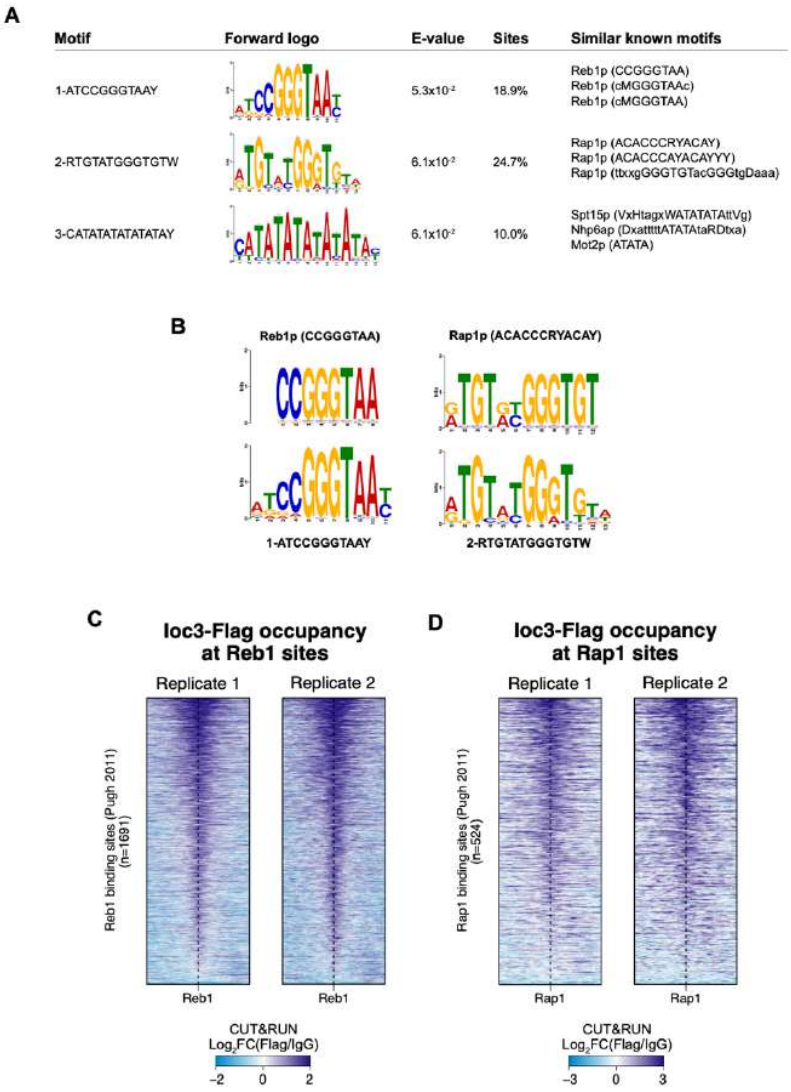

Figure 3.9.2 Ioc3 seems to be enriched at Reb1 and Rap1 binding sites in wild-type yeast. (A) Motif discovery analysis performed by MEME suite on top 500 Ioc3 peaks. The top three most significant motifs are shown. (B) Match between enriched motifs found in Ioc3 peaks and known Reb1 and Rap1 motifs. Left: match between "motif 1" and Reb1 consensus motif. Right: match between "motif 2" and Rap1 consensus motif. (C, D) Ioc3-Flag occupancy over Reb1 and Rap1 binding sites: Heatmaps showing Ioc3-Flag occupancy levels compared to IgG negative control over Reb1 (C) and Rap1 (D) binding sites. Heatmaps for both replicates are displayed, ordered by decreasing log2(Flag/IgG) values, with a flanking window of 500 bps. Reb1 and Rap1 binding sites were obtained from published data (Rhee and Pugh 2011).

These CUT&RUN results seemed promising, but the challenge of reproducibility in library preparation including both wild-type and *htz1Δ* strains posed an obstacle to further investigating ISW1a recruitment through this technique. For this reason, I employed ChIP-qPCR to study the influence of H2A.Z and/or histone acetylation on the recruitment of ISW1a to the start of genes in cells lacking *HTZ1* and/or *GCN5*. Gcn5 is the catalytic acetyltransferase subunit of the SAGA and ADA transcription activator complexes, responsible for the acetylation of multiple lysine residues from histone H3 which were present in the nucleosomes used for testing ISW1a recruitment *in vitro* (Cieniewicz, Moreland et al. 2014, Kuo, Henry et al. 2015). For this purpose, I designed the ChIP-qPCR primers to span an amplicon within the first 200 bps of genes, where +1 nucleosome localizes.

Although I tested several genes for ChIP-qPCR analysis, only a few well-expressed genes, namely *ADH1*, *PDC1*, *PMA1*, and *PYK1*, exhibited an enrichment for Ioc3-Flag compared to untagged wild-type cells. This limitation could derive from the transient activity of ISW1a as a chromatin remodeler. To determine the Ioc3 enrichment, I normalized the input values of target regions to the mean of two control regions, CHRV and *STE3*. These control regions, identified as an intergenic telomeric region within chromosome V and a mid-coding region of the *STE3* gene, were chosen due to their low ISW1a enrichment observed in the microarray data from Michaela Smolle (Smolle, Venkatesh et al. 2012). Results indicated that Ioc3 localization at the gene start remained unaffected in the *gcn5Δ* single mutant, suggesting that ISW1a recruitment to these genomic regions is independent of Gcn5-mediated histone acetylation marks (Figure 3.9.3). On the other hand, cells lacking *HTZ1* exhibited diminished Ioc3 occupancy compared to the wild-type (Figure 3.9.3). The double mutant *htz1Δ gcn5Δ* did not display any additive effect; rather, it mirrored the Ioc3 occupancy pattern observed in the *htz1Δ* single mutant. This observation implies that the absence of H2A.Z is the sole contributor to the reduced Ioc3 occupancy in the double mutant relative to the wild-type. The *in vivo* findings shown by ChIP-qPCR align with the previous *in vitro* evidence generated in our lab regarding ISW1a's binding preference for H2A.Z nucleosomes, but do not correspond with the *in vitro* evidence regarding a binding preference for histone H3

acetylated nucleosomes. While other histone acetyltransferases exist in yeast, there is the possibility that these may compensate for Gcn5 loss. Conversely, H2A-H2A.Z exchange primarily relies on the SWR1C (Zhang, Roberts et al. 2005). Overall, the results herein suggest that ISW1a recruitment to gene starts may be promoted by the presence of H2A.Z at the +1 nucleosome due to a higher affinity to bind H2A.Z-containing nucleosomes. However, a validation across a broader spectrum of genes would be required in order to draw a general conclusion.

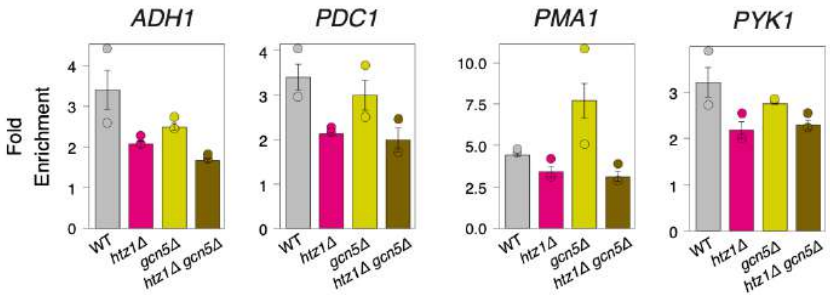

Figure 3.9.3 Potential reduction in Ioc3 recruitment to the start of genes upon loss of H2A.Z. ChIP-qPCR analysis of Ioc3-Flag in wild-type and *htz1Δ*, *gcn5Δ*, and *htz1Δ gcn5Δ* cells. Fold enrichment was obtained by normalizing the input percentage of target genes (*PMA1*, *PDC1*, *ADH1*, and *PYK1*) to the mean of those of control regions (CHRV and *STE3*). Two biological replicates were analyzed and plotted as mean ± SEM. The primer sets used span an amplicon within the first 200 bps of each gene. The colors represent the different yeast strains indicated in the x-axis.

3.10 Supplementary figures

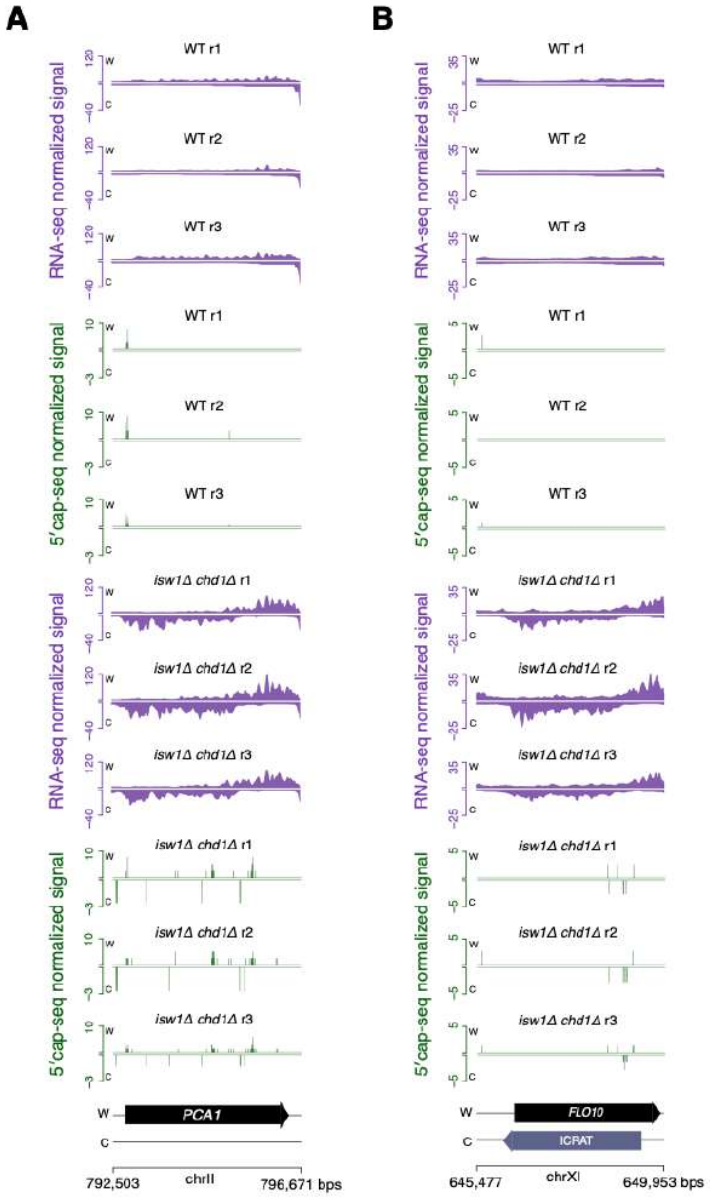

Figure 3.10.1 RNA-seq and 5′cap-seq coverage tracks of three biological replicates from wild-type and *isw1Δ chd1Δ* strains over representative genes *PCA1* (A) and *FLO10* (B). RNA-seq values are represented as the mean of normalized coverage in 10-bp bins. Watson (W) and Crick (C) strands are indicated, as well as genomic coordinates.

A

Rank	Motif	P-value	log P-pvalue	% of Targets	% of Background	STD(Bg STD)	Best Match/Details
1 *		1e-2	-4.797e+00	0.39%	0.07%	120.2bp (359.0bp)	SeqBias: A/T bias(0.767) More Information | Similar Motifs Found
2 *		1e-1	-4.469e+00	1.89%	1.05%	85.8bp (1205.6bp)	TBP(- other)/several species/AthaMap(0.725) More Information | Similar Motifs Found
3 *		1e0	-1.707e+00	0.24%	0.10%	17.0bp (191.5bp)	hb/dmmpmm(Bergman)/fly(0.799) More Information | Similar Motifs Found
4 *		1e0	-9.902e-01	0.47%	0.38%	161.0bp (693.1bp)	SeqBias: CA-repeat(0.913) More Information | Similar Motifs Found
5 *		1e0	-2.949e-01	5.13%	5.57%	104.3bp (1029.4bp)	SeqBias: TA-repeat(0.917) More Information | Similar Motifs Found
6 *		1e0	-2.267e-02	0.08%	0.32%	0.8bp (461.2bp)	Maz(Zf)/HepG2-Maz-ChIP-Seq(GSE31477)/Homer(0.968) More Information | Similar Motifs Found
7 *		1e0	-0.000e+00	59.27%	89.35%	118.5bp (1450.4bp)	HNRNPC(RRM)/Homo_sapiens-RNCMPT00025-PBM/HughesRNA(0.831) More Information | Similar Motifs Found

B

Rank	Motif	P-value	log P-pvalue	% of Targets	% of Background	STD(Bg STD)	Best Match/Details
1 *		1e0	0.000e+00	0.38%	83.71%	36.0bp (277419.7bp)	URC2/MA0422.1/Jaspar(0.802) More Information | Similar Motifs Found
2 *		1e0	0.000e+00	0.57%	100.00%	21.9bp (362222.0bp)	Nab2p(Znf)/Saccharomyces_cerevisiae-RNCMPT00042-PBM/HughesRNA(0.889) More Information | Similar Motifs Found
3 *		1e0	-0.000e+00	0.38%	27.42%	100.5bp (405864.3bp)	br-Z2/dmmpmm(Bergman)/fly(0.713) More Information | Similar Motifs Found
4 *		1e0	-0.000e+00	0.19%	31.86%	0.0bp (295863.3bp)	Tb_0217(RRM)/Trypanosoma_brucei-RNCMPT00217-PBM/HughesRNA(0.672) More Information | Similar Motifs Found
5 *		1e0	-0.000e+00	0.19%	47.20%	0.0bp (324647.1bp)	ATHB-16/MA0951.1/Jaspar(0.787) More Information | Similar Motifs Found
6 *		1e0	-0.000e+00	0.19%	44.15%	0.0bp (305150.6bp)	PH0038.1_Hlx/Jaspar(0.684) More Information | Similar Motifs Found
7 *		1e0	0.000e+00	0.19%	51.97%	0.0bp (296590.2bp)	PB0166.1_Sox12_2/Jaspar(0.790) More Information | Similar Motifs Found

Figure 3.10.2 Results of de-novo motif search performed by HOMER on TSS clusters from capped ICRATs. The red asterisk (*) symbolizes possible false positives. Yeast promoter sequences of protein coding-genes were used as background in (A), while whole *S. cerevisiae* genome was used as background in (B).

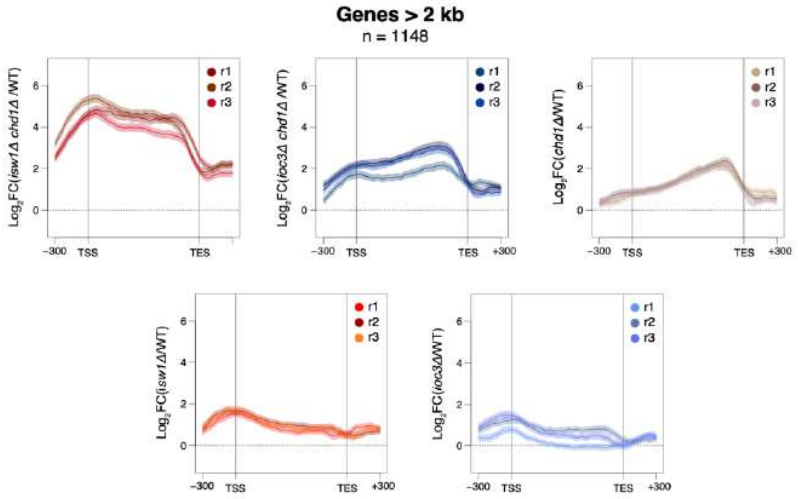

Figure 3.10.3 Individual replicate data from metagene analysis of antisense expression levels across genes longer than 2 kb (n = 1148). The y-axis represents the log2 ratio of normalized antisense RNA-seq coverage for mutant versus wild-type. Data are shown as mean (line) ± SEM (shadow). The TSS and TES are indicated. Gene bodies were scaled to 1000 bps, with a 300 bp flanking window.

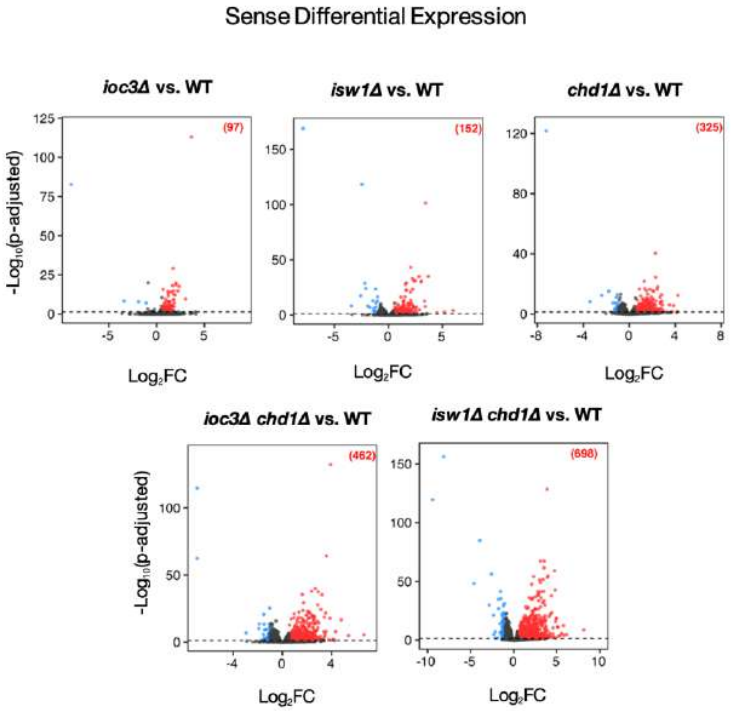

Figure 3.10.4 Results of sense differential expression analysis performed on each remodeler mutant versus wild-type yeast. The dashed line represents significance (adjusted p-value of 0.05). Red indicates upregulated genes, and blue indicates downregulated genes (1.5-fold-change). The number of upregulated or derepressed genes is indicated.

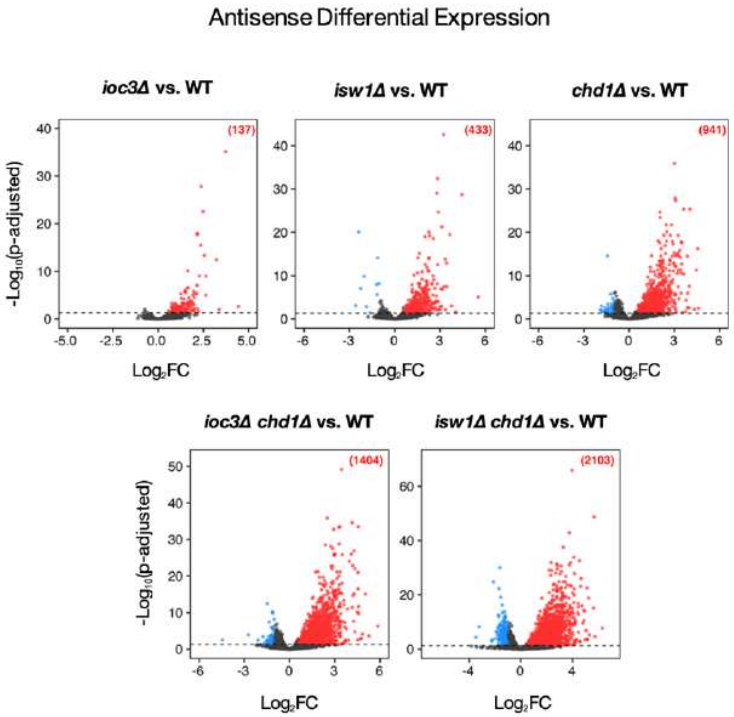

Figure 3.10.5 Results of antisense differential expression analysis performed on each remodeler mutant versus wild-type yeast. The dashed line represents significance (adjusted p-value of 0.05). Red indicates upregulated genes, and blue indicates downregulated genes (1.5-fold-change). The number of upregulated or derepressed genes is indicated.

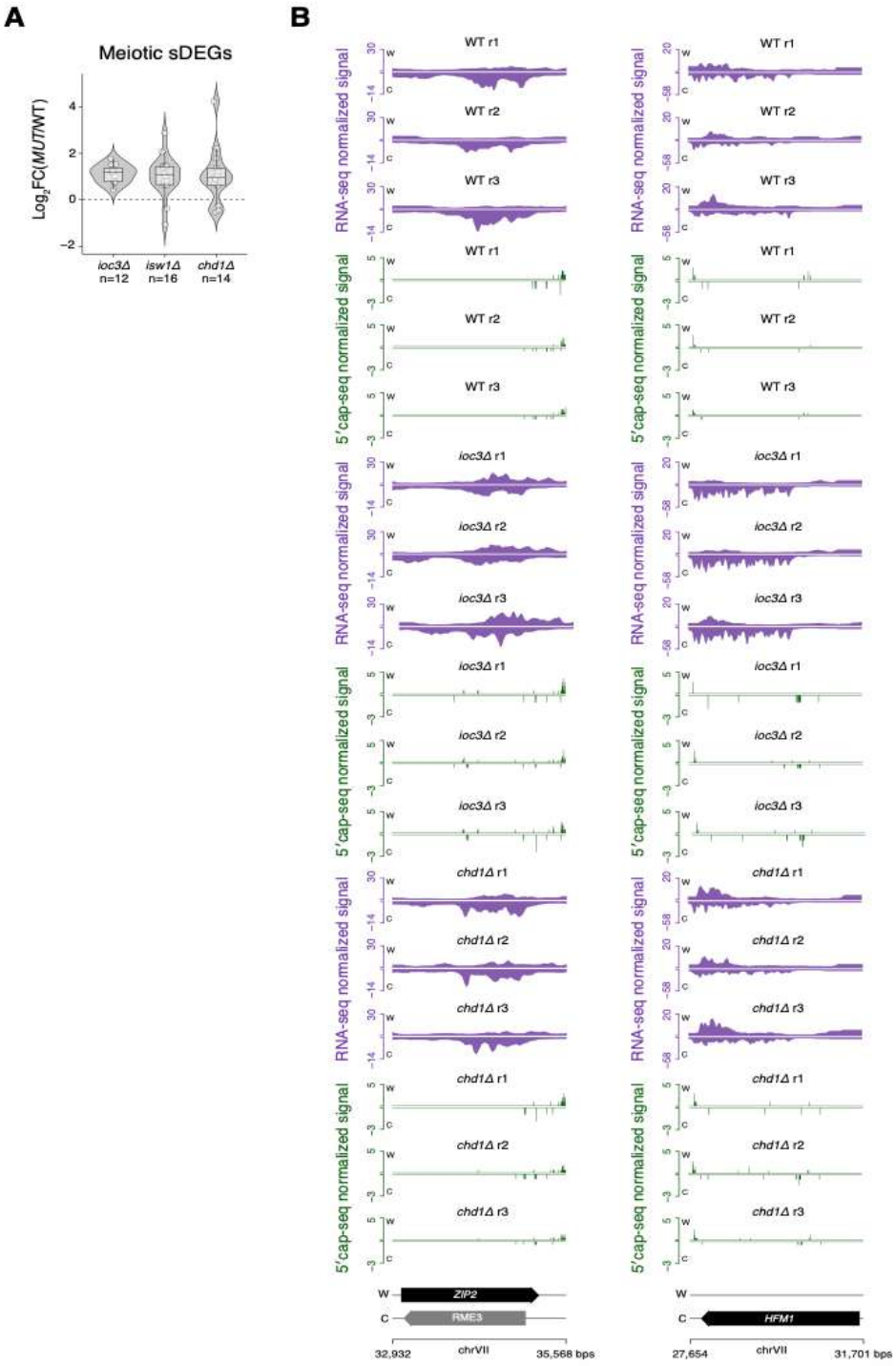

Figure 3.10.6 Individual replicate data for transcriptional changes in meiotic genes caused by deletion of *IOC3*, *ISW1*, and *CHD1*. (A) RNA expression changes of meiosis-related sense differentially expressed genes (n=sDEGs) in each single mutant relative to wild-type. (B) RNA-seq and 5′cap-seq coverage tracks of three biological replicates per strain over meiotic genes *ZIP2* and *HFM1*. RNA-seq values are represented as the mean of normalized coverage in 10-bp bins. Watson (W) and Crick (C) strands are indicated, as well as genomic coordinates.

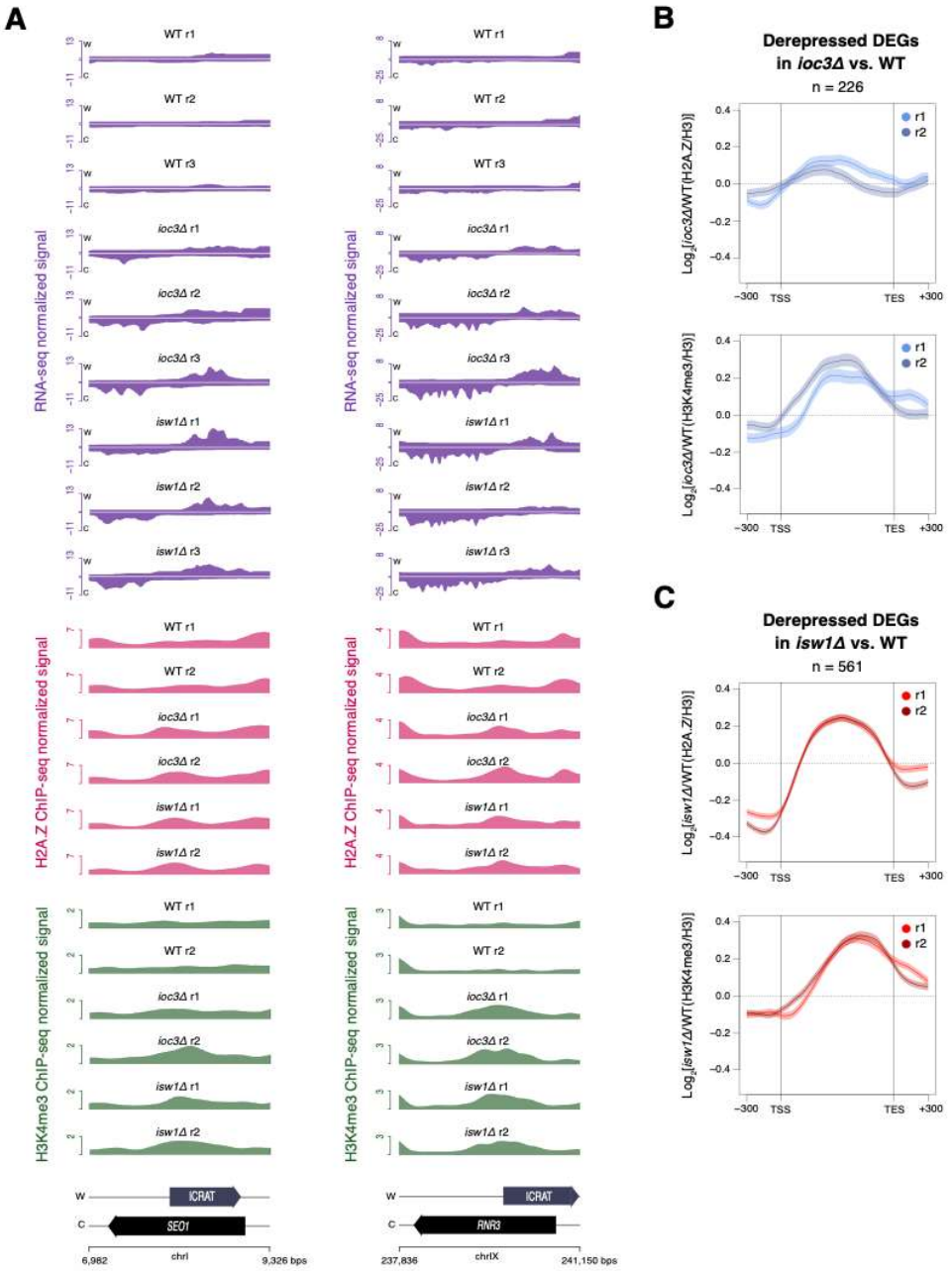

Figure 3.10.7 Individual replicate data for H2A.Z and H3K4me3 levels data over derepressed genes. (A) RNA expression, as well as H2A.Z and H3K4me3 occupancy levels are depicted for representative genes with overlapping ICRATs. RNA-seq values represent the mean of normalized coverage in 10-bp bins, for three biological replicates. ChIP-seq values represent the mean of normalized coverage in 30-bp bins for each replicate. Watson (W) and Crick (C) strands are indicated. (B, C) Metagene representations of H2A.Z and H3K4me3 occupancy over derepressed differentially expressed genes (DEGs) in *ioc3Δ* (B) and *isw1Δ* (C) cells. The y-axis represents the log2 ratio of H2A.Z or H3K4me3 occupancy, as determined using ChIP-seq, in mutant versus wild-type. Data are shown as mean ± SEM. The TSS and TES are indicated. Gene bodies were scaled to 1000 bps, with a 300 bp flanking window.

4 Discussion

4.1 High-resolution characterization of the cryptic transcriptional phenotype in *isw1Δ chd1Δ* cells

This study aimed to investigate the impact of ISW1a on cryptic transcription and to explore the mechanism of ISW1a-mediated cryptic transcription suppression in *Saccharomyces cerevisiae*. To investigate the impact of ISW1a on cryptic transcription, I applied transcriptomics techniques such as RNA-seq and 5′cap-seq. Before delving into the individual contributions of ISW1a and CHD1, I characterized the transcriptional phenotype in *isw1Δ chd1Δ* cells using these high-resolution techniques.

My findings provide a detailed insight into the complex transcriptional landscape induced by the deletion of Isw1 and Chd1 ATPases, highlighting their impact on cryptic transcriptional activity. Key findings demonstrate a strong transcriptional derepression phenotype, particularly for antisense transcription as 35% of yeast genes (n=2103) exhibited a significant increase in antisense RNA expression in the double mutant. A smaller subset of 698 genes showed significantly increased sense expression, and only 72 genes were down-regulated. The increase in antisense transcripts in the absence of major sense down-regulation indicates that there is no negative transcriptional interference, suggesting there are mechanisms taking place to tightly regulate gene expression - one potentially being the rapid degradation of cryptic transcripts.

I conducted a detailed analysis of transcription initiation which demonstrated a considerable increase in both sense and antisense intragenic TSS clusters (TCs) in the double mutant relative to the wild-type. The higher abundance of intragenic TCs in the double mutant aligns with the transcriptional derepression phenotype observed with RNA-seq, pointing to the inappropriate activation of intragenic transcription initiation sites in the absence of Isw1 and Chd1. The increase of intragenic sense TCs, together with the stability of gene

promoter TCs between the double mutant and wild-type suggests that the derepression of sense RNA levels is predominantly due to the accumulation of cryptic transcripts.

In annotating the Isw1 and Chd1-repressed antisense transcripts (ICRATs), I identified 1918 asRNAs, covering 80% of the asDEGs identified in the double mutant. The majority of asDEGs contained a single ICRAT, although longer genes displayed a modestly higher likelihood of harboring multiple overlapping ICRATs. This observation between gene length and ICRAT frequency suggests that longer genes are more susceptible to cryptic transcription initiation events. The identification of TSS clusters near the 5′ ends of the majority of ICRATs indicates that these transcripts are mostly capped. Furthermore, due to the poly(A)-enrichment step performed in both RNA-seq and 5′cap-seq methods, these transcripts are all polyadenylated. Therefore, ICRATs may be processed in a manner similar to mRNAs.

Motif enrichment analysis of the promoter regions of capped and polyadenylated ICRATs using MEME and HOMER tools suggested the presence of a TATA-containing motif within an extended dinucleotide repeat sequence over a limited number of sites. MEME and HOMER identified similar motifs but with distinct interpretations; HOMER's analysis suggested an A/T bias potentially due to systematic background differences. The failure of HOMER to detect this motif when using the entire *S. cerevisiae* genome as a background reinforces the idea that these motifs may represent sequence biases rather than unique regulatory elements specific to the mutant phenotype. I believe the lack of promoter-like DNA regulatory sequences reinforces that the nature of the cryptic transcription initiation is strongly linked to chromatin changes.

In this study, I further demonstrate that ICRATs may not be uniquely repressed by Isw1 and Chd1 remodelers since FACT-impaired cells also exhibited considerably increased ICRAT expression levels compared to wild-type yeast. Chd1 has been demonstrated to facilitate the spreading of FACT across the gene body (Jeronimo, Angel et al. 2021). Further investigation is

needed to explore the potential collaboration between the FACT chaperone and the remodelers Isw1 and Chd1 in preserving transcription fidelity.

In summary, my findings characterize the *isw1Δ chd1Δ* double mutant transcriptional phenotype as one of widespread cryptic intragenic transcriptional activation, with minimal interference to gene expression levels, highlighting the essential role of chromatin organization in preventing cryptic transcription. Beyond confirming the presence of antisense transcripts, these results point to a broader pervasive impact on the protein-coding genome than initially identified. Additionally, mapping TSSs genome-wide allowed me to demonstrate that the increased sense expression observed in the double mutant is often due to sense intragenic RNA accumulation, rather than gene derepression. While this distinction is mostly missed out in the literature, it is unveiled and emphasized herein. And finally, the antisense transcript regions annotated herein could serve as a valuable resource for the scientific community, with the potential to contribute to the accelerated comprehension of the non-coding transcriptome. Moreover, these annotated asRNAs could hold particular significance when integrated with future or existing datasets generated in cells lacking Isw1 and Chd1. Such integration could potentially improve the comprehension of chromatin dynamics by these remodelers during RNAPII-mediated transcription.

Isw1 (longer spacing) and Chd1 (shorter spacing) remodelers engage in a reported competition to establish regularly spaced nucleosome arrays within gene bodies (Ocampo, Chereji et al. 2016, Kubik, Bruzzone et al. 2019). In *isw1Δ chd1Δ* cells, intragenic nucleosome spacing is altered, with the +2 nucleosome being pushed toward either the +1 or +3 nucleosome (Ocampo, Chereji et al. 2019). Ocampo and colleagues have proposed that the closely packed nucleosomes in the double mutant may slow down RNAPII elongation, potentially resulting in collisions between elongating sense polymerases, and consequently leading to antisense transcription (Ocampo, Chereji et al. 2019). Further studies combining Ocampo's MNase-seq data and the ICRATs identified in this work could provide deeper insights into the mechanism by which Isw1 and Chd1 suppress cryptic transcription. For instance, it would be valuable to

determine whether the disrupted nucleosome spacing observed in *isw1Δ chd1Δ* cells is a phenomenon particularly pronounced in genes with overlapping ICRATs or a general one.

4.2 Distinct and overlapping contributions of ISW1a and CHD1 remodelers to cryptic transcription

In this study, I describe the distinct and overlapping roles of ISW1a and CHD1 remodelers during gene expression, highlighting their specific impact on suppressing sense and antisense cryptic transcription. All single and double remodeler mutants demonstrated a proneness for transcriptional derepression.

Among the tested single remodeler mutants, *CHD1* single deletion stood out as exhibiting the largest alterations in both sense (325 sDEGs) and antisense transcription (941 asDEGs). Deleting *IOC3* resulted in a more subtle transcription derepression phenotype (97 sDEGs and 137 asDEGs). And as expected, deletion of *ISW1* had a transcription derepression impact greater than the one in *ioc3Δ* cells (152 sDEGs and 233 asDEGs), as deleting this ATPase inhibits the formation of both ISW1a and ISW1b complexes. The broader impact of Chd1 compared to Isw1 has been previously reported in the context of transcription-coupled histone turnover, notably heightened at mid-3′ end regions of genes in *chd1Δ* and *isw1Δ chd1Δ* cells compared to *isw1Δ* cells (Smolle, Venkatesh et al. 2012).

My work identifies the genes whose antisense transcription is suppressed exclusively by ISW1a or CHD1, the genes where ISW1a can compensate for the loss of CHD1 and vice versa, and a larger subset of genes where both ISW1a and CHD1 are jointly required for effective suppression of antisense transcription. These results suggest that ISW1a and CHD1 can function independently as well as in collaboration to suppress cryptic transcription.

I uncovered how ISW1a and CHD1 differ in their roles in suppressing antisense transcription. First, I showed that Isw1 and Chd1 repress different asRNAs annotated in the *isw1Δ chd1Δ* double mutant. Additionally, I showed

that RNAPII density at ICRATs derepressed in *chd1Δ* cells was lower in *isw1Δ* cells and the other way around, supporting the differences in suppressing antisense transcription. These differences were particularly evident at longer genes, where Isw1 and Chd1 remodelers prevent antisense transcription at opposite ends of the gene body. In *ioc3Δ* cells, the derepression of asRNAs and antisense TCs was particularly distinguishable at the 5′ regions of genes, indicating that ISW1a is critical for preventing antisense transcription in these regions. In *chd1Δ* cells, antisense transcription predominantly accumulated at the 3′ ends of genes, a pattern I highlight as being associated with increased antisense intragenic TSSs at the 3′ ends, as well as TSSs immediately downstream of the TES. This elucidates the complementary nature of ISW1a and CHD1, with ISW1a acting primarily at the 5′ end and CHD1 acting at the 3′ end of genes to ensure cryptic transcription suppression over the gene body.

Regarding the identity of genes with derepressed asRNAs, I show that ISW1a primarily targets less transcribed genes, while CHD1 regulates both active and inactive genes. Furthermore, across all remodeler mutants, derepressed asDEGs showed an enrichment for genes involved in transmembrane transport. The implication of overlapping antisense RNAs in regulating transmembrane transport genes in *S. cerevisiae* is limited. The *PHO84* gene, which encodes for an inorganic phosphate transporter, contains an overlapping asRNA that accumulates upon loss of Rrp6 (Castelnuovo, Rahman et al. 2013). The transcription of this asRNA represses the sense transcription through *PHO84* promoter deacetylation (Castelnuovo, Rahman et al. 2013). Additionally, asRNAs overlapping with hexose transporter genes have been shown to be upregulated upon loss of the RNA Helicase Dbp2, or in wild-type cells under glucose depletion (Beck, Cloutier et al. 2014).

In the context of sense transcription, I show that ISW1a primarily suppresses transcription initiation within intragenic regions, as shown by increased sense intragenic TSSs in *ioc3Δ* cells, preventing the accumulation of sense cryptic transcripts over mid-to-end regions of genes. CHD1 not only suppresses sense cryptic initiation at intragenic regions but also appears to

repress gene expression, as shown by the presence of both increased sense intragenic TSSs and gene promoter TSSs in *chd1Δ* cells. This distinction was accurately achieved by combining both RNA-seq and 5′cap-seq datasets.

In all remodeler mutants, derepressed sDEGs consisted of less transcribed genes, with a significant portion being TATA-containing. Published Northern blot data uncovered the involvement of Isw2 in repressing meiotic genes during mitotic growth (Goldmark, Fazzio et al. 2000). Goldmark and colleagues attributed this effect to the repression of chromatin structure at the promoter region by Isw2, whose recruitment onto meiotic genes is proposed to occur via the upstream repression sequence (URS1)-binding protein, Ume6 (Goldmark, Fazzio et al. 2000). In the investigation conducted herein, I show that the depletion of Isw1 or Chd1 remodelers resulted in a significant increase in the sense expression of meiotic/sporulation genes – a finding not documented before. During mitotic growth, meiotic genes are either kept silent or very lowly transcribed. The heightened sense expression in the meiotic genes was primarily attributed to RNAs originated from sense intragenic sites, which I particularly highlighted in yeast lacking the ISW1a remodeling complex. In *ioc3Δ* cells, the derepression of sense intragenic transcription in these genes was accompanied by reduced antisense RNA levels, indicating a cis-regulatory mechanism. This regulatory mechanism may be critical for modulating gene expression during meiosis and sporulation, which raises the question of how these genes would behave in *ioc3Δ* cells undergoing or preparing for meiosis. Employing RNA-seq and 5′cap-seq on meiotic growth and vegetative diploids in *ioc3Δ* and wild-type backgrounds could provide valuable insights to address this question. Given these observations, ISW1a may be particularly important for repressing cryptic transcription at genes poised for transcriptional activation under specific environmental or developmental conditions.

Given that the analysis of the transcriptional implications of an *IOC3* deletion revealed a subtle impact, I further explored the ISW1a-associated cryptic phenotype in *ioc3Δ* cells within a *rrp6Δ* background using 5′cap-seq. First, my studies nicely reproduced the cryptic phenotype from *rrp6Δ* cells. Cells

lacking only the exosome catalytic subunit exhibited the most pronounced increase of TSS expression at intergenic regions, including those marking the start site of cryptic unstable transcripts (CUTs). This effect was further exacerbated in *ioc3Δ rpp6Δ* cells, indicating a previously undocumented role for ISW1a in suppressing divergent transcription from intergenic regions. One potential mechanism for suppressing CUTs could be ISW1a's capacity to counteract NDR widening through nucleosome reassembly or sliding upstream of NDRs, as proposed in previous research (Parnell, Schlichter et al. 2015). Another notable observation in this study is the increased expression of intragenic TSSs in the *ioc3Δ rrp6Δ* double mutant compared to single mutants, suggesting that transcripts originating from these promoters in *ioc3Δ* cells are partially degraded via the nuclear exosome. To further validate these findings, I recommend performing RNA-seq followed by differential expression analysis. Alternatively, RT-qPCR experiments targeting specific CUTs could confirm the role of ISW1a in preventing their transcription in *ioc3Δ rrp6Δ* cells.

Overall, I identified key findings regarding the roles of ISW1a and CHD1 in regulating transcription. These include (1) ISW1a and CHD1 can function independently or synergistically to suppress cryptic transcription; (2) ISW1a and CHD1 prevent antisense transcription at opposite ends of genes; (3) while ISW1a primarily suppresses sense intragenic transcription initiation, CHD1 also represses mRNA transcription initiation; and (4) ISW1a may also prevent cryptic transcription initiation within intergenic regions, including initiation of CUTs. By dissecting the individual contributions of ISW1a and CHD1 to transcription regulation, my studies provide new insights into the impact of ISW1a in suppressing cryptic transcription in yeast.

4.3 Why do cryptic intragenic RNAs accumulate in chromatin remodeler-deficient cells?

The cryptic intragenic transcripts observed in the remodeler mutants are polyadenylated and predominantly capped. In eukaryotes, the collaboration between the 7-methylguanosine cap situated at the 5′end of the mRNA and the 3′ poly(A) tail is known to influence RNA stability and stimulate translation (Passmore and Coller 2022). However, deadenylation pathways can target poly(A) molecules to degradation (Passmore and Coller 2022). In yeast, a fraction of chromatin-sensitive intragenic RNAs has been suggested to undergo degradation through nonsense-mediated decay (NMD) (Malabat, Feuerbach et al. 2015). Given that NMD is a translation-dependent RNA quality surveillance mechanism, some intragenic RNAs in yeast may potentially interact with the translation machinery.

While the translational potential of the detected cryptic transcripts in this study has not been explored, earlier work from Pelechano's lab has investigated the association between ribosomes and cryptic transcripts present in a variety of chromatin factor mutants (Wei, Hennig et al. 2019). In cells lacking the Set2 methyltransferase, the authors could detect 618 intragenic sense TSSs associated with polyribosomes, suggesting that transcripts emerging from intragenic promoters can be stable and may putatively lead to the production of truncated proteins (Wei, Hennig et al. 2019).

When Isw1 and Chd1 remodelers are abolished, previously concealed cryptic promoters are exposed, resulting in the production of cryptic transcripts. Instead of undergoing rapid degradation, these transcripts visibly accumulate in cells lacking Isw1 and/or Chd1 remodelers, raising questions regarding RNA degradation escape. In the present study, I found no significant alterations in the expression levels of genes related to RNA decapping, deadenylation, or decay in the remodeler mutant cells compared to wild-type, suggesting that these cells contain a fully functional nuclear exosome and termination complexes. While it is plausible that cells lacking chromatin remodelers in this study may exhibit a higher ratio of cryptic transcript abundance to free nuclear exosome abundance,

resulting in a slower degradation rate, the possibility of export and translation cannot be ruled out. Future experiments such as polyribosome fractionation and HT-5Pseq could help elucidate the translation efficiency of cryptic transcripts (Panda, Martindale et al. 2017, Wei, Hennig et al. 2019, Zhang and Pelechano 2021).

4.4 H2A.Z is important for the cryptic phenotype in cells lacking Isw1 chromatin remodelers

The second fundamental question addressed in this thesis is: how does ISW1a suppress cryptic transcription? The collaborative efforts between Lingling Yang and I determined an association between cryptic transcription and alterations in the distribution of H2A.Z and H3K4me3 in *ioc3Δ* and *isw1Δ* cells. We observed increased accumulation of H2A.Z H3K4me3 at intragenic regions in *ioc3Δ* cells, and to a bigger extent in *isw1Δ* cells.

By coupling the H2A.Z and H3K4me3 occupancy data with my transcriptomic data, I uncovered that the increased levels of both H2A.Z and H3K4me3 were not global effects resulting from the depletion of Isw1 remodelers. They were rather pronounced at intragenic regions of genes exhibiting cryptic transcription in these mutants, particularly at the start of the overlapping cryptic transcripts. To gain insight into the causal or consequential roles of these chromatin changes in *ioc3Δ* and *isw1Δ* cells, I measured specific antisense transcripts identified by RNA-seq in the *isw1Δ* single mutant. The RT-qPCR studies I present here revealed that the deletion of *HTZ1* suppresses antisense transcription in the remodeler mutants. This indicates the critical role of H2A.Z in enabling antisense transcription upon loss of Isw1 or ISW1a additional subunit, Ioc3. The incorporation of H2A.Z at the start of the tested antisense transcripts seems to rely on Swr1 activity, particularly in *isw1Δ* cells, as similar results could be reproduced in a *swr1Δ* background.

In contrast to the discernible effect of *HTZ1* deletion in *isw1Δ* and *ioc3Δ* cells, the deletion of Set1 methytransferase or Set3 deacetylase did not yield a

prevalent outcome on the expression of antisense transcripts. Although Set1 is responsible for depositing H3K4me3, its depletion did not suppress the cryptic phenotype in the remodeler mutants. This suggests that H3K4me3 may not play a critical role in the initiation of antisense transcription but is more likely a consequence of the early elongation of antisense transcripts.

By combining my RNA-seq data with published NET-seq data, I could observe an increase in RNAPII occupancy across most across most ICRATs identified in *isw1Δ* and *chd1Δ* single mutants. Since Set1 is recruited by early elongating RNAPII, I would suggest that for cells lacking Isw1 or Ioc3, an increased occupancy of antisense elongating RNAPII could result in Set1 depositing methylation marks on unmethylated or already methylated H3K4 residues. This would then lead to the accumulation of H3K4me3 at the 5′ end of antisense transcripts, located within intragenic regions. Concerning Chd1, the literature on H3K4me3 reveals contrasting results. Radman-Livaja and colleagues previously observed a slight rise in H3K4me3 at the 3′ end of genes in *chd1Δ* yeast cells, whereas Lee et al. did not identify a statistically significant increase in H3K4me3 in the same gene regions (Radman-Livaja, Quan et al. 2012, Lee, Park et al. 2017). However, these studies employed different resolution tools to generate chromatin profiles for H3K4me3, namely ChIP-chip and ChIP-seq. Resolving these discrepancies requires additional studies focused on comprehending the chromatin changes resulting from CHD1 deletion.

Overall, my findings support published work pinpointing the general role of H2A.Z in transcription initiation (Gu, Naiyachit et al. 2015, Bagchi, Battenhouse et al. 2020). Published work has linked increased H2A.Z occupancy at 3′ end of genes to the start sites of antisense transcripts in wild-type yeast (Gu, Naiyachit et al. 2015). In humans, intragenic H2A.Z has also been found in transcriptionally silent genes although the association with cryptic transcription was not investigated (Hardy and Robert 2010). In this study, I propose that the absence of Isw1 and Ioc3 compromises chromatin establishment and lead to the formation of intragenic nucleosome-depleted regions. Then the Swr1 complex

could sense these regions due to its affinity for extended DNA stretches, leading to the incorporation of H2A.Z (Ranjan, Mizuguchi et al. 2013, Carcamo, Poyton et al. 2022). Consequently, H2A.Z-containing nucleosomes at intragenic sites destabilizes histone-DNA contacts, promoting cryptic transcription initiation. The accumulation of intragenic H2A.Z, facilitated by Swr1-mediated deposition, has been previously reported in cells lacking FACT and Spt6 histone chaperones (Jeronimo, Watanabe et al. 2015). The authors have also observed that deletion of *HTZ1* suppresses cryptic transcription in the chaperone mutants, similar to the findings observed herein (Jeronimo, Watanabe et al. 2015). This study also revealed that Isw1 and Chd1-repressed asRNAs are also expressed in yeast cells impaired for FACT or Spt6. Similar to Isw1 and Chd1, these chaperones have been reported to play a role in preserving chromatin structure during RNA polymerase II elongation (Formosa and Winston 2020, Miller, Warner et al. 2023). Consequently, it is plausible that they act in parallel to suppress cryptic transcription. However, further studies are required to elucidate and assess the extent of their putative collaborative mechanisms.

4.5 ISW1a recruitment may be facilitated by H2A.Z

The genome-wide strategy CUT&RUN has proven effective in capturing the occupancy of chromatin remodelers like SWI/SNF and RSC (Brahma and Henikoff 2019, Wolf, Zhao et al. 2023). Consistent with published data, my study successfully replicated the recruitment of Ioc3 to gene boundaries in wild-type yeast (Smolle, Venkatesh et al. 2012, Yen, Vinayachandran et al. 2012). However, due technical challenges involving CUT&RUN libraries, I proceeded to investigate the recruitment of ISW1a by ChIP-qPCR. My findings revealed a trend of reduced Ioc3 recruitment onto the start of genes upon *HTZ1* deletion, indicating a partial contribution from H2A.Z to the recruitment of ISW1a to the start of genes. Because Ioc3 occupancy was not completely abolished but rather reduced in the absence of H2A.Z, other factors are required to ISW1a recruitment *in vivo*. Nevertheless, my study provides *in vivo* evidence that

supports previous *in vitro* findings where ISW1a complex was shown to preferably bind to H2A.Z-containing nucleosomes and slide these faster than H2A-containing nucleosomes (Bergmann 2021).

In moving forward, additional research on ISW1a recruitment onto chromatin should be explored. Although chromatin remodelers can interact with DNA, the interaction or affinity of ISW1a to DNA may be more critical given that CUT&RUN revealed Ioc3 peaks at gene boundaries, which are characterized by longer stretches of DNA. The enrichment in Reb1 and Rap1 consensus motifs found in Ioc3 peaks from CUT&RUN could either suggest Ioc3 affinity for NDRs or for Reb1 and Rap1 transcription factors which are involved in NDR formation (Yarragudi, Miyake et al. 2004, Hartley and Madhani 2009, Krietenstein, Wal et al. 2016). Thus, I would recommend future ISW1a recruitment studies in cells depleted for Reb1 or Rap1. Furthermore, genome-wide sequencing studies on the occupancy of Ioc3 in cells deficient for early elongating RNAPII form and associated factors could also help elucidating ISW1a recruitment to the start of genes.

4.6 Proposed model for Isw1 remodeling complexes in suppressing cryptic transcription in wild-type yeast

Proper chromatin organization helps – among other processes - maintaining transcription fidelity. The findings from my studies, combined with unpublished data from our lab and insights from published literature, have led me to develop a working model that outlines the molecular mechanisms driving cryptic transcription events in budding yeast (Figure 4.6.1).

In wild-type yeast, Isw1 and Chd1 remodeling complexes generate regularly spaced nucleosome arrays within intragenic regions (Ocampo, Chereji et al. 2016, Kubik, Bruzzone et al. 2019). ISW1a is recruited to the start of genes, partially due to its affinity for H2A.Z, where it rapidly repositions the first nucleosomes, thus maintaining chromatin structure at the 5′ end of genes. ISW1b is recruited to the mid-3′ end of genes, preserving chromatin structure in

these regions (Smolle, Venkatesh et al. 2012, Li, Bergmann et al. 2022). Chd1 is recruited by the Paf1 complex, which binds to RNAPII, contributing to regularly spaced arrays throughout the gene body and facilitating FACT spreading throughout the gene body (Lee, Park et al. 2017, Jeronimo, Angel et al. 2021). Intragenic promoters are thereby concealed within a repressed chromatin state after RNAPII passage, and histone variant H2A.Z is restricted to the +1 nucleosome rather than inappropriately incorporated at intragenic regions.

In the absence of Ioc3, the ISW1a remodeling complex is unable to form, resulting in the accumulation of cryptic transcripts over intragenic regions, particularly antisense transcripts overlapping with the 5′ end of genes. I believe this occurs due to a disruption in chromatin organization in these regions, which could contribute to the exposure of DNA stretches longer than the average linker DNA. Due to the inconclusive motif searches in this study, the presence of intragenic promoter-like elements remains elusive. Although additional research is needed to identify how longer linker DNA is exposed in *ioc3Δ* cells, I propose two possibilities: higher histone turnover at the 5′ end of genes in *ioc3Δ* cells (Figure 1.6.4 B) or a disruption in nucleosome spacing that leads to unresolved dinucleosomes over the 5′ end of genes (Eriksson and Clark 2021). The SWR1 complex is then recruited to cryptic promoters, possibly through its affinity for longer DNA stretches. This complex exchanges the canonical H2A histone for the variant H2A.Z, crucial for facilitating the disassembly of the nucleosome marking the cryptic TSS, and potentially enabling additional RNAPII engagement and passage. During early cryptic elongation, Set1 recruitment by RNAPII likely methylates nucleosomes bearing H3K4me2 marks, thereby promoting the transition to H3K4me3-enriched nucleosomes and altering the chromatin at intragenic regions.

Deleting the Isw1 ATPase abolishes both the ISW1a and ISW1b complexes, resulting in a heightened cryptic phenotype compared to *ioc3Δ* cells. In yeast lacking *ISW1*, the chromatin structure at the mid-3′ end of genes is not properly maintained due to elevated histone turnover levels - a consequence from the loss of ISW1b (Smolle, Venkatesh et al. 2012). Conversely, histone

turnover is diminished around the gene start sites. The molecular mechanisms underlying cryptic transcription in *isw1Δ*, particularly regarding H2A.Z, resemble those in *ioc3Δ* yeast but to a greater extent, correlating with the worse cryptic transcription phenotype present in the *isw1Δ* mutant. This study also unveiled decreased levels of the histone variant H2A.Z at gene promoters, which could be correlated with the reduced levels of histone turnover in these regions. Neither of these effects is observed in *ioc3Δ* yeast. This could imply that Isw1 alone or ISW1b may play a crucial role in promoting histone turnover near the 5′ end of genes. Alternatively, the heightened production of cryptic transcripts in *isw1Δ* compared to *ioc3Δ*, particularly those overlapping with the 5′ end, may interfere with the activity of the SWR1 complex, thereby disrupting H2A.Z levels at gene promoters. Despite the presence of a functional nuclear exosome, cryptic RNA transcripts persistently accumulate within remodeler mutants. However, the precise mechanisms governing their termination and ultimate fate remain areas to further explore.

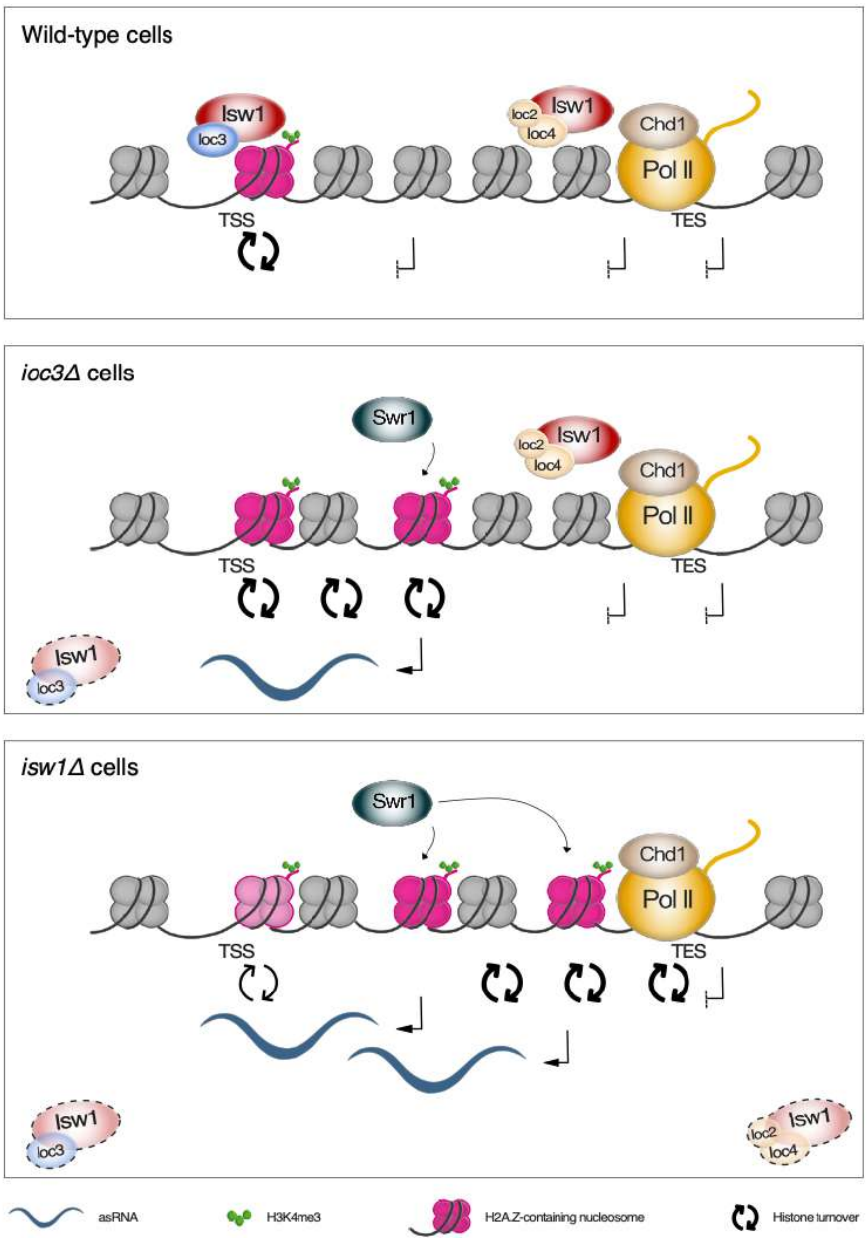

Figure 4.6.1 Proposed model for the role of Isw1 and Chd1 remodelers in the suppression of cryptic transcription. In wild-type yeast, intragenic chromatin organization by Isw1 and Chd1 remodelers suppresses cryptic transcription. Isw1 and Chd1 complexes generate evenly spaced nucleosome arrays within intragenic regions. ISW1a and ISW1b maintain chromatin at the 5′ and mid-3′ gene ends, respectively, while Chd1 spreads with RNAPII to conceal intragenic promoters. In *ioc3Δ* mutants, ISW1a loss leads to faulty H2A.Z incorporation, facilitating intragenic transcription initiation and accumulation of antisense transcripts over the 5′ end of genes. Deleting Isw1 abolishes both ISW1a and ISW1b, leading to higher faulty H2A.Z incorporation, and consequent higher cryptic transcription phenotype.

4.7 Outlook

This thesis uncovers key insights into ISW1a's role in suppressing cryptic transcription, but several questions remain. Targeted experiments will be essential to further elucidate the mechanisms of cryptic transcription repression by this chromatin remodeler.

4.7.1 Link between intragenic DNA exposure and cryptic transcription

One aspect of the proposed model is the exposure of DNA at intragenic regions in *ioc3Δ* and *isw1Δ* cells. This could result from either increased histone turnover or disrupted nucleosome spacing and consequent unresolved dinucleosomes. I would recommend integrating epigenomics data (MNase-seq and ATAC-seq) with transcriptomics data (RNA-seq and 5′cap-seq) data over intragenic regions of asDEGs identified in *ioc3Δ* and *isw1Δ* mutants, alongside ICRAT annotations. Integrating MNase-seq data with the asDEGs could help elucidate whether genes with overlapping ICRATs are disproportionately affected by nucleosome disruptions including unsolved dinucleosomes. ATAC-seq could also help identify if the chromatin accessibility near the intragenic TSS clusters correlates with cryptic transcription. The analysis of nucleosome positioning and DNA accessibility in these regions by this multi-comics combination could provide more direct evidence for the model's proposed chromatin disruption.

Regarding histone turnover, *ioc3Δ* and *isw1Δ* cells display different altered patterns relative to wild-type yeast, as shown by preliminary microarray data from our lab (Figure 1.6.4 B). Future studies, with higher resolution, could contribute to a better coverage of histone turnover changes in these mutants, such as ChIP-seq targeting H3K56ac, as this acetylation mark is deposited solely on soluble histones (Tsubota, Berndsen et al. 2007). Another way of studying histone turnover could be by using a yeast strain with constitutively expressed Myc-tagged histone H3 and *GAL1* promoter-controlled Flag-tagged

histone H3, then briefly inducing Flag-H3 expression with galactose, and comparing Flag-H3 over Myc-H3 occupancy levels using ChIP-seq.

Furthermore, to assess whether changes in histone dynamics and DNA accessibility around the start of antisense intragenic transcripts support the proposed model, I suggest including *ioc3Δ htz1Δ* and *isw1Δ htz1Δ* double mutants. Since *HTZ1* deletion suppresses antisense transcription in the remodeler mutants (e.g., at genes tested by RT-qPCR), observing increased histone dynamics and/or DNA accessibility at these regions in both *isw1Δ* and *ioc3Δ* single mutants, as well as in *isw1Δ htz1Δ* and *ioc3Δ htz1Δ* double mutants, would suggest that these chromatin changes are a cause, rather than a consequence, of antisense transcription.

4.7.2 Role of ISW1a in suppressing cryptic transcription initiation at intergenic regions

5′cap-seq analysis from *ioc3Δ rrp6Δ* cells suggested a role of ISW1a in preventing cryptic transcript expression from emerging at intergenic regions, including NDRs. While 5′cap-seq allows for genome-wide map of precise TSSs and quantification of transcription initiation levels, RNA-seq is a more direct way of measuring transcript abundance and differential expression.

Therefore, it would be relevant to employ RNA-seq to confirm the observations captured by 5′cap-seq analysis. Alternatively, CUT-specific RT-qPCRs could be conducted to quantify intergenic transcription in *ioc3Δ rrp6Δ* cells. In addition, I would also compare ATAC-seq data from *ioc3Δ* cells surrounding CUTs transcription start site, whose expression was increased within NDRs, in order to elucidate the mechanism by which ISW1a prevents divergent transcription from these regions.

Ioc3 has been shown to be strongly bound to the terminal nucleosome of genes (Yen, Vinayachandran et al. 2012). This interaction may likely be important to preventing NDR widening in the direction opposite to that of the gene

promoter, preventing accumulation of divergent cryptic transcripts. However further studies would be needed to investigate this hypothesis.

4.7.3 Stability and fate of remodeler-repressed cryptic transcripts

The stability and polyadenylation of ICRATs raise the question of whether these transcripts undergo similar processing to canonical mRNAs. Investigations using RNA immunoprecipitation followed by high-throughput sequencing (RIP-seq) in *isw1Δ* and *ioc3Δ* cells could help identify RNA-binding proteins involved in the stability, localization, translation, and decay of ICRATs (Zambelli and Pavesi 2015). RNA-FISH and cellular fractionation followed by RT-qPCR could determine whether these cryptic transcripts accumulate in the nucleus or are exported to the cytoplasm. Previous studies have shown ribosome association with cryptic transcripts in certain chromatin factor mutants by conducting polyribosome fractionation followed by 5′cap-seq (Wei, Hennig et al. 2019). The same approach could be employed to determine whether cryptic transcripts in ISW1a-deficient cells associate with ribosomes, and potentially undergo translation.

4.7.4 Relationship between Isw1, Chd1, and the FACT complex

The observation that FACT-impaired cells exhibit elevated ICRAT expression suggests a potential cooperation between Isw1 and/or Chd1, and FACT. To dissect this relationship, ICRAT-specific RT-qPCR experiments should be performed on both single mutants (*isw1Δ, chd1Δ,* Spt16-deficient cells) and double mutants (*isw1Δ* and *chd1Δ* in a Spt16-deficient background). This would help elucidate the functional overlap between these factors in suppressing cryptic transcription. Additionally, co-immunoprecipitation or proximity labelling could reveal physical interactions between FACT complex subunits and those of Isw1 and Chd1.

4.7.5 The importance of Swr1 and H2A.Z in enabling cryptic transcription in *ioc3Δ* cells

In the working model I propose that without ISW1a, SWR1C may be recruited to accessible DNA at intragenic regions, leading to the incorporation of H2A.Z in these regions. The RT-qPCR results I present in this study indicate the importance of H2A.Z to the production of antisense transcripts in *isw1Δ* and *ioc3Δ* cells. However, I believe RNA-seq would provide a broader and more comprehensive understanding of the impact of *HTZ1* and *SWR1* deletion on the cryptic transcriptional phenotype in these mutants. This is especially important since the deletion of *SWR1* in the *ioc3Δ* mutant did not fully replicate the effects observed in the *isw1Δ* mutant for most genes tested by RT-qPCR.

4.7.6 Recruitment of ISW1a

Genome-wide mapping of Ioc3-Flag in *htz1Δ* cells would help determine if the reduction of Ioc3 binding in the absence of H2A.Z at gene starts, as observed in specific genes by ChIP-qPCR, represents a broader and more significant finding. The current CUT&RUN findings suggest that ISW1a's association with chromatin may depend on (1) its interaction with DNA at nucleosome-depleted regions (NDRs), (2) histone modifications near gene boundaries, and/or (3) other factors recruited to NDRs.

The Ioc3-Flag occupancy peaks I identified in wild-type yeast were enriched for Reb1 and Rap1 binding motifs, suggesting a potential link between these transcription factors and ISW1a recruitment. To further explore this, I recommend genome-wide mapping of Ioc3-Flag in cells with *reb1* temperature sensitive allele and in *RAP1-AID* cells. To uncover additional factors contributing to ISW1a recruitment, I propose examining the roles of transcriptional initiation and early elongation factors, including RNAPII-associated factors, as well as histone modifications near NDRs. These studies could identify stronger candidates for the recruitment of the ISW1a complex *in vivo*, providing deeper insights into its regulatory mechanisms.

4.7.7 Concluding remarks

By addressing these gaps, future research could deepen our understanding of the mechanisms governing chromatin dynamics and transcription fidelity. This will not only enhance our understanding of transcriptional regulation in yeast but may also offer insights into similar processes in higher eukaryotes and their potential implications in human disease context.

References

Amigo, R., C. Farkas, C. Gidi, M. I. Hepp, N. Cartes, E. Tarifeno, J. L. Workman and J. L. Gutierrez (2022). "The linker histone Hho1 modulates the activity of ATP-dependent chromatin remodeling complexes." Biochim Biophys Acta Gene Regul Mech **1865**(1): 194781.

Amigo, R., F. Raiqueo, E. Tarifeno, C. Farkas and J. L. Gutierrez (2023). "Poly(dA:dT) Tracts Differentially Modulate Nucleosome Remodeling Activity of RSC and ISW1a Complexes, Exerting Tract Orientation-Dependent and -Independent Effects." Int J Mol Sci **24**(20).

Auger, A., L. Galarneau, M. Altaf, A. Nourani, Y. Doyon, R. T. Utley, D. Cronier, S. Allard and J. Cote (2008). "Eaf1 is the platform for NuA4 molecular assembly that evolutionarily links chromatin acetylation to ATP-dependent exchange of histone H2A variants." Mol Cell Biol **28**(7): 2257.

Aydin, O. Z., W. Vermeulen and H. Lans (2014). "ISWI chromatin remodeling complexes in the DNA damage response." Cell Cycle **13**(19): 3016.

Babour, A., Q. Shen, J. Dos-Santos, S. Murray, A. Gay, D. Challal, M. Fasken, B. Palancade, A. Corbett, D. Libri, J. Mellor and C. Dargemont (2016). "The Chromatin Remodeler ISW1 Is a Quality Control Factor that Surveys Nuclear mRNP Biogenesis." Cell **167**(5): 1201.

Bagchi, D. N., A. M. Battenhouse, D. Park and V. R. Iyer (2020). "The histone variant H2A.Z in yeast is almost exclusively incorporated into the +1 nucleosome in the direction of transcription." Nucleic Acids Res **48**(1): 157.

Balarezo-Cisneros, L. N., S. Parker, M. G. Fraczek, S. Timouma, P. Wang, R. T. O'Keefe, C. B. Millar and D. Delneri (2021). "Functional and transcriptional profiling of non-coding RNAs in yeast reveal context-dependent phenotypes and in trans effects on the protein regulatory network." PLoS Genet **17**(1): e1008761.

Baldi, S., P. Korber and P. B. Becker (2020). "Beads on a string-nucleosome array arrangements and folding of the chromatin fiber." Nat Struct Mol Biol **27**(2): 109.

Basehoar, A. D., S. J. Zanton and B. F. Pugh (2004). "Identification and distinct regulation of yeast TATA box-containing genes." Cell **116**(5): 699.

Bassett, A., S. Cooper, C. Wu and A. Travers (2009). "The folding and unfolding of eukaryotic chromatin." Curr Opin Genet Dev **19**(2): 159.

Beck, Z. T., S. C. Cloutier, M. J. Schipma, C. J. Petell, W. K. Ma and E. J. Tran (2014). "Regulation of glucose-dependent gene expression by the RNA helicase Dbp2 in Saccharomyces cerevisiae." Genetics **198**(3): 1001.

Bellush, J. M. and I. Whitehouse (2017). "DNA replication through a chromatin environment." Philos Trans R Soc Lond B Biol Sci **372**(1731).

Bergmann, L. (2021). Elucidating the molecular mechanism of Isw1a and Isw1b chromatin remodeler recruitment, Ludwig Maximilian University of Munich.

Bhardwaj, S. K., S. G. Hailu, L. Olufemi, S. Brahma, S. Kundu, S. K. Hota, J. Persinger and B. Bartholomew (2020). "Dinucleosome specificity and allosteric switch of the ISW1a ATP-dependent chromatin remodeler in transcription regulation." Nat Commun **11**(1): 5913.

Brahma, S. and S. Henikoff (2019). "RSC-Associated Subnucleosomes Define MNase-Sensitive Promoters in Yeast." Mol Cell **73**(2): 238.

Carcamo, C. C., M. F. Poyton, A. Ranjan, G. Park, R. K. Louder, X. A. Feng, J. M. Kim, T. Dzu, C. Wu and T. Ha (2022). "ATP binding facilitates target search of SWR1 chromatin remodeler by promoting one-dimensional diffusion on DNA." Elife **11**.

Castelnuovo, M., S. Rahman, E. Guffanti, V. Infantino, F. Stutz and D. Zenklusen (2013). "Bimodal expression of PHO84 is modulated by early termination of antisense transcription." Nat Struct Mol Biol **20**(7): 851.

Chen, H., H. Kharerin, A. Dhasarathy, M. Kladde and L. Bai (2022). "Partitioned usage of chromatin remodelers by nucleosome-displacing factors." Cell Rep **40**(8): 111250.

Chen, H. M. and A. M. Neiman (2011). "A conserved regulatory role for antisense RNA in meiotic gene expression in yeast." Curr Opin Microbiol **14**(6): 655.

Cieniewicz, A. M., L. Moreland, A. E. Ringel, S. G. Mackintosh, A. Raman, T. M. Gilbert, C. Wolberger, A. J. Tackett and S. D. Taverna (2014). "The bromodomain of Gcn5 regulates site specificity of lysine acetylation on histone H3." Mol Cell Proteomics **13**(11): 2896.

Clapier, C. R. and B. R. Cairns (2012). "Regulation of ISWI involves inhibitory modules antagonized by nucleosomal epitopes." Nature **492**(7428): 280.

Clapier, C. R., J. Iwasa, B. R. Cairns and C. L. Peterson (2017). "Mechanisms of action and regulation of ATP-dependent chromatin-remodeling complexes." Nat Rev Mol Cell Biol **18**(7): 407.

Couvillion, M., K. M. Harlen, K. C. Lachance, K. L. Trotta, E. Smith, C. Brion, B. M. Smalec and L. S. Churchman (2022). "Transcription elongation is finely tuned by dozens of regulatory factors." Elife **11**.

Cuperus, G. and D. Shore (2002). "Restoration of silencing in Saccharomyces cerevisiae by tethering of a novel Sir2-interacting protein, Esc8." Genetics **162**(2): 633.

Dollard, C., S. L. Ricupero-Hovasse, G. Natsoulis, J. D. Boeke and F. Winston (1994). "SPT10 and SPT21 are required for transcription of particular histone genes in Saccharomyces cerevisiae." Mol Cell Biol **14**(8): 5223.

Draghici, S., P. Khatri, A. C. Eklund and Z. Szallasi (2006). "Reliability and reproducibility issues in DNA microarray measurements." Trends Genet **22**(2): 101.

Duina, A. A. (2011). "Histone Chaperones Spt6 and FACT: Similarities and Differences in Modes of Action at Transcribed Genes." Genet Res Int **2011**: 625210.

Eriksson, P. R. and D. J. Clark (2021). "The yeast ISW1b ATP-dependent chromatin remodeler is critical for nucleosome spacing and dinucleosome resolution." Sci Rep **11**(1): 4195.

Eustermann, S., A. B. Patel, K. P. Hopfner, Y. He and P. Korber (2023). "Energy-driven genome regulation by ATP-dependent chromatin remodelers." Nat Rev Mol Cell Biol.

Ferrari, P. and M. Strubin (2015). "Uncoupling histone turnover from transcription-associated histone H3 modifications." Nucleic Acids Res **43**(8): 3972.

Formosa, T. and F. Winston (2020). "The role of FACT in managing chromatin: disruption, assembly, or repair?" Nucleic Acids Res **48**(21): 11929.

Gangaraju, V. K. and B. Bartholomew (2007). "Dependency of ISW1a chromatin remodeling on extranucleosomal DNA." Mol Cell Biol **27**(8): 3217.

Garcia-Martinez, J., G. Ayala, V. Pelechano, S. Chavez, E. Herrero and J. E. Perez-Ortin (2012). "The relative importance of transcription rate, cryptic transcription and mRNA stability on shaping stress responses in yeast." Transcription **3**(1): 39.

Gelfand, B., J. Mead, A. Bruning, N. Apostolopoulos, V. Tadigotla, V. Nagaraj, A. M. Sengupta and A. K. Vershon (2011). "Regulated antisense transcription controls expression of cell-type-specific genes in yeast." Mol Cell Biol **31**(8): 1701.

Goldmark, J. P., T. G. Fazzio, P. W. Estep, G. M. Church and T. Tsukiyama (2000). "The Isw2 chromatin remodeling complex represses early meiotic genes upon recruitment by Ume6p." Cell **103**(3): 423.

Goodwin, L. R. and D. J. Picketts (2018). "The role of ISWI chromatin remodeling complexes in brain development and neurodevelopmental disorders." Mol Cell Neurosci **87**: 55.

Gu, M., Y. Naiyachit, T. J. Wood and C. B. Millar (2015). "H2A.Z marks antisense promoters and has positive effects on antisense transcript levels in budding yeast." BMC Genomics **16**(1): 99.

Gurova, K., H. W. Chang, M. E. Valieva, P. Sandlesh and V. M. Studitsky (2018). "Structure and function of the histone chaperone FACT - Resolving FACTual issues." Biochim Biophys Acta Gene Regul Mech.

Hahn, S., E. T. Hoar and L. Guarente (1985). "Each of three "TATA elements" specifies a subset of the transcription initiation sites at the CYC-1 promoter of Saccharomyces cerevisiae." Proc Natl Acad Sci U S A **82**(24): 8562.

Hardy, S. and F. Robert (2010). "Random deposition of histone variants: A cellular mistake or a novel regulatory mechanism?" Epigenetics **5**(5): 368.

Hartley, P. D. and H. D. Madhani (2009). "Mechanisms that specify promoter nucleosome location and identity." Cell **137**(3): 445.

Hepp, M. I., V. Alarcon, A. Dutta, J. L. Workman and J. L. Gutierrez (2014). "Nucleosome remodeling by the SWI/SNF complex is enhanced by yeast high mobility group box (HMGB) proteins." Biochim Biophys Acta **1839**(9): 764.

Hongay, C. F., P. L. Grisafi, T. Galitski and G. R. Fink (2006). "Antisense transcription controls cell fate in Saccharomyces cerevisiae." Cell **127**(4): 735.

Huang da, W., B. T. Sherman and R. A. Lempicki (2009). "Systematic and integrative analysis of large gene lists using DAVID bioinformatics resources." Nat Protoc **4**(1): 44.

Jeronimo, C., A. Angel, V. Q. Nguyen, J. M. Kim, C. Poitras, E. Lambert, P. Collin, J. Mellor, C. Wu and F. Robert (2021). "FACT is recruited to the +1 nucleosome of transcribed genes and spreads in a Chd1-dependent manner." Mol Cell **81**(17): 3542.

Jeronimo, C. and F. Robert (2022). "The histone chaperone FACT: a guardian of chromatin structure integrity." Transcription **13**(1-3): 16.

Jeronimo, C., S. Watanabe, C. D. Kaplan, C. L. Peterson and F. Robert (2015). "The Histone Chaperones FACT and Spt6 Restrict H2A.Z from Intragenic Locations." Mol Cell **58**(6): 1113.

Jiang, C. and B. F. Pugh (2009). "Nucleosome positioning and gene regulation: advances through genomics." Nat Rev Genet **10**(3): 161.

Kalashnikova, A. A., R. A. Rogge and J. C. Hansen (2016). "Linker histone H1 and protein-protein interactions." Biochim Biophys Acta **1859**(3): 455.

Kim, J. M., P. Visanpattanasin, V. Jou, S. Liu, X. Tang, Q. Zheng, K. Y. Li, J. Snedeker, L. D. Lavis, T. Lionnet and C. Wu (2021). "Single-molecule imaging of chromatin remodelers reveals role of ATPase in promoting fast kinetics of target search and dissociation from chromatin." Elife **10**.

Kim, T. and S. Buratowski (2009). "Dimethylation of H3K4 by Set1 recruits the Set3 histone deacetylase complex to 5' transcribed regions." Cell **137**(2): 259.

Kim, T. S., C. L. Liu, M. Yassour, J. Holik, N. Friedman, S. Buratowski and O. J. Rando (2010). "RNA polymerase mapping during stress responses reveals widespread nonproductive transcription in yeast." Genome Biol **11**(7): R75.

Koch, M. R., N. C. M. House, C. M. Cosetta, R. M. Jong, C. G. Salomon, C. E. Joyce, E. A. Philips, X. A. Su and C. H. Freudenreich (2018). "The Chromatin Remodeler Isw1 Prevents CAG Repeat Expansions During Transcription in Saccharomyces cerevisiae." Genetics **208**(3): 963.

Krietenstein, N., M. Wal, S. Watanabe, B. Park, C. L. Peterson, B. F. Pugh and P. Korber (2016). "Genomic Nucleosome Organization Reconstituted with Pure Proteins." Cell **167**(3): 709.

Kubik, S., M. J. Bruzzone, D. Challal, R. Dreos, S. Mattarocci, P. Bucher, D. Libri and D. Shore (2019). "Opposing chromatin remodelers control transcription initiation frequency and start site selection." Nat Struct Mol Biol **26**(8): 744.

Kubik, S., E. O'Duibhir, W. J. de Jonge, S. Mattarocci, B. Albert, J. L. Falcone, M. J. Bruzzone, F. C. P. Holstege and D. Shore (2018). "Sequence-Directed Action of RSC Remodeler and General Regulatory Factors Modulates +1 Nucleosome Position to Facilitate Transcription." Mol Cell **71**(1): 89.

Kuo, Y. M., R. A. Henry, S. Tan, J. Cote and A. J. Andrews (2015). "Site specificity analysis of Piccolo NuA4-mediated acetylation for different histone complexes." Biochem J **472**(2): 239.

Lazzaro, M. A. and D. J. Picketts (2001). "Cloning and characterization of the murine Imitation Switch (ISWI) genes: differential expression patterns suggest distinct developmental roles for Snf2h and Snf2l." J Neurochem **77**(4): 1145.

Lee, Y., D. Park and V. R. Iyer (2017). "The ATP-dependent chromatin remodeler Chd1 is recruited by transcription elongation factors and maintains H3K4me3/H3K36me3 domains at actively transcribed and spliced genes." Nucleic Acids Res **45**(12): 7180.

Li, J., L. Bergmann, A. Rafael de Almeida, K. M. Webb, M. M. Gogol, P. Voigt, Y. Liu, H. Liang and M. M. Smolle (2022). "H3K36 methylation and DNA-binding both promote Ioc4 recruitment and Isw1b remodeler function." Nucleic Acids Res **50**(5): 2549.

Li, J., X. Liu, Z. Yin, Z. Hu and K. Q. Zhang (2021). "An Overview on Identification and Regulatory Mechanisms of Long Non-coding RNAs in Fungi." Front Microbiol **12**: 638617.

Li, L., K. Chen, Y. Sia, P. Hu, Y. Ye and Z. Chen (2024). "Structure of the ISW1a complex bound to the dinucleosome." Nat Struct Mol Biol **31**(2): 266.

Li, M., A. Hada, P. Sen, L. Olufemi, M. A. Hall, B. Y. Smith, S. Forth, J. N. McKnight, A. Patel, G. D. Bowman, B. Bartholomew and M. D. Wang (2015). "Dynamic regulation of transcription factors by nucleosome remodeling." Elife **4**.

Li, S., T. Wei and A. R. Panchenko (2023). "Histone variant H2A.Z modulates nucleosome dynamics to promote DNA accessibility." Nat Commun **14**(1): 769.

Li, Y., H. Gong, P. Wang, Y. Zhu, H. Peng, Y. Cui, H. Li, J. Liu and Z. Wang (2021). "The emerging role of ISWI chromatin remodeling complexes in cancer." J Exp Clin Cancer Res **40**(1): 346.

Lindstrom, K. C., J. C. Vary, Jr., M. R. Parthun, J. Delrow and T. Tsukiyama (2006). "Isw1 functions in parallel with the NuA4 and Swr1 complexes in stress-induced gene repression." Mol Cell Biol **26**(16): 6117.

Litwin, I., M. Nowicka, K. Markowska, E. Maciaszczyk-Dziubinska, P. Tomaszewska, R. Wysocki and K. Kramarz (2023). "ISW1a modulates cohesin distribution in centromeric and pericentromeric regions." Nucleic Acids Res **51**(17): 9101.

Malabat, C., F. Feuerbach, L. Ma, C. Saveanu and A. Jacquier (2015). "Quality control of transcription start site selection by nonsense-mediated-mRNA decay." Elife **4**.

Mattick, J. S., P. P. Amaral, P. Carninci, S. Carpenter, H. Y. Chang, L. L. Chen, R. Chen, C. Dean, M. E. Dinger, K. A. Fitzgerald, T. R. Gingeras, M. Guttman, T. Hirose, M. Huarte, R. Johnson, C. Kanduri, P. Kapranov, J. B. Lawrence, J. T. Lee, J. T. Mendell, T. R. Mercer, K. J. Moore, S. Nakagawa, J. L. Rinn, D. L. Spector, I. Ulitsky, Y. Wan, J. E. Wilusz and M. Wu (2023). "Long non-coding RNAs: definitions, functions, challenges and recommendations." Nat Rev Mol Cell Biol **24**(6): 430.

Miller, C., B. Schwalb, K. Maier, D. Schulz, S. Dumcke, B. Zacher, A. Mayer, J. Sydow, L. Marcinowski, L. Dolken, D. E. Martin, A. Tresch and P. Cramer (2011). "Dynamic transcriptome analysis measures rates of mRNA synthesis and decay in yeast." Mol Syst Biol **7**: 458.

Miller, C. L. W., J. L. Warner and F. Winston (2023). "Insights into Spt6: a histone chaperone that functions in transcription, DNA replication, and genome stability." Trends Genet **39**(11): 858.

Mivelaz, M., A. M. Cao, S. Kubik, S. Zencir, R. Hovius, I. Boichenko, A. M. Stachowicz, C. F. Kurat, D. Shore and B. Fierz (2020). "Chromatin Fiber Invasion and Nucleosome Displacement by the Rap1 Transcription Factor." Mol Cell **77**(3): 488.

Mizuguchi, G., X. Shen, J. Landry, W. H. Wu, S. Sen and C. Wu (2004). "ATP-driven exchange of histone H2AZ variant catalyzed by SWR1 chromatin remodeling complex." Science **303**(5656): 343.

Morillon, A., N. Karabetsou, A. Nair and J. Mellor (2005). "Dynamic lysine methylation on histone H3 defines the regulatory phase of gene transcription." Mol Cell **18**(6): 723.

Morillon, A., N. Karabetsou, J. O'Sullivan, N. Kent, N. Proudfoot and J. Mellor (2003). "Isw1 chromatin remodeling ATPase coordinates transcription elongation and termination by RNA polymerase II." Cell **115**(4): 425.

Oberbeckmann, E., V. Niebauer, S. Watanabe, L. Farnung, M. Moldt, A. Schmid, P. Cramer, C. L. Peterson, S. Eustermann, K. P. Hopfner and P. Korber (2021). "Ruler elements in chromatin remodelers set nucleosome array spacing and phasing." Nat Commun **12**(1): 3232.

Ocampo, J., R. V. Chereji, P. R. Eriksson and D. J. Clark (2016). "The ISW1 and CHD1 ATP-dependent chromatin remodelers compete to set nucleosome spacing in vivo." Nucleic Acids Res **44**(10): 4625.

Ocampo, J., R. V. Chereji, P. R. Eriksson and D. J. Clark (2019). "Contrasting roles of the RSC and ISW1/CHD1 chromatin remodelers in RNA polymerase II elongation and termination." Genome Res **29**(3): 407.

Panda, A. C., J. L. Martindale and M. Gorospe (2017). "Polysome Fractionation to Analyze mRNA Distribution Profiles." Bio Protoc **7**(3).

Park, D., H. Shivram and V. R. Iyer (2014). "Chd1 co-localizes with early transcription elongation factors independently of H3K36 methylation and releases stalled RNA polymerase II at introns." Epigenetics Chromatin **7**(1): 32.

Parnell, T. J., A. Schlichter, B. G. Wilson and B. R. Cairns (2015). "The chromatin remodelers RSC and ISW1 display functional and chromatin-based promoter antagonism." Elife **4**: e06073.

Passmore, L. A. and J. Coller (2022). "Roles of mRNA poly(A) tails in regulation of eukaryotic gene expression." Nat Rev Mol Cell Biol **23**(2): 93.

Pelechano, V., W. Wei and L. M. Steinmetz (2016). "Genome-wide quantification of 5'-phosphorylated mRNA degradation intermediates for analysis of ribosome dynamics." Nat Protoc **11**(2): 359.

Pinskaya, M., A. Nair, D. Clynes, A. Morillon and J. Mellor (2009). "Nucleosome remodeling and transcriptional repression are distinct functions of Isw1 in Saccharomyces cerevisiae." Mol Cell Biol **29**(9): 2419.

Piovesan, A., M. C. Pelleri, F. Antonaros, P. Strippoli, M. Caracausi and L. Vitale (2019). "On the length, weight and GC content of the human genome." BMC Res Notes **12**(1): 106.

Pondugala, V. V. and K. Mishra (2022). "RNA-Mediated Regulation of Meiosis in Budding Yeast." Noncoding RNA **8**(6).

Radman-Livaja, M., T. K. Quan, L. Valenzuela, J. A. Armstrong, T. van Welsem, T. Kim, L. J. Lee, S. Buratowski, F. van Leeuwen, O. J. Rando and G. A. Hartzog (2012). "A key role for Chd1 in histone H3 dynamics at the 3' ends of long genes in yeast." PLoS Genet **8**(7): e1002811.

Ramanathan, A., G. B. Robb and S. H. Chan (2016). "mRNA capping: biological functions and applications." Nucleic Acids Res **44**(16): 7511.

Ranjan, A., G. Mizuguchi, P. C. FitzGerald, D. Wei, F. Wang, Y. Huang, E. Luk, C. L. Woodcock and C. Wu (2013). "Nucleosome-free region dominates histone acetylation in targeting SWR1 to promoters for H2A.Z replacement." Cell **154**(6): 1232.

Reyes, A. A., R. D. Marcum and Y. He (2021). "Structure and Function of Chromatin Remodelers." J Mol Biol **433**(14): 166929.

Rhee, H. S. and B. F. Pugh (2011). "Comprehensive genome-wide protein-DNA interactions detected at single-nucleotide resolution." Cell **147**(6): 1408.

Ricci, M. A., C. Manzo, M. F. Garcia-Parajo, M. Lakadamyali and M. P. Cosma (2015). "Chromatin fibers are formed by heterogeneous groups of nucleosomes in vivo." Cell **160**(6): 1145.

Shahbazian, M. D., K. Zhang and M. Grunstein (2005). "Histone H2B ubiquitylation controls processive methylation but not monomethylation by Dot1 and Set1." Mol Cell **19**(2): 271.

Shen, Q., N. Beyrouthy, L. Matabishi-Bibi and C. Dargemont (2017). "The chromatin remodeling Isw1a complex is regulated by SUMOylation." Biochem J **474**(20): 3455.

Sherman, B. T., M. Hao, J. Qiu, X. Jiao, M. W. Baseler, H. C. Lane, T. Imamichi and W. Chang (2022). "DAVID: a web server for functional enrichment analysis and functional annotation of gene lists (2021 update)." Nucleic Acids Res **50**(W1): W216.

Singh, A. K. and F. Mueller-Planitz (2021). "Nucleosome Positioning and Spacing: From Mechanism to Function." J Mol Biol **433**(6): 166847.

Smolle, M., S. Venkatesh, M. M. Gogol, H. Li, Y. Zhang, L. Florens, M. P. Washburn and J. L. Workman (2012). "Chromatin remodelers Isw1 and Chd1 maintain chromatin structure during transcription by preventing histone exchange." Nat Struct Mol Biol **19**(9): 884.

Soares, L. M., P. C. He, Y. Chun, H. Suh, T. Kim and S. Buratowski (2017). "Determinants of Histone H3K4 Methylation Patterns." Mol Cell **68**(4): 773.

Sun, Z. W. and C. D. Allis (2002). "Ubiquitination of histone H2B regulates H3 methylation and gene silencing in yeast." Nature **418**(6893): 104.

Thelen, N., J. Defourny, D. L. J. Lafontaine and M. Thiry (2021). "Visualization of Chromatin in the Yeast Nucleus and Nucleolus Using Hyperosmotic Shock." Int J Mol Sci **22**(3).

Topal, S., P. Vasseur, M. Radman-Livaja and C. L. Peterson (2019). "Distinct transcriptional roles for Histone H3-K56 acetylation during the cell cycle in Yeast." Nat Commun **10**(1): 4372.

Tsubota, T., C. E. Berndsen, J. A. Erkmann, C. L. Smith, L. Yang, M. A. Freitas, J. M. Denu and P. D. Kaufman (2007). "Histone H3-K56 acetylation is catalyzed by histone chaperone-dependent complexes." Mol Cell **25**(5): 703.

Tsukiyama, T., J. Palmer, C. C. Landel, J. Shiloach and C. Wu (1999). "Characterization of the imitation switch subfamily of ATP-dependent chromatin-remodeling factors in Saccharomyces cerevisiae." Genes Dev **13**(6): 686.

Vary, J. C., Jr., V. K. Gangaraju, J. Qin, C. C. Landel, C. Kooperberg, B. Bartholomew and T. Tsukiyama (2003). "Yeast Isw1p forms two separable complexes in vivo." Mol Cell Biol **23**(1): 80.

Venkatesh, S., H. Li, M. M. Gogol and J. L. Workman (2016). "Selective suppression of antisense transcription by Set2-mediated H3K36 methylation." Nat Commun **7**: 13610.

Venkatesh, S., M. Smolle, H. Li, M. M. Gogol, M. Saint, S. Kumar, K. Natarajan and J. L. Workman (2012). "Set2 methylation of histone H3 lysine 36 suppresses histone exchange on transcribed genes." Nature **489**(7416): 452.

Venkatesh, S., J. L. Workman and M. Smolle (2013). "UpSETing chromatin during non-coding RNA production." Epigenetics Chromatin **6**(1): 16.

Vera, J. M. and R. D. Dowell (2016). "Survey of cryptic unstable transcripts in yeast." BMC Genomics **17**: 305.

Viktorovskaya, O., J. Chuang, D. Jain, N. I. Reim, F. Lopez-Rivera, M. Murawska, D. Spatt, L. S. Churchman, P. J. Park and F. Winston (2021). "Essential histone chaperones collaborate to regulate transcription and chromatin integrity." Genes Dev **35**(9-10): 698.

Wei, W., B. P. Hennig, J. Wang, Y. Zhang, I. Piazza, Y. Pareja Sanchez, C. D. Chabbert, S. H. Adjalley, L. M. Steinmetz and V. Pelechano (2019). "Chromatin-sensitive cryptic promoters putatively drive expression of alternative protein isoforms in yeast." Genome Res **29**(12): 1974.

White, C. L., R. K. Suto and K. Luger (2001). "Structure of the yeast nucleosome core particle reveals fundamental changes in internucleosome interactions." EMBO J **20**(18): 5207.

Wolf, B. K., Y. Zhao, A. McCray, W. H. Hawk, L. T. Deary, N. W. Sugiarto, I. S. LaCroix, S. A. Gerber, C. Cheng and X. Wang (2023). "Cooperation of chromatin remodeling SWI/SNF complex and pioneer factor AP-1 shapes 3D enhancer landscapes." Nat Struct Mol Biol **30**(1): 10.

Woo, H., S. Dam Ha, S. B. Lee, S. Buratowski and T. Kim (2017). "Modulation of gene expression dynamics by co-transcriptional histone methylations." Exp Mol Med **49**(4): e326.

Woodcock, C. L. and S. Dimitrov (2001). "Higher-order structure of chromatin and chromosomes." Curr Opin Genet Dev **11**(2): 130.

Wu, A. C. K., H. Patel, M. Chia, F. Moretto, D. Frith, A. P. Snijders and F. J. van Werven (2018). "Repression of Divergent Noncoding Transcription by a Sequence-Specific Transcription Factor." Mol Cell **72**(6): 942.

Xu, Z., W. Wei, J. Gagneur, F. Perocchi, S. Clauder-Munster, J. Camblong, E. Guffanti, F. Stutz, W. Huber and L. M. Steinmetz (2009). "Bidirectional promoters generate pervasive transcription in yeast." Nature **457**(7232): 1033.

Yamada, K., T. D. Frouws, B. Angst, D. J. Fitzgerald, C. DeLuca, K. Schimmele, D. F. Sargent and T. J. Richmond (2011). "Structure and mechanism of the chromatin remodeling factor ISW1a." Nature **472**(7344): 448.

Yang, C., E. Bolotin, T. Jiang, F. M. Sladek and E. Martinez (2007). "Prevalence of the initiator over the TATA box in human and yeast genes and identification of DNA motifs enriched in human TATA-less core promoters." Gene **389**(1): 52.

Yarragudi, A., T. Miyake, R. Li and R. H. Morse (2004). "Comparison of ABF1 and RAP1 in chromatin opening and transactivator potentiation in the budding yeast Saccharomyces cerevisiae." Mol Cell Biol **24**(20): 9152.

Yen, K., V. Vinayachandran, K. Batta, R. T. Koerber and B. F. Pugh (2012). "Genome-wide nucleosome specificity and directionality of chromatin remodelers." Cell **149**(7): 1461.

Yen, K., V. Vinayachandran and B. F. Pugh (2013). "SWR-C and INO80 chromatin remodelers recognize nucleosome-free regions near +1 nucleosomes." Cell **154**(6): 1246.

Zambelli, F. and G. Pavesi (2015). "RIP-Seq data analysis to determine RNA-protein associations." Methods Mol Biol **1269**: 293.

Zentner, G. E., T. Tsukiyama and S. Henikoff (2013). "ISWI and CHD chromatin remodelers bind promoters but act in gene bodies." PLoS Genet **9**(2): e1003317.

Zhang, H., D. N. Roberts and B. R. Cairns (2005). "Genome-wide dynamics of Htz1, a histone H2A variant that poises repressed/basal promoters for activation through histone loss." Cell **123**(2): 219.

Zhang, Y. and V. Pelechano (2021). "High-throughput 5'P sequencing enables the study of degradation-associated ribosome stalls." Cell Rep Methods **1**(1): 100001.

Zhu, Q., N. Liu, S. H. Orkin and G. C. Yuan (2019). "CUT&RUNTools: a flexible pipeline for CUT&RUN processing and footprint analysis." Genome Biol **20**(1): 192.